UNIVERSIDADE FEDERAL DA BAHIA
INSTITUTO DE GEOCIÊNCIAS
PROGRAMA DE PESQUISA E PÓS-GRADUAÇÃO EM GEOLOGIA
ÁREA DE CONCENTRAÇÃO:
PETROLOGIA, METALOGÊNESE E EXPLORAÇÃO MINERAL

DISSERTAÇÃO DE MESTRADO

CARACTERIZAÇÃO DOS PROCESSOS CRÍTICOS DO SISTEMA MINERALIZANTE AURÍFERO EPIGENÉTICO DA SERRA DE JACOBINA, BAHIA

DANIEL AUGUSTO DE MIRANDA

SALVADOR
2020

CARACTERIZAÇÃO DOS PROCESSOS CRÍTICOS DO SISTEMA MINERALIZANTE AURÍFERO EPIGENÉTICO DA SERRA DE JACOBINA, BAHIA

Daniel Augusto de Miranda

Orientador: Prof. Dr. Aroldo Misi

Dissertação de Mestrado apresentada ao Programa de Pós-Graduação em Geologia do Instituto de Geociências da Universidade Federal da Bahia como requisito parcial à obtenção do Título de Mestre em Geologia, Área de Concentração: Petrologia, Metalogênese e Exploração Mineral.

SALVADOR

2020

M672 Miranda, Daniel Augusto de

Caracterização dos processos críticos do sistema mineralizante aurífero epigenético da Serra de Jacobina, Bahia/ Daniel Augusto de Miranda. – Salvador, 2020.

91 f.

Orientador: Prof. Dr. Aroldo Misi

Dissertação (Mestrado) – Universidade Federal da Bahia. Instituto de Geociências, 2020.

1. Geologia. 2. Petrografia. 3. Ouro. 4. Serra. I. Misi, Aroldo. II. Universidade Federal da Bahia. III. Título.

CDU552.1

DANIEL AUGUSTO DE MIRANDA

"CARACTERIZAÇÃO DOS PROCESSOS CRÍTICOS DO SISTEMA MINERALIZANTE AURÍFERO EPIGENÉTICO DA SERRA DE JACOBINA, BAHIA"

Trabalho apresentado ao Programa de Pós-Graduação em Geologia da Universidade Federal da Bahia, como requisito parcial para a obtenção do Grau de Mestre em Geologia na área de concentração em PETROLOGIA, METALOGÊNESE E EXPLORAÇÃO MINERAL em 09/03/2020.

APROVADO PELA BANCA EXAMINADORA:

Dr. Aroldo Misi (Orientador) - UFBA

Dr. Carlos D. Marques de Sá (Examinador Externo) – UFS

Dr. Luiz Cesar Corrêa Gomes (Examinador Interno) – UFBA

Salvador – BA
2020

Aos meus familiares e esposa, com muito carinho.

RESUMO

A Serra de Jacobina está localizada na porção nordeste do estado da Bahia, Brasil. Trata-se de uma cadeia de montanhas com direção N-S e duzentos e cinquenta quilômetros de extensão que está na borda leste do bloco Gavião-Lençóis. Ela corresponde à porção norte do Lineamento Contendas-Mirante-Jacobina. Existem diversos garimpos em veios de quartzo auríferos hospedados nas rochas metassedimentares siliciclásticas do Grupo Jacobina e metaultramáficas da Suíte Vale do Coxo. Quatro destes garimpos foram mapeados: Maravilha, Jaqueira, Morro da Palmeirinha e Mina Velha. Estes depósitos são hospedados por dois sistemas de falhas de idade Paleoproterozoica, com direção aproximada N-S, denominados de leste para oeste de Pindobaçu e Maravilha. O Sistema de Falhas Pindobaçu é uma estrutura transcrustal que representa o contato entre os blocos Gavião-Lençóis e Mairi. O sistema de falha Maravilha é composto por estruturas rasas limitadas à crosta continental superior. Os veios mineralizados são hospedados por estruturas de segunda ordem pertencentes a estes sistemas de falhas. A alteração sericítica disseminada ocorre de maneira ampla nos quartzitos e conglomerados do Grupo Jacobina. Nos xistos Vale do Coxo a alteração é pervasiva com substituição da biotita pela clorita. Nos veios de quartzo a sericitização ocorre como preenchimento de fraturas. A sulfetação é subordinada à alteração sericítica tanto nas rochas siliciclásticas quanto nas metaultramáficas. O ouro ocorre como cristais isolados nos veios de quartzo e subordinado à sericitização e à sulfetação nas hospedeiras. Petrografia e microtermometria de inclusões fluidas nos veios de quartzo indicaram três principais tipos de fluidos. O tipo WC, bifásico, é composto por H_2O+CO_2+NaCl e ocorre nos garimpos Maravilha e Jaqueira. O tipo W, bifásico ou trifásico, é composto por H_2O +NaCl ou H_2O+NaCl+sólido respectivamente, ocorrem nos garimpos Jaqueira, Morro da Palmeirinha e Mina Velha. O fluido do tipo C, de cor escura, é monofásico ou bifásico, composto por CO_2-CH_4 e/ou N_2 e ocorre tanto no Maravilha quanto no Morro da Palmeirinha. No garimpo da Jaqueira a integração entre os resultados de microtermometria com geotermometria de cloritas indica condições de pressão e temperatura de 1,6-2,0 kbar e 302-346°C. A mineralização aurífera em veios de quartzo da Serra de Jacobina pode ser interpretada como produto de um sistema mineral hidrotermal orogênico composto pelos seguintes processos críticos: "gatilho" representado pela colisão Paleoproterozoica entre as paleoplacas Gavião e Mairi; produção de fluidos orogênicos de composição variada; fluxo de fluido induzido por sistemas de falhas compressionais que serviram como condutos; dois principais indutores da deposição de ouro foram a imiscibilidade de fluidos e interação fluido-rocha; concentração de ouro nos veios de quartzo e rochas hospedeiras; depósitos estão hospedados em uma litosfera cratônica estável e foram preservados do ciclo de denudação que moldou a paisagem do cráton do São Francisco.

Palavras-chave: Lineamento Contendas-Mirante-Jacobina. Inclusão fluida. Geotermometria de clorita. Ouro orogênico.

ABSTRACT

The Serra de Jacobina mountain range is located in the northeastern part of the Bahia state, Brazil. It consists of a 250-km-long, N-S mountain chain at the eastern border of the Gavião-Lençóis block and corresponds to the Contendas-Mirante-Jacobina Lineament northern portion. There are several structurally controlled Au-bearing quartz veins hosted by metasedimentary rocks of the siliciclastic Jacobina Group and Vale do Coxo metaultramafic rocks exploited by artisanal miners. Four of these occurrences, named Maravilha, Jaqueira, Morro da Palmeirinha and Mina Velha were mapped. They are hosted by two fault systems of Paleoproterozoic age, named from east to west, Pindobaçu and Maravilha. The Pindobaçu fault system is a transcrustal structure and represents the contact between the Gavião-Lençóis and Mairi blocks. The Maravilha fault system is a shallower structure limited to the upper crust. Mineralized veins are hosted by second-order structures related to these two fault systems. The hydrothermal alteration varies according to the host rock. Disseminated sericitic alteration is widespread within Jacobina Group quartzites and metaconglomerates. At Vale do Coxo schists, the alteration is pervasive, with chlorite replacing biotite, and of the fissure-filling type as quartz veins. Sulfidation is subordinated to the sericitic alteration, both at quartzites and schists from the Jacobina Group and Vale do Coxo, respectively. Gold occurs as isolated crystals within quartz veins or subordinated to sericitic and/or sulfidation assemblages in host rocks. Petrography and fluid inclusion microthermometry revealed three main types of fluids. The type WC is a two-phase H_2O+CO_2+NaCl fluid which occurs at Maravilha and Jaqueira. The type W is a two-phase H_2O +NaCl or three-phase H_2O +NaCl+solid fluid which occur at Jaqueira, Morro da Palmeirinha and Mina Velha. The type C is a dark color, one- or two-phase CO_2-CH_4 and/or N_2 fluid which occurs at Maravilha and Morro da Palmeirinha. At Jaqueira, combined microthermometric results with chlorite geothermometry, reveals that the hydrothermal alteration and gold deposition occurs with P-T conditions of 1.6-2.0 kbar and 302-346°C. The main mechanisms of gold deposition were fluid immiscibility and fluid-rock interaction. The hydrothermal mineralization at Serra de Jacobina is interpreted as an orogenic mineral system and the following elements were characterized: (1) The production of orogenic fluids with variable composition; (2) the fault systems in a compression-driven fluid flow type are conduits and driver; (3) the inductors of gold precipitation were fluid immiscibility and fluid-rock interaction.

Keywords: Contendas-Mirante-Jacobina Lineament. Fluid inclusion. Chlorite geothermometry. Orogenic gold.

SUMÁRIO

CAPÍTULO 1
INTRODUÇÃO GERAL

O conceito de sistema mineralizante se refere à "todos os fatores geológicos que controlam a geração e preservação de depósitos minerais" (Wyborn *et al*., 1994). McCuaig *et. al*. (2010) propõe um método pragmático para geração de alvos de exploração com aplicação do conceito de sistemas mineralizantes. Para isto devem ser identificados os chamados processos críticos deste sistema. Para depósitos auríferos orogênicos, por exemplo, estes elementos são determinados inicialmente pela caracterização dos fatores que identificam a fonte dos fluidos hidrotermais, o arcabouço litoestrutural envolvido no transporte destes fluidos bem como a alteração hidrotermal observada nas imediações da mineralização. Segundo McCuaig & Hronsky (2014), diferentes depósitos minerais são tratados como expressões menores dentro de um sistema de processos muito mais amplos, que operam em uma variedade de escalas, balanceando massa e fluxo de energia. Embora cada tipo de sistema mineralizante possua suas particularidades, estes autores apontam uma generalização dos processos críticos mais práticos e fáceis de serem utilizados na aplicação deste conceito. São eles a arquitetura litosférica, ambiência geodinâmica e fertilidade, além da preservação de região de deposição da mineralização. A vetorização destes processos críticos em ambiente de Sistemas de Informações Geográficas (SIG) permite e elaboração de mapas de potencialidade mineral que auxiliam na geração de alvos em projetos de exploração mineral (Hagemann *et al*., 2016).

A Serra de Jacobina está localizada na porção nordeste do estado da Bahia, Brasil. Situa-se na porção nordeste do cráton do São Francisco (Almeida, 1977) e trata-se de uma cadeia de montanhas com direção N-S e duzentos e cinquenta quilômetros de extensão que está na borda leste da paleoplaca Gavião. Esta serra corresponde à porção norte do Lineamento Contendas-Mirante-Jacobina. O interesse geológico sobre a Serra de Jacobina remonta ao século XVIII com a descoberta de ouro na região em 1701 (Mascarenhas *et al*., 1998). Além do ouro associado aos metaconglomerados da Formação Serra do Córrego classicamente comparado às mineralizações de Witwatersrand (Bateman, 1958) ocorrem outros tipos de mineralizações auríferas hospedadas em veios de quartzo estruturalmente controlados na Serra de Jacobina denominados Bahia Gold Belt, *trend* aurífero de direção N-S e aproximadamente noventa quilômetros de extensão (Pearson *et al*., 2005). As rochas encaixantes dos veios de quartzo são: (i) rochas siliciclásticas do Grupo Jacobina; (ii) às rochas metaultramáficas de direção N-S da Suíte Vale do Coxo (Reis *et al*., 2019); (iii) aos diques máficos a intermediários de direção E-W. Teixeira *et al*.(2001) e Pearson *et al*. (2005) classificam estas tipologias em função da sua rocha hospedeira. Baseados na observação do controle estrutural de corpos mineralizados com alteração hidrotermal e na ocorrência de ouro nestas diferentes unidades os autores propõe um modelo de mineralização epigenética para estas tipologias.

O objetivo geral do presente estudo é o uso das diversas ocorrências auríferas em veios de quartzo para o entendimento do sistema mineralizante que produziu estas mineralizações epigenéticas. Para isto os objetivos específicos buscam a caracterização dos processos críticos deste sistema. Foram utilizados: (i)

petrografia por microscópio óptico de transmissão e reflexão, microscópio eletrônico de varredura e microssonda eletrônica para caracterização da mineralogia hidrotermal; (ii) Dados de mapeamento litoestrutural conjugados à trabalhos regionais caracterizam o processo crítico arquitetura litosférica; (iii) microtermometria em inclusões fluidas aliados à dados de geocronologia explicam o processo evolução geodinâmica; (iv) Considerações sobre a evolução da paisagem do cráton do São Francisco ajudam a compreender o fator de preservação destes depósitos.

O entendimento dos sistemas mineralizantes induz a uma compreensão dos depósitos minerais de forma ampla e regional. A vetorização dos processos críticos do sistema mineralizante em ambiente SIG permite a confecção de mapas de predição de potencialidade mineral para geração de alvos para exploração mineral. A proposta de dissertação *Caracterização dos Processos Críticos do Sistema Mineralizante Aurífero Epigenético da Serra de Jacobina, BA* visa o entendimento regional do Bahia Gold Belt. Assim propõe-se o uso desta província metalogenética relativamente bem conhecida como área escola para aplicação do conceito de sistemas mineralizantes. Tais conceitos serão utilizados em outras áreas estudadas pela CPRM - Serviço Geológico do Brasil cujos resultados serão divulgados com o intuito de contribuir para evolução do conhecimento geológico do país.

A revista em que o artigo será submetido é a *Journal of South American Earth Sciences*, ISSN 0895-9811, classificação A3 *qualis capes*.

Referencias

ALMEIDA, F.F.M. O cráton do São Francisco. **Revista Brasileira de Geociências**, São Paulo, v. 7, n. 4, p. 349-367, 1977.

BATEMAN, J.D. Uranium-bearing auriferous reefs at Jacobina, Brazil. **Economic Geology**, Lancaster, v. 54, p. 417-425, 1958.

HAGEMANN, S.G.; LISITSIN, V.A.; HUSTON, D.L. Mineral system analysis: quo vadis. **Ore Geology Review**, Perth, Austrália, v. 76, p. 504-522, 2016. DOI: 10.1016/j.oregeorev.2015.12.012

MASCARENHAS, J.F. *et al*. **Geologia e recursos minerais do Grupo Jacobina e da parte sul do Greenstone Belt de Mundo Novo**. Salvador: CBPM, 1998. (Série Arquivos Abertos, 13).

McCUAIG, T.C.; BERESFORD, S.; HRONSKY, J. Translating the mineral system approach into an effective exploration targeting system. **Ore Geology Reviews**, Perth, Austrália, v. 38, p. 128-138, 2010. DOI: 10.1016/j.oregeorev.2010.05.008.

McCUAIG, T.C.; HRONSKY, J.M.A. **The mineral system concept**: the key to exploration targeting. Lancaster, PA: Society of Economic Geologists, 2014. p.153-176. (Special Publications, 18). DOI: 10.5382/SP.18.08

PEARSON, W.; MACÊDO, P.M., RÚBIO, A., LORENZO, C.L., KARPETA, P. Geology and gold mineralization of the Jacobina Mine and Bahia Gold Belt, Bahia, Brazil and a comparison to Tarkwa and Witwatersrand. *In*: RHODEN, H.N.; STEININGER, R.C.; VIKRE, P.G. (Ed.) **Geological Society of Nevada Symposium 2005**. Reno, Nevada: GSN, 2005. p.757-785.

REIS, C.; MENEZES, R.C.L.; MIRANDA, D.A.; SANTOS, F.P.; LOUREIRO, H.S.C.; NEVES, J.P.; VIEIRA, R. **ARIM - Serra de Jacobina**: Mapa Geológico. Salvador : CPRM, 2019. 1 mapa color., 90,0 x 130,0 cm. Escala 1:250.000. Programa Gestão Estratégica da Geologia, da Mineração e da Transformação Mineral.

TEIXEIRA, J.B.G.; SOUZA, J.A.B.; SILVA, M.G.; LEITE, C.M.M.; BARBOSA, J.S.F.; COELHO, C.E.S.; ABRAM, M.B.; FILHO, V.M.C.; IYER, S.S.S. Gold mineralization in the Serra de Jacobina region, Bahia Brazil: tectonic framework and metallogenesis. **Mineralium Deposita**, Alemanha, v. 36, p. 332-344, 2001. DOI: 10.1007/s001260100174.

WYBORN, L.A.I.; HEINRICH, C.A.; JAQUES, A.L. Australian proterozoic mineral systems: essential ingredients and mappable criteria. *In*: AUSTRALIAN INSTITUTE OF MINING AND METALLURGY ANNUAL CONFERENCE, 1994, Melbourne. **Procedings** […] Melbourne: Australian Institute of Mining and Metallurgy, 1994. p.109-115.

CAPÍTULO 2

ARTIGO 1 - A MINERAL SYSTEM APPROACH ON THE PALEOPROTEROZOIC AU-BEARING QUARTZ VEINS OF THE SERRA DE JACOBINA, NORTHEASTERN OF THE SÃO FRANCISCO CRATON, BRAZIL

TITLE: A mineral system approach on the Paleoproterozoic Au-bearing quartz veins of the Serra de Jacobina, Northeastern of the São Francisco Craton, Brazil

Daniel Augusto de Miranda [a,b,*]

a CPRM/Geological Survey of Brazil, Av. Ulysses Guimarães, 2862, Salvador, BA, CEP 41213-000, Brazil.

b Curso de Pós-Graduação em Geologia, Instituto de Geociências, Universidade Federal da Bahia, Salvador, BA, Brazil.

Aroldo Misi [b]

b Curso de Pós-Graduação em Geologia, Instituto de Geociências, Universidade Federal da Bahia, Salvador, BA, Brazil. aroldo.misi@gmail.com

Evandro Luiz Klein [c, d]

c CPRM/Geological Survey of Brazil, SBN, Quadra 02, Bloco H, Ed. Central Brasília, 1° andar, Brasília, DF, Brazil. evandro.klein@cprm.gov.br

d GPGE – Grupo de Pesquisa em Geologia Econômica, PPGG-UFPA – Programa de Pós-Graduação em Geologia e Geoquímica, Universidade Federal do Pará, Belém-PA, Brazil

Marco Paulo de Castro [e]

e Departamento de Geologia, Escola de Minas, Universidade Federal de Ouro Preto, Morro do Cruzeiro, 35400-000, Ouro Preto, MG, Brazil. marco_pcastro@yahoo.com

Gláucia Queiroga [e]

e Departamento de Geologia, Escola de Minas, Universidade Federal de Ouro Preto, Morro do Cruzeiro, 35400-000, Ouro Preto, MG, Brazil. glauciaqueiroga@yahoo.com.br

* Corresponding author: daniel.miranda@cprm.gov.br

HIGHLIGHTS

- Structurally controlled Au-bearing quartz veins hosted by fault systems.
- Initial ore-forming fluids were a mixture of two immiscible fluids.
- Classic Q-S-P (quartz-sericite-pyrite) sericitic hydrothermal assemblage.
- Au-deposition P-T conditions 1.6-2.0 kbar and 302-346°C.
- The deposits represent a Paleoproterozoic orogenic hydrothermal mineral system.

ABSTRACT

The Serra de Jacobina mountain range is located in the northeastern part of the Bahia state, Brazil. It consists of a 250-km-long, N-S mountain chain at the eastern border of the Gavião-Lençóis block and corresponds to the Contendas-Mirante-Jacobina Lineament northern portion. There are several structurally controlled Au-bearing quartz veins hosted by metasedimentary rocks of the siliciclastic Jacobina Group and Vale do Coxo metaultramafic rocks exploited by artisanal miners.

Four of these occurrences, named Maravilha, Jaqueira, Morro da Palmeirinha and Mina Velha were mapped. They are hosted by two fault systems of Paleoproterozoic age, named from east to west, Pindobaçu and Maravilha. The Pindobaçu fault system is a transcrustal structure and represents the contact between the Gavião-Lençóis and Mairi blocks. The Maravilha fault system is a shallower structure limited to the upper crust. Mineralized veins are hosted by second-order structures related to these two fault systems. The hydrothermal alteration varies according to the host rock. Disseminated sericitic alteration is widespread within Jacobina Group quartzites and metaconglomerates. At Vale do Coxo schists the alteration is pervasive, with chlorite replacing biotite, and of the fissure-filling type in the quartz veins. Sulfidation is subordinated to the sericitic alteration, both at quartzites and schists from the Jacobina Group and Vale do Coxo, respectively. Gold occurs as isolated crystals within quartz veins or subordinated to sericitic and/or sulfidation assemblages in host rocks.

Petrography and fluid inclusion microthermometry revealed three main types of fluids. The type WC is a two-phase H_2O+CO_2+NaCl fluid which occurs at Maravilha and Jaqueira. The type W is a two-phase H_2O +NaCl or three-phase H_2O +NaCl+solid fluid which occur at Jaqueira, Morro da Palmeirinha and Mina Velha. The type C is a dark color, one- or two-phase CO_2-CH_4 and/or N_2 fluid which occurs at Maravilha and Morro da Palmeirinha.

At Jaqueira, combined microthermometric results with chlorite geothermometry, reveals that the hydrothermal alteration and gold deposition occurs with P-T conditions of 1.6-2.0 kbar and 302-346°C. The main mechanisms of gold deposition were fluid immiscibility and fluid-rock interaction.

The hydrothermal mineralization at Serra de Jacobina is interpreted as an orogenic mineral system and the following elements were characterized: (1) The production of orogenic fluids with variable composition; (2) the fault systems in a compression-driven fluid flow type are conduits and driver; (3) the inductors of gold precipitation were fluid immiscibility and fluid-rock interaction.

Keywords: Contendas-Mirante-Jacobina Lineament, fluid inclusions, chlorite geothermometry, orogenic gold

1. Introduction

The mineral system concept refers to "all geological factors that control the generation and preservation of mineral deposits, and stress the processes that are involved in mobilizing ore components from a source, transporting and accumulating them in a more concentrated form and them preserving them throughout the subsequent geological history" (Wyborn et al., 1994). This concept recognizes that mineral deposits are the local expressions of much larger processes, resulting from focused mass and energy flows in certain regions of the crust (McCuaig et al., 2010). McCuaig and Hronsky (2014) described the interaction of critical elements, such as fertility, lithospheric architecture, geodynamic evolution plus the preservation of the deposit as the goal to exploration targeting. Thus, a mineral system description should refer to the trigger, or main geotectonic event, source of mineralized fluids, conduits for fluid flow, process that drive fluid flow, mechanisms that concentrate (throttle) and/or induce to precipitation of metals (trap), geochemical conditions that prevent dispersion of metals and process that preserves deposit. Vectorization of these elements into GIS platforms allows the elaboration of mineral prospectivity maps, which improves the effectiveness of exploration targeting (Hagemann et al., 2016).

The geological interest over the Serra de Jacobina region dates back to the 18th century with the discovery of gold in 1701 (Mascarenhas et al., 1998). The Au-U deposits in conglomerates of the Archean siliciclastic Jacobina Group are known worldwide for characteristics that allow correlating them with Witwatersrand-like paleoplacer deposits in South Africa (Bateman, 1958). From 1983 to 1998 Canavieiras, Itapicuru and João Belo mines produced 700,000 ounces of gold at an average recovered grade of 2.62 g/t. Early 2000's measured and indicated resources were 24.8 Mt grading 2.53 g/t Au (Pearson et al., 2005). Now, seven mines are under operation by Jacobina Mineração e Comércio JMC, Yamana Gold Inc. subsidiary, named Canavieiras Norte, Canavieiras Sul, João Belo, Morro do Vento Norte, Morro do Vento Sul, Basal and Lagartixa. Measured and indicated resources are 40.7 Mt grading 2.47 g/t Au (Yamana Annual Report, 2018).

In addition, Paleoproterozoic (ca. 1.9 Ga) epigenetic auriferous deposits in structurally-controlled quartz veins hosted by metaconglomerates, quartzites and schists from Jacobina Group and metaultramafic rocks from Vale do Coxo Suite, are exploited from artisanal gold mines, locally called *garimpos*, and occur along a 90-km-long N-S structural trend known as Bahia Gold Belt (Teixeira et al., 2001; Pearson et al., 2005).

Previous fluid inclusion studies in hydrothermal mineralization of Serra de Jacobina were performed by Carvalho (2001). The author used laser Raman microspectroscopy and microthermometric techniques in Au-bearing quartz veins from the Maravilha, Jaqueira and Goela da Ema *garimpos*, besides amethyst occurrences from the Coxo de Dentro *garimpo*. He also worked at the barren quartz veins and hydraulic breccia hosted by the Serra do Córrego metaconglomerate. The author identified fluid immiscibility between aqueous and aqueous carbonic fluids as the main mechanism for gold deposition in quartz veins and estimated 1.0-2.5kb and 200-350°C pressure and temperature conditions.

In this work, new data of composition and microthermometric determinations of fluid inclusions integrated to petrographic studies and microprobe analysis from Au-bearing quartz veins are presented. An effort at Maravilha and Jaqueira studies were performed as well as an expansion of the sampling towards the northern part of the mountain range at the Morro da Palmeirinha and Mina Velha *garimpos*.

These data allow a better understanding of the hydrothermal system that has generated the gold deposits. Regional works and local structural mapping, allied to geochronological data available, gives support to the interpretation.

2. Geological setting

2.1. Regional Geology

The Serra de Jacobina mountain range is located in the São Francisco Craton (Almeida, 1977) northeastern portion (Fig.1). The range is a physiographic feature that represents the Contendas-Mirante-Jacobina Lineament northern segment. This N-S lineament is located on the eastern border of the Gavião-Lençóis block and sets the boundary with the Jequié and Serrinha blocks (Sabaté et al., 1990). The lineament represents the result of the collision between these blocks which involved a series of crustal accretions that occurred between 2.2 and 1.8 Ga (Barbosa et al., 2003; Cruz et al., 2016). At the Serra de Jacobina, the lineament is parallel to the contact with the Itabuna-Savador-Curaçá Orogen (ISCO), which, according to Barbosa and Sabaté (2004), could be a fourth block reworked during the Paleoproterozoic collision. Santos et al. (2019 and references therein) named this Mairi Block.

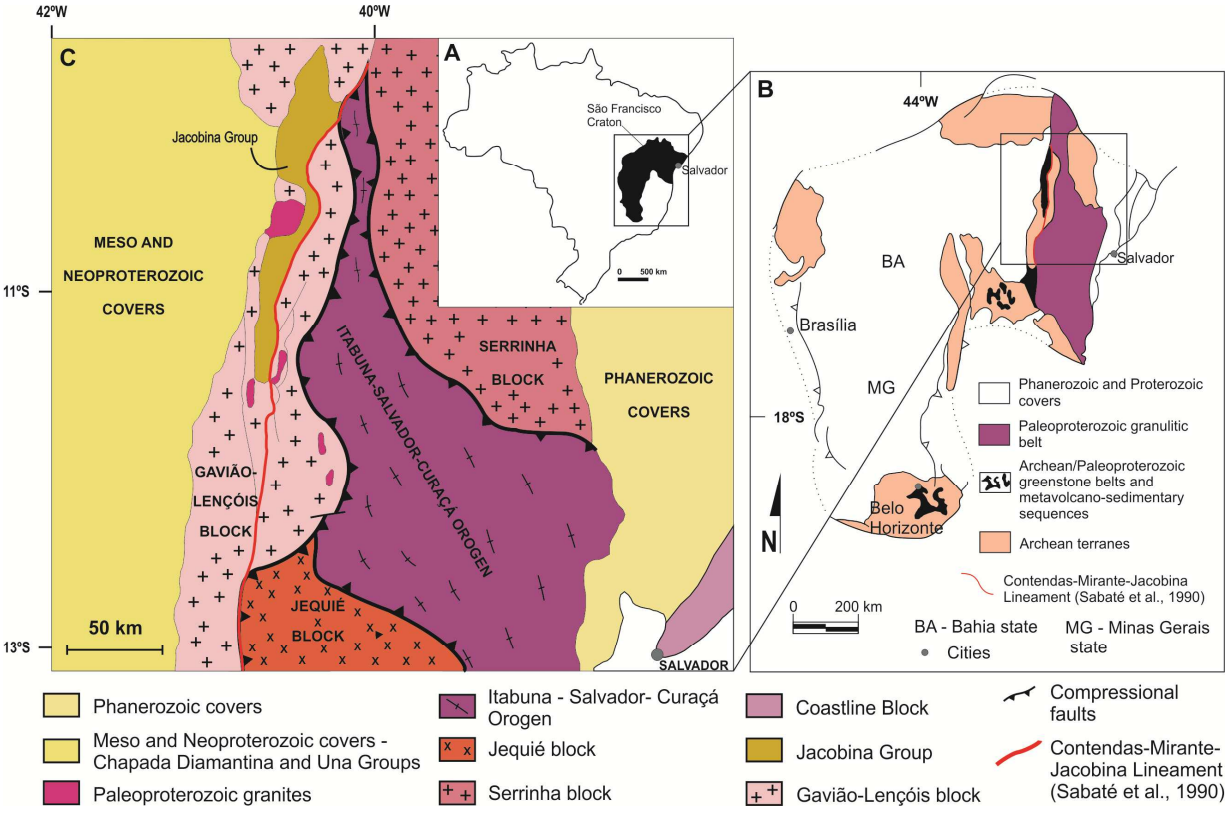

Fig. 1. São Francisco Craton (SFC) main features. (A) Geographic position relatively to Brazil limits. (B) Main geotectonic terranes with focus on the Contendas-Mirante-Jacobina Lineament highlighted by the black square. (C) SFC northeastern portion with Jacobina Group parallel to the Contendas-Mirante-Jacobina Lineament (red solid line highlighted). Modified from Santos et al. (2019 and references therein).

The Gavião-Lençóis Block consists mainly of tonalitic-trondhjemitic-granodioritic (TTG) orthogneisses and gneissic-amphibolitic associations, which are sometimes migmatized (Cruz et al., 2009). TTG massifs have zircons with ages between 3.4 and 3.1 Ga and Sm-Nd ages of 3.6 Ga (Martin et al., 1997; Santos-Pinto et al., 2012). It corresponds to Serra de Jacobina basement and named Mairi Complex at that region. It is characterized by the presence of mafic enclaves in the tonalitic-granodioritic orthogneisses and the occurrence of sporadic kinzigitic gneisses (Barbosa et al., 2012).

In terms of metasedimentary rocks, Leo et al. (1964) defined the Jacobina Group, suggesting their stratigraphic units. From bottom to top, the Group comprises the Serra do Córrego Formation metaconglomerates and quartzites, Rio do Ouro Formation quartzites with herringbone structures, Cruz das Almas Formation quartzites with schists intercalations and Fazenda Bananeira Formation quartzites, rhythmic schists, banded iron formations, manganesiferous schists and metacherts. Afterwards, several studies adopted different stratigraphic stackings and controversial interpretations, concerning the basin type and tectonic setting (e.g., rift basin: Mascarenhas et al., 1996 and Teles et al., 2015; foreland basin: Ledru et al., 1997; passive margin basin: Teixeira et al., 2001). Reis et al. (2018) reinterpret this lithological association as a rift basin with fluvial and shallow marine sedimentation, which evolves to a passive margin with mixed detrital and volcano-chemical sediments. Sulfur isotopic compositions of detrital pyrites from the auriferous Serra do Córrego metaconglomerate are similar to those proposed for the Witwatersrand deposits and indicates pre-GOE conditions for Jacobina Basin (Teles et al., 2020).

Serpentinized and talcified rocks occur parallel to the N-S Jacobina Group structure and were recently named Vale do Coxo Suite by Reis et al. (2019).

The Campo Formoso Mafic-Ultramafic Complex is mainly made up of serpentinized cumulate peridotites. The cumulate texture of the ultramafic rocks, rhythmic alternation of the sequence, and interlayered chromitites characterize it as a stratiform massif (Lord et al., 2004; Misi et al., 2012). Menezes et al. (2018) publish Sm-Nd whole rock model ages coupled with U-Pb (LA-ICPMS) zircon ages indicating a 3.2Ga for massif crystallization.

The Archean-Paleoproterozoic ISCO is composed of rocks metamorphosed at amphibolite- to granulite-facies conditions, including tonalite, charnockite with basic to ultrabasic enclaves, and supracrustal rocks (Barbosa and Sabaté, 2004).

The Caraíba Complex is composed of tonalites, granodiorites, trondhjemites and granites metamorphosed to granulite and/or upper amphibolite facies and is part of the the ISCO (Teixeira, 1997). U-Pb zircon ages from several methods give this complex ages ranging from 2.69 to 2.25 Ga (Silva et al., 1997; Silva et al., 2002; Oliveira et al., 2010).

The Saúde Complex is composed of aluminous, kinzigitic paragneisses, migmatites, quartzites, calcsilicate rocks, iron formations and mafic-ultramafic bodies, whose protolith were metamorphosed into the lower amphibolite facies (Leite et al., 2005). Zincone et al. (2017) presented ages ranging from 2.20 to 2.07 Ga and 2.68 to 2.50 Ga and interpreted this complex as part of a foreland basin developed during the Paleoproterozoic.

Granitoid suites at the northern portion of Contendas-Mirante-Jacobina Lineament, are mainly composed of muscovite-garnet peraluminous granites (Sabaté et al., 1990). Whole rock Rb-Sr ages range from 2.08 to 1.88 Ga. At Gavião-Lençóis block they intrude Jacobina Group, Vale do Coxo

metaultramafic rocks and Campo Formoso Mafic-Ultramafic Complex, while at ISCO, intrudes Saúde Complex (Barbosa et al., 2012 and references therein).

Subvertical intrusive mafic dikes with E-W orientation occur along the Serra de Jacobina. They are composed of gabbro and diorite, and locally diabase (Couto et al., 1978; Reis et al., 2019).

Mesoproterozoic and Neoproterozoic units that occur west of Serra de Jacobina comprise the Espinhaço and São Francisco Supergroups, respectively. Espinhaço is composed of metasedimentary and metavolcanic rocks and São Francisco by carbonate (mainly) and siliciclastic lithofacies (Guimarães et al., 2012).

In terms of lithospheric architecture two recent works have investigated the northern portion São Francisco Craton structural framework, using deep-probing geophysical survey (Fig.2). Padilha et al. (2019) carried out, east-west direction magnetotelluric (MT) profile that crosscut the Serra de Jacobina. They identified a conductive zone that extends from the upper crust to the mantle and is coincident with the superficial trace of the Contendas-Mirante-Jacobina Lineament. Santos et al. (2019) performed an east-west, terrestrial gravimetric profile and their modelling indicates a transcrustal structure that separates two blocks: Gavião-Lençóis to the west and Mairi to east. This structure is coincident with Pindobaçu Fault System superficial trace, which represents the Contendas-Mirante-Jacobina Lineament northern portion. Their model also showed that Jacobina and Maravilha fault systems are shallow structures restricted to the upper crust. Ledru et al. (1997) using $^{40}Ar/^{39}Ar$ ages of micas hosted by these fault systems, indicates 1918 Ma for the Jacobina fault system and 1988 to 1938 Ma for Maravilha fault system.

3. Gold mineralization at Serra de Jacobina

The most important auriferous deposit at Serra de Jacobina mountain range is hosted by quartz-pebble metaconglomerates from the Serra do Córrego formation. There are two mineralized layers, upper and lower metaconglomerates, separated by a quartzite layer. The metaconglomerate is oligomictic dominated by rounded quartz pebble, but also composed of green quartzite, chert and arkose pebbles. Gold occurs as free particles in the conglomerate matrix, filling fractures and also within sulfides (Teixeira et al., 2001). There are also deposits (locally called *garimpos*), composed of structurally-controlled Au-bearing quartz veins hosted by quartzites, conglomerates and schists from the Jacobina Group and metaultramafic rocks from Vale do Coxo Suite (Teixeira et al., 2001; Pearson et al., 2005).

Some models concerning the origin of the Au-U mineralization hosted by the Serra do Córrego Formation metaconglomerates have been proposed: Bateman (1958) suggested a sedimentary origin (paleoplacer model), Gross (1968) indicated a modified sedimentary origin (modified paleoplacer), while White (1961) and Cox (1967) argued for an epigenetic origin for the mineralization. Milesi et al. (2002) presented the “hydrothermal shear-reservoir” model, in which they admit an epigenetic gold enrichment related to shear zones but without highlighting a possible primary sedimentary origin associated with the metaconglomerates. Teixeira et al. (2001) and Pearson et al. (2005) indicate structural shear zones and reefs intense sericitization and sulfidation from orogenic origin. Teixeira et al. (2010) related metaconglomerates mineralizations to Paleoproterozoic collision and Teixeira et al. (2019) use these orogenic features on their new reconstruction hypothesis for São Francisco Craton.

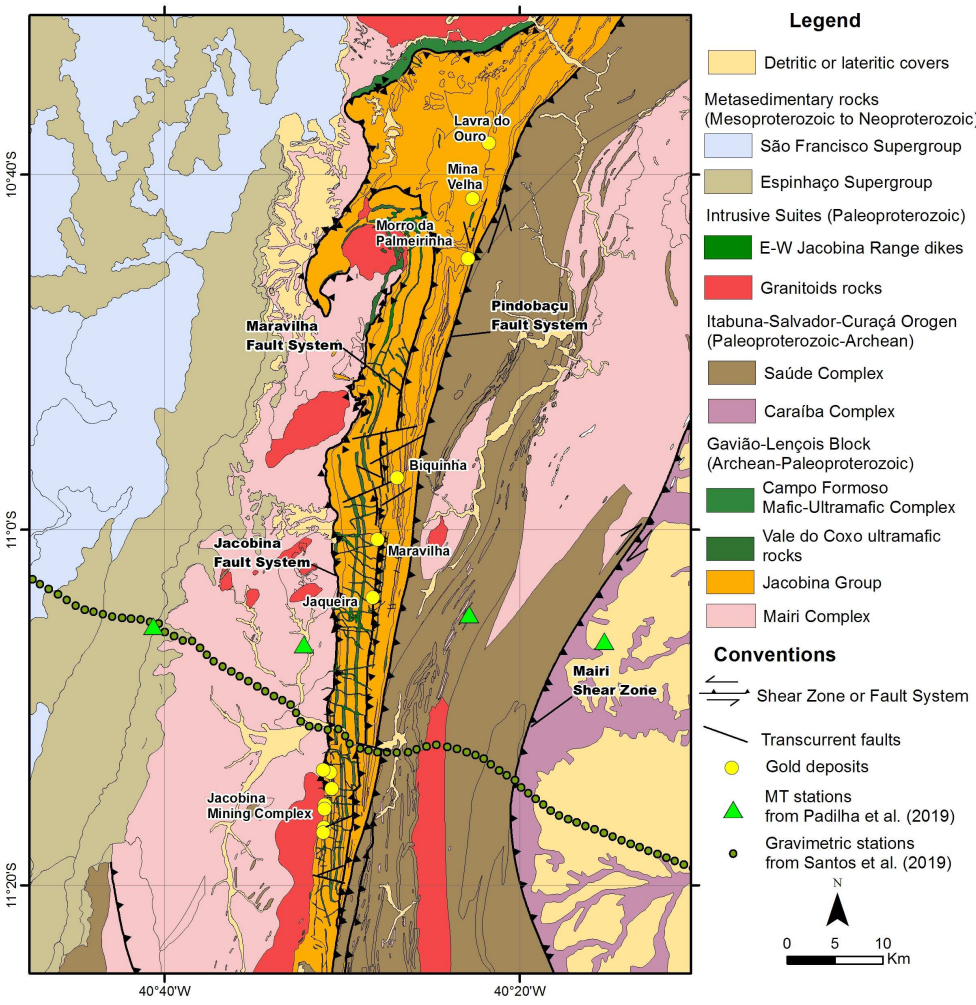

Fig. 2. Serra de Jacobina simplified geological map. Modified from Reis et al. (2019).

In this work we focused on structurally-controlled Au-bearing quartz veins hosted by quartzites of the Jacobina Group, and meta-ultramafic rocks of the Vale do Coxo Suite. Four *garimpos* were mapped: Maravilha, Jaqueira, Morro da Palmeirinha and Mina Velha (Fig.2).

3.1. Host Rocks

For the Jacobina Group we adopted the classic stratigraphic proposition from Leo et al. (1964) recently revised by Reis et al. (2019).

3.1.1. Jacobina Group

At Maravilha (Fig.3A) and Jaqueira (Fig.3B) *garimpos* host rocks from the Jacobina Group are hanging-wall quartzites from the Rio do Ouro Formation. They exhibit white to greenish color together with asymmetric ripple marks. Petrography reveals anhedral, fine-to-medium, and equidimensional quartz crystals.

Both at Morro da Palmeirinha (Fig.4A) and Mina Velha (Fig.4B) host quartzites are from Cruz das Almas Formation. At Morro da Palmeirinha they occur like hanging- and foot-wall host rocks. It consists of fine-to-medium quartzites, which have grey to white color, and herringbone structures, that grade to medium-to-coarse green quartzites, with ripple marks. At Mina Velha they occur like foot-wall quartzites. They have green color with herringbone structure and cross-bedding stratification. Under the microscope, some preserved sedimentary characteristics were observed, with rounded to subrounded quartz grains ranging in size from 0.5 to 3.7 mm and forming stratification.

3.1.2. Vale do Coxo Suite

Vale do Coxo host rocks at Maravilha and Jaqueira *garimpos* occurs like a foot-wall biotite-schist. It is a strongly weathered greenish rock, mainly composed of biotite, sericite, chlorite and quartz. Biotite has brown to pale brown pleochroism and defines a penetrative foliation. At Mina Velha they occur like a hanging-wall chlorite-schist. It is also a strongly weathered rock with green to red colors. It is mainly composed of chlorite, sericite and quartz. Chlorite has green to pale green pleochroism and defines mylonitic foliation. At Morro da Palmeirinha some exploited veins are hosted between quartzites and green phyllonites interpreted as Vale do Coxo rocks intensely deformed. Its penetrative foliation is defined by interlayered sheets of sericite, chlorite and quartz ribbons.

3.2. Structures and quartz veins

3.2.1. Maravilha Fault System

The Maravilha Fault System is the first-order structure which hosts the Maravilha and Jaqueira *garimpos*. The system has an N-S-striking main thrust fault dipping 80° to east.

The metasedimentary layers have an N-S-direction at both *garimpos*, dipping 83° to the west at Maravilha and between 62 and 68° to the east at Jaqueira.

The Maravilha *garimpo* quartz vein is hosted by a second-order, N-S-striking thrust fault, dipping 75° to the west that crosscuts metasedimentary layers. The vein is 1.5 m thick and is composed of smoky quartz, sericite, pyrite and gold (Fig.5 A-B).

At Jaqueira the quartz veins are hosted by a second-order thrust fault NW-SE, dipping between 75 and 80° to the southwest. This fault also intercepts metasedimentary layers. The veins show > 50 cm in thickness and are composed of smoky quartz, sericite and pyrite (Fig.5 C-D).

3.2.2. Pindobaçu Fault System

The Pindobaçu Fault System (PFS) is the first-order structure which hosts Morro da Palmeirinha and Mina Velha *garimpos*.

At Morro da Palmeirinha the PFS has N-S-striking main thrust fault dipping 60° to 80° to the east. The metasedimentary layers have N-S-direction, dipping 70° to 80° to the east. The quartz veins are hosted by second-order thrust fault, oriented to N-S, and dipping 63-70° to the east that crosscut metasedimentary layers. The veins are mostly narrow, 10 to 50 cm thick, and are mostly composed of smoky quartz, sericite and pyrite (Fig.5 E-F).

At Mina Velha the PFS has NE-SW-striking main thrust fault dipping 60° - 80° to the southeast. Metasedimentary layers dip 5° to NNW-SSE. The veins are hosted by a second-order, NNE-SSW thrust fault, which dips 63° to the southeast that intercepts metasedimentary layers. The veins are mostly narrow with 10 to 30 centimeters thickness, usually composed of massive pyrite and smoky quartz (Fig.5 G-H).

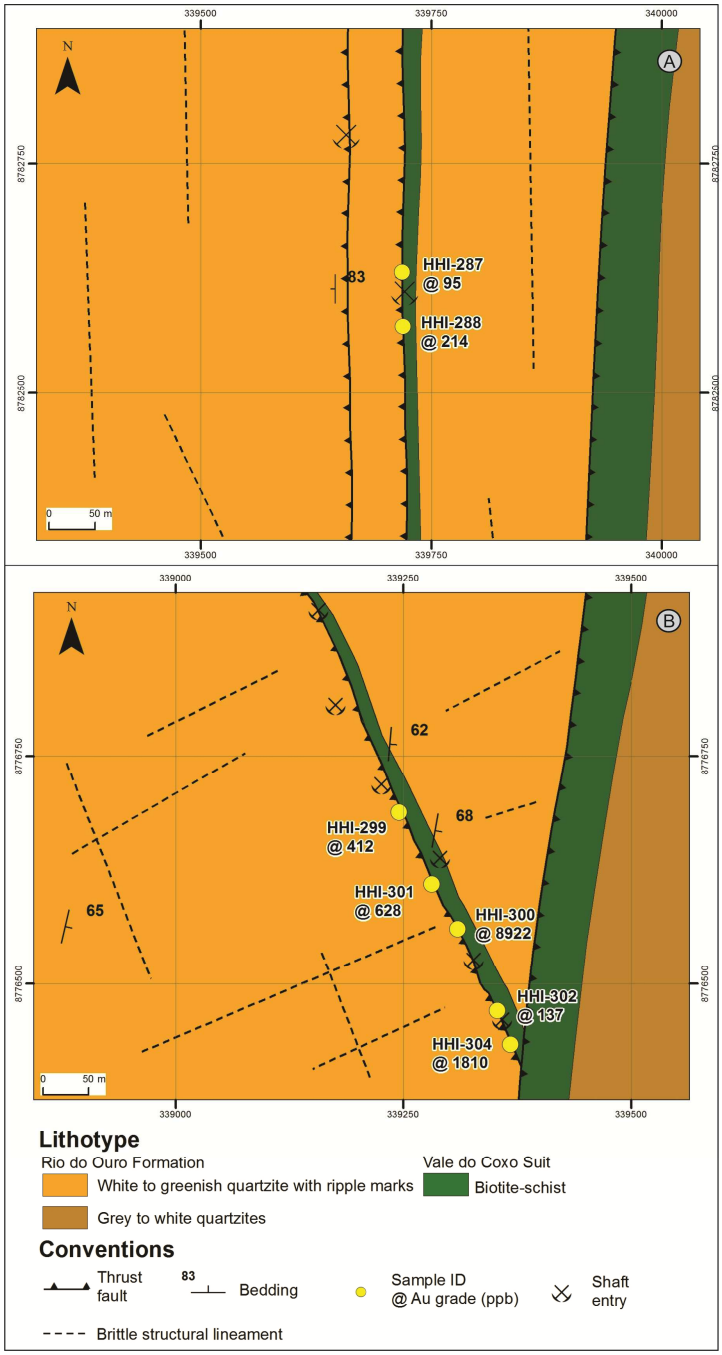

Fig. 3. Simplified geological map from (A) Maravilha and (B) Jaqueira *garimpos*.

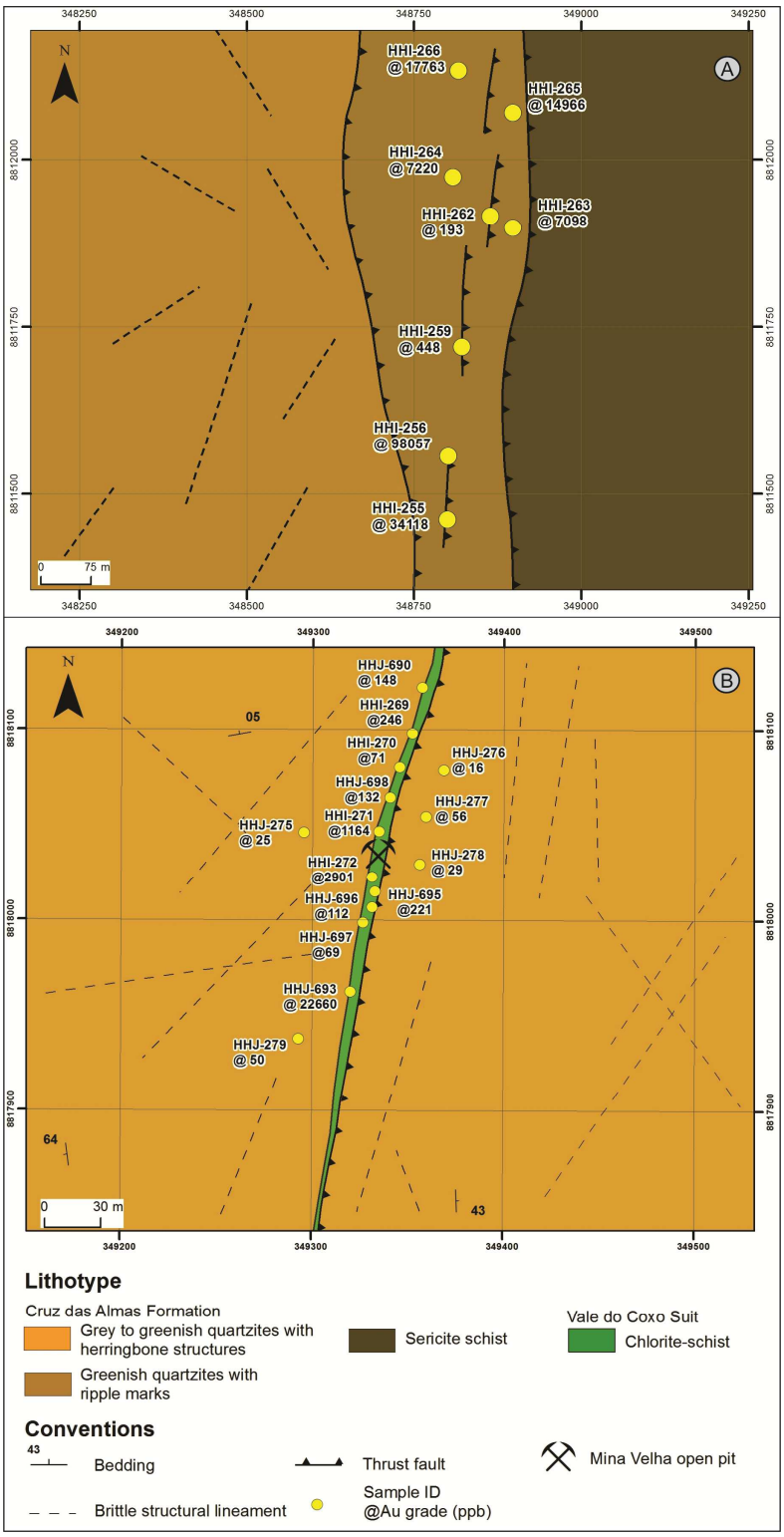

Fig. 4. Simplified geological map from the (A) Morro da Palmeirinha and (B) Mina Velha *garimpos.*

Fig. 5. Quartz veins features from Maravilha. (A) General view from underground artisanal shaft. (B) Visible gold, right side of the pencil. Quartz veins features from Jaqueira. (C) Narrow quartz vein, yellow highlighted, hosted by hanging-wall quartzite and foot-wall schist. (D) Detail of massive pyrite within quartz vein. Quartz veins features from Morro da Palmeirinha. (E) Narrow quartz vein, yellow highlighted, hosted by quartzite. (F) Detail on smoky quartz vein. Quartz veins features from Mina Velha. (G) Narrow quartz vein, yellow highlighted, hosted by hanging-wall chlorite-schist and foot-wall quartzite. (H) Detail of massive pyrite vein with smoky quartz.

3.3. Hydrothermal Alteration and Gold Mineralization

3.3.1. Petrography

3.3.1.1 Jacobina Group

Optical microscopy analyses of hanging-wall quartzites from the Rio do Ouro Formation at Maravilha and Jaqueira *garimpos* reveals anhedral, fine- to medium-grained, recrystallized quartz crystals. Sericite occurs between quartz crystals, usually accompanied by fine grained, anhedral to subhedral, tourmaline crystals.

At Morro da Palmeirinha, Cruz das Almas Formation hanging- and foot-wall quartzites, the petrographic study shows that quartz is anhedral with wavy extinction. Sericite occurs in two forms: as very fine-grained crystals between quartz; as subhedral crystals when filling fractures. Subhedral to anhedral tourmaline crystals are usually spatially related to both sericitic assemblages (Fig.6 A). Pyrite occurs in two forms: as subhedral to euhedral crystals when spatially related to filling-fracture sericite + tourmaline assemblage; subhedral to euhedral disseminated between quartz crystals. Gold occur spatially related to filling-fracture type sericite + pyrite + tourmaline assemblage.

At Mina Velha, Cruz das Almas Formation, the foot-wall quartzites show rounded to subrounded quartz crystals with wavy extinction. Sericitic assemblage occurs like crenulated ribbons between quartz stratification (Fig.6 B), with tourmaline, pyrite and ilmenite frequently associated. Anhedral to subhedral tourmaline crystals are spatially related to sericitic ribbons. Pyrite occurs in two forms: i) rounded to subrounded with quartz grains stratifications, ii) euhedral to subhedral, when related to sericitic ribbons. In one sample it was possible to observe gold in the contact between crenulated sericitic ribbons and subrounded pyrite (Fig.6 C-D).

3.3.1.2 Vale do Coxo Suite

The foot-wall biotite-schist at Maravilha and Jaqueira is mainly composed of biotite, sericite, chlorite, quartz and gold. The biotite has brown to pale brown pleochroism and defines a penetrative foliation. Chlorite and sericite replace biotite (Fig.7 A-B). Sericite is probably fuchsite. Chlorite has green to pale green pleochroism and blue to purple birefringence. It is frequently spatially related to sericite and pyrite. Fine-grained tourmaline crystals usually occur spatially related to sericite and chlorite. Quartz occurs as ribbons parallel to the main foliation and usually has wavy extinction (Fig.7 C-D). Pyrite and chalcopyrite are anhedral to subhedral and occur spatially related to chlorite. Gold crystals occur spatially related to the chlorite + pyrite assemblage.

Both host meta-ultramafic phyllonite from Morro da Palmeirinha and Mina Velha hanging-wall chlorite-schist share similar mineralogy. They are mainly composed of chlorite, sericite and quartz. Chlorite has green to pale green pleochroism, grey birefringence and is spatially related to sericite and rutile assemblage. It also occurs spatially related to pyrite + chalcopyrite assemblage and locally is replaced by talc. Sericite occurs subordinated to chlorite. Quartz occurs as ribbons parallel to mylonitic foliation and usually has wavy extinction. Pyrite and chalcopyrite are anhedral to subhedral and occurs spatially related to chlorite. Ilmenite is frequently altered to leucoxene.

3.3.1.3 Quartz veins

The petrographic analysis of quartz veins from both Maravilha and Jaqueira *garimpos* is quite similar. Quartz is anhedral with wavy extinction. Sericite occurs as very fine-grained crystals between quartz. Chlorite is subhedral to anhedral and usually is filling fractures (Fig.8 A-B) and the crystals have green to pale green and pale grey pleochroism. They are usually spatially related to rutile, ilmenite and/or leucoxene, and pyrite. Subhedral to anhedral tourmaline occurs disseminated between quartz crystals and anhedral when filling fractures. Pyrite is euhedral when disseminated between quartz crystals and anhedral when filling fractures. Chalcopyrite is anhedral and spatially related to filling-fracture type pyrite. Ilmenite and leucoxene are usually filling fractures spatially related to chlorite. Gold occurs as isolated crystals between quartz and spatially related to the filling fractures chlorite + pyrite + tourmaline assemblage.

In the veins of the Morro da Palmeirinha *garimpo* quartz is anhedral with wavy extinction. Sericite is anhedral when filling fractures and usually spatially related to tourmaline. Besides spatially related to sericite, tourmaline occurs as subhedral to euhedral crystals disseminated between quartz, with colorless to pale green pleochroism. The rutile crystals are isolated or spatially related to tourmaline and pyrite, frequently altered to leucoxene. Pyrite is euhedral to subhedral and usually is related to chalcopyrite and/or chalcocite/covellite. A massive pyrite + chalcopyrite assemblage occurs as filling fractures in some veins. Gold occurs as: i) isolated crystals between quartz, ii) included and/or spatially related to filling fracture sericite + tourmaline assemblage (Fig.8 C-D), iii) included and/or spatially related to disseminated subhedral to euhedral tourmaline (Fig.8 E-F), iv) spatially related to pyrite + rutile assemblage.

The petrographic analysis of quartz veins from the Mina Velha *garimpo* exhibit anhedral quartz with wavy extinction. Sericites are in very fine grained crystals between quartz and subhedral to anhedral when filling fractures. Subhedral to anhedral tourmaline is usually spatially related to sericite. Tourmaline also occurs as subhedral to euhedral crystals when disseminated between quartz crystals. Rutile is anhedral, spatially related to anhedral sericite + tourmaline assemblage, frequently altered to ilmenite and/or leucoxene. Pyrite is the main sulfide. It is anhedral to subhedral and is filling fractures or disseminated between quartz crystals. Chalcopyrite occurs subordinated to, and sometimes included in pyrite.

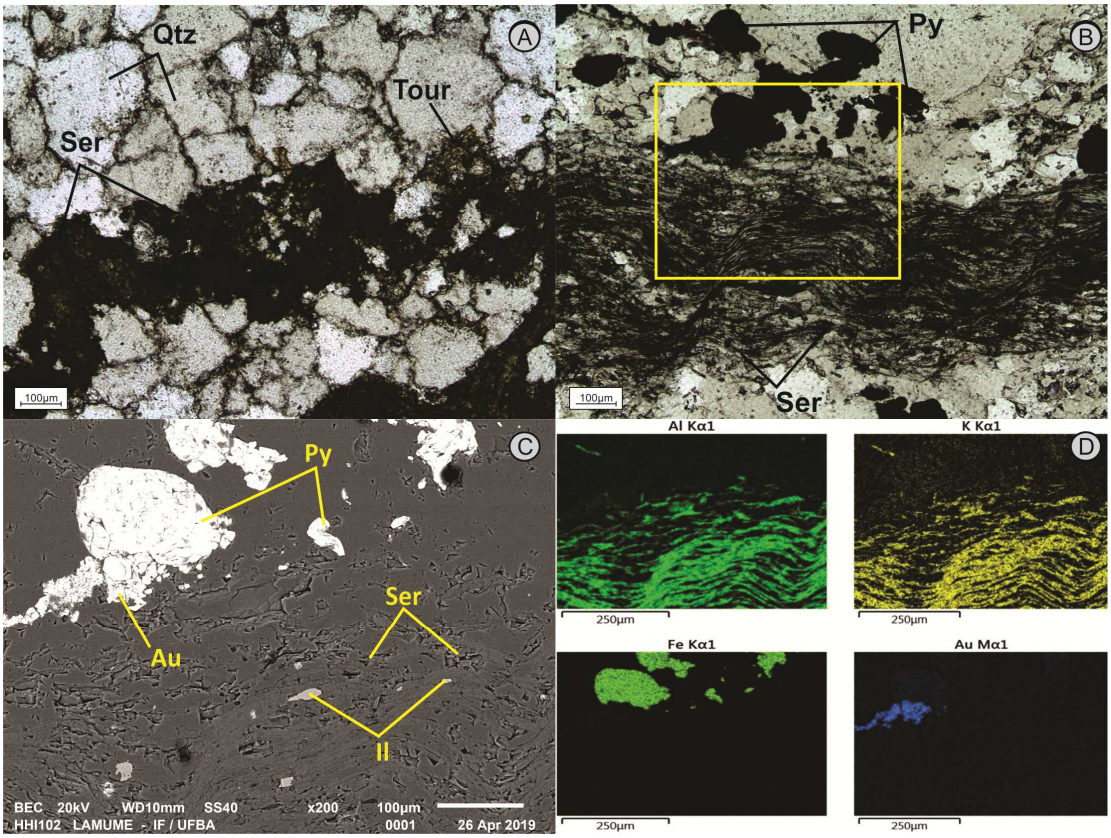

Fig. 6. Jacobina Group features. (A) Sericite + tourmaline assemblage filling-fracture type in quartzite. (B) Photomicrography showing crenulated sericite and subrounded pyrites. Yellow box indicates SEM images from (C) and (D). (C) BSE image with gold crystal between sericitic ribbon and pyrite. (D) SEM EDS element mapping. Mineral abbreviations: Au: gold, Il: ilmenite, Ser: sericite, Py: pyrite, Tour: tourmaline, Qtz: quartz.

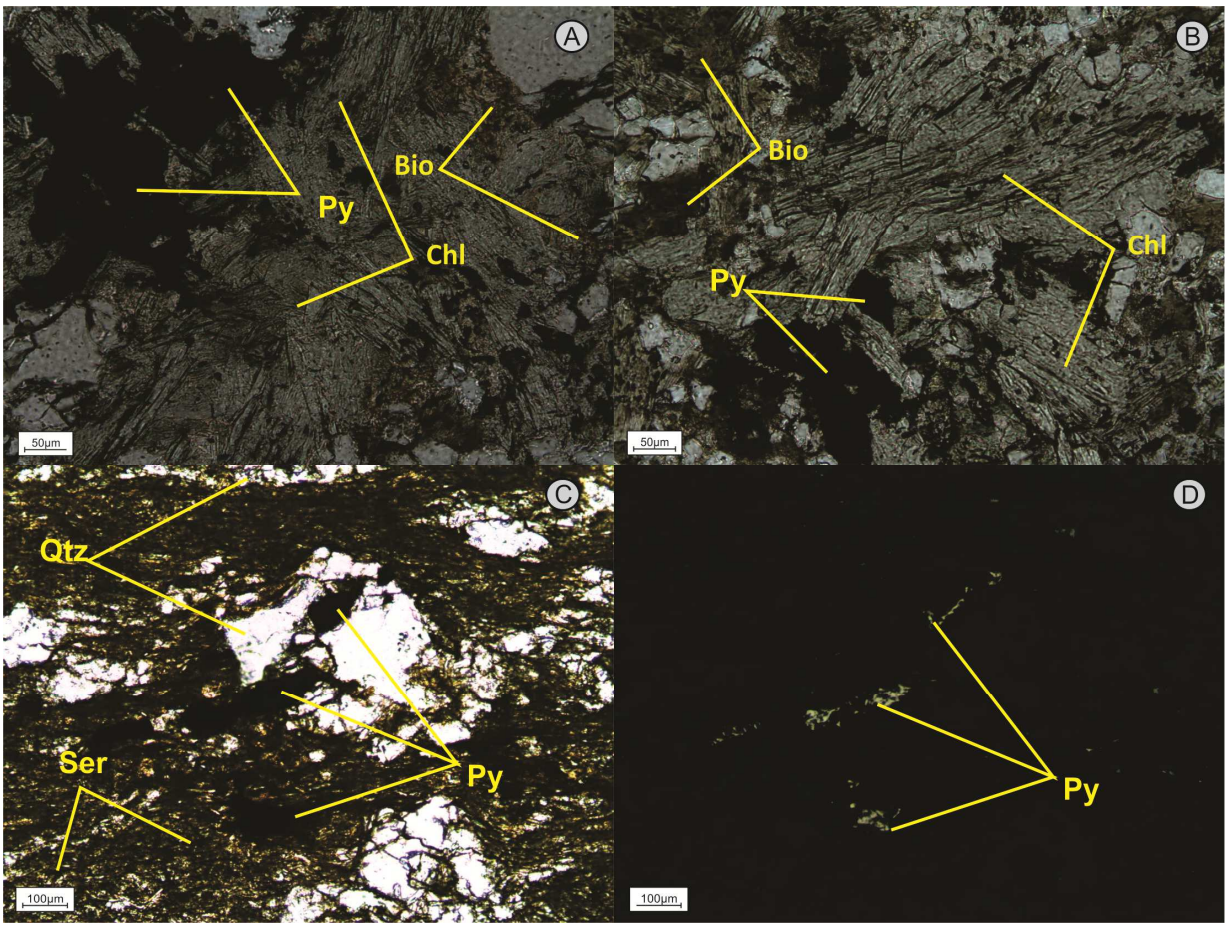

Fig. 7. Vale do Coxo Suite features. (A-B) Photomicrograph showing chlorite replacing biotite. (C-D) Photomicrography showing quartz and pyrite crystals parallel to main foliation. Mineral abbreviations: Qtz: quartz, Chl: chlorite, Py: pyrite, Bio: biotite, Ser: sericite.

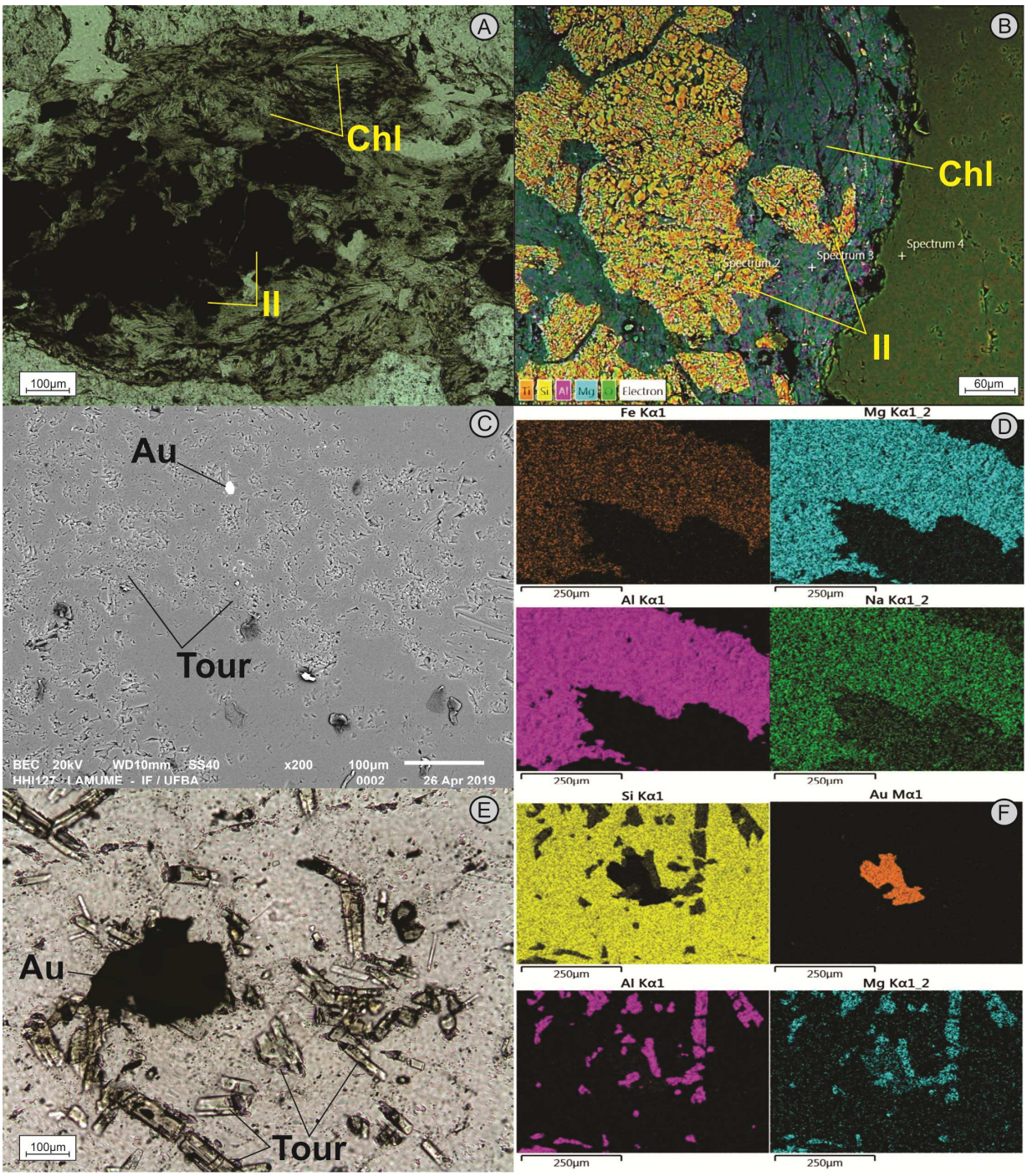

Fig. 8. Quartz veins features. (A) Photomicrograph of chlorite + ilmenite assemblage. (B) SEM EDS layered image of chlorite + ilmenite assemblage. (C) SEM BSE image showing gold included in anhedral tourmaline. (D) SEM EDS element mapping from SEM BSE image C. (E) Subhedral tourmaline spatially related to gold. (F) SEM EDS element mapping showing gold crystal and tourmaline from photomicrograph E. Mineral abbreviations: Chl: chlorite, Il: ilmenite, Au: gold, Tour: tourmaline.

The Figure 9 shows our proposal of paragenetic succession. Because the assemblages from both quartz vein and host rocks are relatively simple, we believe the proposed timing is reasonable. During the pre-ore stage the host rock mineralogy is represented by the biotite from Vale do Coxo Suite and rounded to subrounded quartz and pyrite crystals from Jacobina Group. During the ore stage biotite was replaced by sericite and chlorite in the host rock from Vale do Coxo Suite. The filling-fracture assemblage sericite + chlorite + tourmaline + gold were precipitated in the quartz veins. The sulfides from the ore stage were pyrite and chalcopyrite, and the oxides were rutile and ilmenite. During the post-ore stage the assemblage sericte + chlorite has finished precipitation and in only one sample chlorite was replaced by talc. Tourmaline also occurs during this final stage. The rutile and ilmenite are altered to leucoxene and chalcopyrite is altered to covellite and chalcocite.

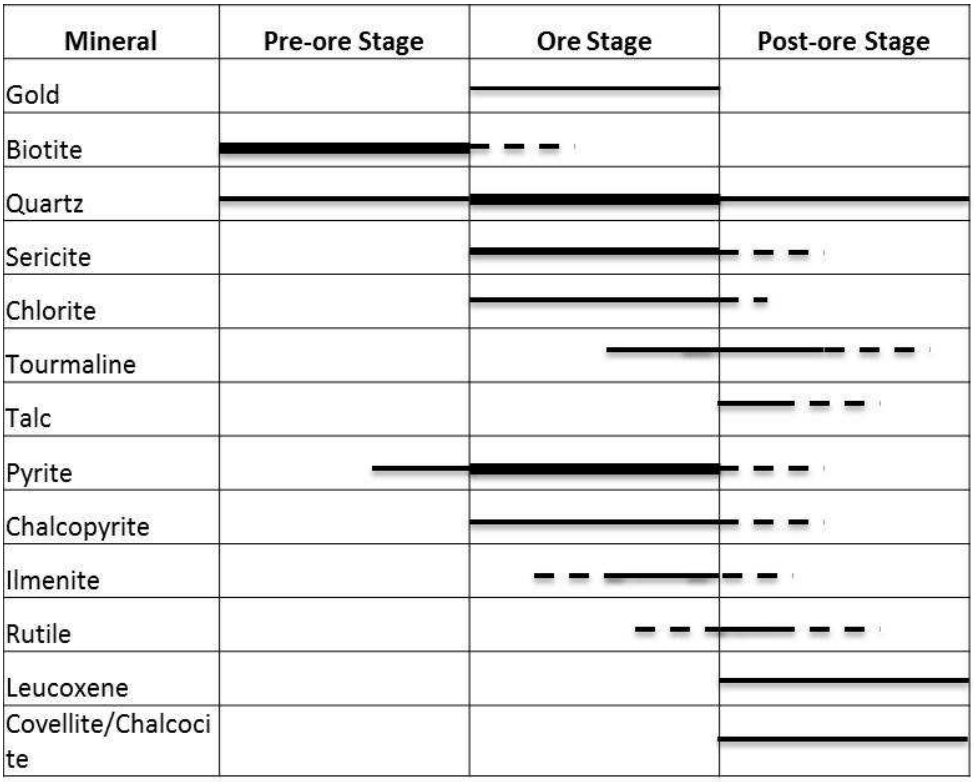

Fig. 9. Evolution of the ore and gangue mineralogy schematic representation. Line thickness denotes relative mineral abundance.

3.3.2. Sericitic Alteration

In the quartzites from the Jacobina Group, sericitic assemblage is represented by mica + chlorite and occurs in two different types. It is widespread disseminated between quartz crystals and also occurs like anhedral crystals in a fissure-filling type.

In the meta-ultramafic rocks from the Vale do Coxo Suite sericitic alteration is pervasive with sericite replacing biotite. It tends to be more intense nearby mineralized veins, but this is not a rule. Locally argillic alteration has occurred. It is selectively with talc replacing chlorite and observed in one sample.

In quartz veins, sericitic alteration occurs in two types. A fissure-filling type when anhedral crystals are filling fractures; a second non-pervasive type, when assemblage is widely disseminated between quartz crystals.

3.3.3. Sulfidation

In the Jacobina Group quartzites sulfidation is represented by the assemblage pyrite + chalcopyrite. The minerals occur like subhedral to euhedral crystals subordinated to sericitic fissure-filling type alteration. It is also represented by subhedral to euhedral, disseminated pyrite between quartz crystals.

In the schists from the Vale do Coxo Suite sulfidation is selectively with pyrite + chalcopyrite assemblage subordinated to sericitic alteration.

In quartz veins sulfidation occurs in two types: disseminated, subhedral to euhedral pyrite + chalcopyrite assemblage subordinated to sericitic alteration; and massive pyrite veins.

4. Analytical procedures

4.1. Scanning Electron Microscopy (SEM)

Eight samples were investigated by SEM analyses. It carried out at Laboratório Multiusuário de Microscopia Eletrônica (LAMUME) of the Universidade Federal da Bahia, Brazil. A JEOL JSM 6610LV SEM operating at 20kV accelerating voltage was used to identify minerals, providing semi-quantitative geochemical measurements, backscattered electrons (BSE) images and energy dispersion spectroscopy (EDS) maps.

4.2. Whole Rock Geochemistry

A total of 30 samples were analyzed for their geochemical composition with the following distribution: nine samples were used to investigate Jacobina Group quartzites at the Morro da Palmeirinha (n = 4) and Mina Velha (n = 5) *garimpos*; eight samples were analyzed for the Vale do Coxo Suite composition at Mina Velha; thirteen quartz veins samples from Maravilha (n = 2), Jaqueira (n = 5), Morro da Palmeirinha (n = 4) and Mina Velha (n = 2). Analysis of whole rock major and trace elements were performed at the SGS Geosol Laboratory, Vespasiano unit, Brazil. The samples were washed, dried to 105°C, crushed to 3mm in crusher machine, homogenized, quartered, crushed to 150 meshes in agate ball mill 95% and melted with lithium metaborate. Major elements were determinate by X-ray fluorescence spectrometry and trace elements by Inductively Coupled Plasma Mass Spectroscopy (ICP-MS) method. The Au, Pd and Pt were detected by the Inductively Coupled Plasma Absorption Emission Spectroscopy (ICP-AES) method. The LOI was calculated by weight difference after 1000°C heating.

4.3. Fluid Inclusion Analyses

Eight samples of Au-bearing quartz veins have been collected on surface exposures and underground artisanal shafts and prepared for fluid inclusion (FI) analyses. The double-polished thin sections were examined under the petrographic microscope to characterize the distribution, size, types and textural relationships and to establish the fluid inclusion assemblages (FIA). Microthermometric measurements were performed at the Fluid Inclusion Laboratory of the Geoscience Institute, Universidade Federal da Bahia, Brazil. A THMS-600 heating-freezing stage coupled to a petrographic microscope Olympus, BX60 model was used. The equipment was previously calibrated with synthetic standards including pure CO_2 (-56.6 °C) and water (0.0°C). General heating-freezing rate was 1-5 °C/min, reduced to 0.5-1 °C/min close to periods of phase transitions and accuracy is estimated at +/- 0.1°C. Measurements properties include temperatures of final melting of CO_2 ($TmCO_2$), final melting of clathrate (Tm cla), halite dissolution (Tm halite), partial homogenization of CO_2 (Th CO_2), final melting of ice (Tm ice) and final homogenization (Tht). Other abbreviations used here include L and V, for liquid and vapor phases respectively. Estimation of volume fractions of liquid and vapor phases were performed according to Bakker and Diamond (2006). Chemical properties were calculated using the Flincor computer software (Brown, 1989). For salinity and bulk density from H_2O-NaCl inclusions we used equations of state from Brown and Lamb (1989). For halite-bearing H_2O-NaCl inclusions salinities were obtained from dissolution temperatures of halite (Roedder, 1984). For H_2O-CO_2-NaCl salinities, CO_2 and bulk densities we used the final melting temperature of clathrate as recommended by Collins (1979) using equations of state from Bowers and Helgeson (1983). The salinities are expressed as wt. % NaCl equivalent (wt. % NaCl eq.) and densities as grams per cubic centimeter (g/cm^3).

4.4. Electron Microprobe Analysis

Electron Microprobe Analysis (EMPA) were performed using a JEOL JXA-8230 superprobe, equipped with five wavelength dispersive spectrometers (WDS), at the Microscopy and Microanalysis Laboratory (LMic) of the Department of Geology, Universidade Federal de Ouro Preto, Brazil. The JEOL EMPA software Ver3.0.1.16 package was used to perform the calibration, overlap correction and quantification. Operating conditions were 15kV accelerating voltage, 20nA beam current and 2 µm beam diameter. The work distance on EMPA is fixed at 11 mm with no variation during the analysis. Counting time for Ba, Ni, Cr and Sr was set at 30s at peak and 15s at background; while Na, F, Si, Al, Mg, Fe, Cl, P, Ti, Ca, K, Mn was set at 10s at peak and 5s at background. The major spectral interferences were corrected during the standard analysis and during the quantification. Lα X-ray was used for Ba and Sr while Kα X-ray was used for Na, F, Si, Al, Mg, Fe, Cl, Ni, P, Cr, Ti, Ca, K, Mn. The standard deviation to each element was: Na (1.01%), F (1.12%), Si (0.3%), Al (0.51%), Mg (0.47%), Ba (0.34%), Fe (0.43%), Cl (1.74%), Cr (0.26%), Ni (0.72%), P (0.87%), Sr (1.31%), Ti (0.21%), Ca (0.19%), K (0.5%), Mn (0.41%).

5. Whole rock geochemistry results

In this section are presented only the main elements composition ranges. The whole rock geochemistry complete results are listed in Supplementary Table 1. Major elements results are presented in weight percent (wt. %), trace and rare earth elements (REE) in parts per million (ppm), Au, Pd and Pt in parts per billion (ppb).

5.1. Jacobina Group geochemical composition and REE pattern

Most of the samples of quartzites from the Jacobina Group at Morro da Palmeirinha and Mina Velha *garimpos* share similar major elements, which are mainly SiO_2 (85.20-95.50), with minor Al_2O_3 (2.01-9.08), Fe_2O_3 (1.50-4.41), TiO_2 (0.13-0.63) and K_2O (0.01-0.61). The exception was a pyrite-rich quartzite sample from Morro da Palmeirinha with lower SiO_2 (66.40), higher Al_2O_3 (14.40) and Fe_2O_3 (8.26) than the rest of the samples. Considering the trace elements, it is worth mentioning the abundance of Cr (68-329), Cu (9.6-57.3) and Ni (10.1-70.8) in the analyzed samples. The main geochemical difference between the quartzites is the gold content. At the Morro da Palmeirinha *garimpo* the gold grades are higher (7098-17763) than those from Mina Velha (16-56).

The total rare earth elements concentration (ΣREE) of the quartzite samples ranges from 176 to 1283 ppm, with $(La/Yb)_N$ values from 5 to 37, showing enrichment of light rare earth elements (115-947) relatively to heavy earth elements (43-336). All samples presented slightly negative Eu anomaly which ranges from 0.57 to 0.77.

5.2. Vale do Coxo Suite geochemical composition and REE pattern

The biotite schist samples from Vale do Coxo Suite are mainly composed of SiO_2 (45.10-57.90), Fe_2O_3 (14.90-21.40), Al_2O_3 (10.70-14.80), MgO (6.16-13.7) and minor TiO_2 (0.34-0.56) and K_2O (0.04-0.74). Considering the trace elements, the results reveal high contents of Co (41-138), Cr (201-585), Cu (98-873), Ni (157-279) and V (124-198). The gold grades range from 69 to 2901 ppb.

The total rare earth elements concentration (ΣREE) of the biotite schist samples ranges from 108 to 177 ppm, with $(La/Yb)_N$ values from 1 to 5, showing slightly enrichment of light rare earth elements (52-95 ppm) relatively to heavy earth elements (41-81 ppm). All samples presented weak negative Eu anomaly which ranges from 0.63 to 0.84.

5.3. Quartz veins geochemical composition and REE pattern

The quartz veins samples from the Maravilha, Jaqueira and Morro da Palmeirinha *garimpos* share similar major elements, which are mainly SiO_2 (93.90-99.00), with minor Fe_2O_3 (0.78-3.83), Al_2O_3 (0.07-1.66) and TiO_2 (0.02-0.32). On the other side, massive pyrite quartz veins samples from Mina Velha showed lower SiO_2 (16.50-58.10) and higher Fe_2O_3 (21.60-52.30) contents relatively to the other *garimpos*, with minor amounts of Al_2O_3 (0.52-4.41), MgO (0.23-3.95) and TiO_2 (0.02-0.14). Considering the trace elements, the Co (0.9-25.9), Cr (3-47), Cu (7.7-50.1), Mo (0.21-2.27), Ni (2.3-85.3) and V (1-24) contents from samples of the Maravilha, Jaqueira and Morro da Palmeirinha *garimpos* are lower than those from Mina Velha which are Co (338-833.5), Cr (8-83), Cu (177.3-895.8), Mo (6.56-8.18), Ni (794-2159.6) and V (10-60). The gold grades ranges from 95 to 214 ppb at Maravilha, 137 to 8922 ppb at Jaqueira, 193 to 98057 ppb at Morro da Palmeirinha and from 148 to 22660 ppb at the Mina Velha *garimpo*.

In terms of rare earth elements, the four *garimpos* have similar concentration. The total concentration (ΣREE) ranges from 38 to 145 ppm, with $(La/Yb)_N$ values from 4 to 58, showing enrichment of light rare earth elements (28-112) relatively to heavy earth elements (9-46). The samples from Jaqueira, Morro da Palmeirinha and Mina Velha presented weak negative Eu anomaly which ranges from 0.42 to 0.94, while the two samples from Maravilha showed no Eu anomaly with values of 0.98 and 1.09.

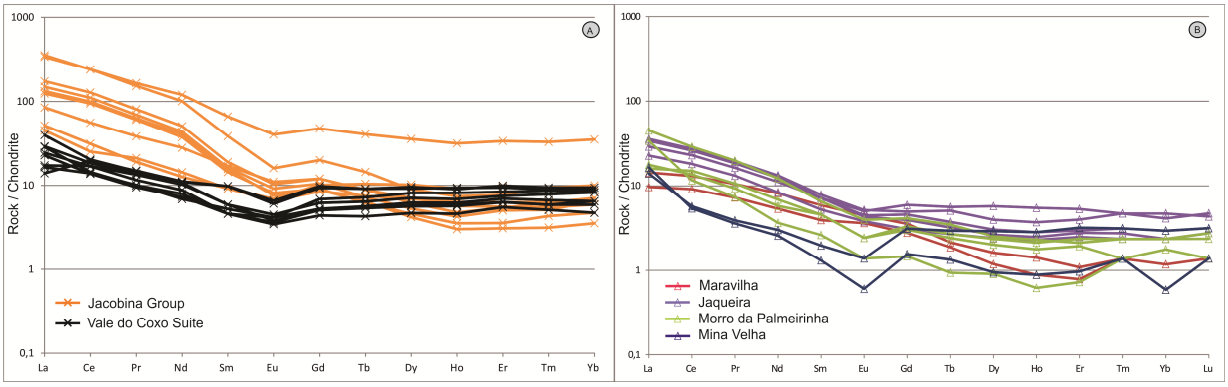

Fig. 10. Chondrite-normalized patterns of REE for quartzite from Jacobina Group and biotite schist from Vale do Coxo Suite (A), and quartz veins from Maravilha, Jaqueira, Morro da Palmeirinha and Mina Velha (B). Chondrite normalization values are from Sun and McDonough (1989).

6. Fluid Inclusions results

6.1. Petrography

The fluid inclusions occur as primary clusters or trails, pseudosecondary intragranular trails and as secondary transgranular trail ubiquitous in all quartz samples. Thus, the measurements were performed following the fluid inclusion assemblage (FIA) concept (Goldstein and Reynolds, 1994), which represents a group (trail or cluster) of related inclusions contained in a single crystal or occurring in a single domain of a crystal. Recrystallized portions of the host quartz and crystals with numerous crosscutting fractures, decrepitation clusters as well as fluid inclusions with necking down and irregular morphologies were rejected.

Based on the number of phases at room temperature (~25°C) and on phase changes during freezing and heating runs, three main types of fluid inclusions have been identified.

6.1.1. Type WC

Type WC comprises aqueous-carbonic inclusions. They are usually two-phase (CO_2L+H_2OL) at room temperature (Fig. 11A) but, with a little depression in temperature, classic three-phase ($CO_2V+CO_2L+H_2OL$) is observed. This type is observed at the Maravilha and Jaqueira samples.

At Maravilha FI, the volumetric proportion of CO_2 vapor phase (VCO_2) varies between 30% and 95% with predominance of those with VCO_2 > 80%. The inclusions range in size from 5 to 30 μm (mainly 8-15 μm) and display oval to elongate shapes (Fig. 11B). They occur like primary clusters or pseudosecondary trails usually spatially related to carbonic type C inclusions.

At Jaqueira, VCO_2 varies between 15% and 95% with no predominance of VCO_2. The inclusions range in size from 2 to 15 μm (mainly 8-12 μm) and display oval to elongate shapes. They occur like primary clusters (Fig. 11C) and pseudosecondary trails usually spatially related to aqueous type W (subtype We) inclusion (Fig. 11D).

6.1.2. Type W

Type W comprises mono-phase (H_2OL), two-phase (H_2OL+H_2OV) and three-phase (H_2OL+H_2OV+solid) aqueous inclusions that can be subdivided according their size, shape and/or mode of occurrence.

Subtype We consists of two-phase (H_2OL+H_2OV) aqueous inclusions with volumetric proportion of vapor H_2O varies between 1 and 10%. They range in size from 7 to 18 μm (mainly 8-12 μm) and display oval to elongate shapes. They occur as primary clusters spatially related to type WC inclusions at Jaqueira (Fig. 11C-D).

Subtype Wmp comprises two-phase (H_2OL+H_2OV) aqueous inclusions with volumetric proportion of vapor H_2O varies between 5 and 20%. They range in size from 8 to 15 μm and display oval to subrounded shapes. They occur in three different ways: i) isolated primary inclusions (Fig. 12A), ii) short pseudosecondary trails and iii) as primary clusters usually spatially related to carbonic type C inclusions (Fig. 12B). This subtype occurs at Morro da Palmeirinha *garimpo*.

Subtype Wmv is composed of two-phase (H_2OL+H_2OV) aqueous inclusions with distinctive characteristic of higher volumetric proportion of vapor H_2O than liquid H_2O. In some inclusions this proportion is higher than 50% (Fig. 12C). Their size ranges from 5 to 20 μm and have subrounded to polygonal shapes. They occur like primary clusters in single quartz crystals, frequently intercepted by Wl FIAs. They were observed only at samples from the Mina Velha *garimpo*.

Subtype Wl occurs in the Jaqueira, Morro da Palmeirinha and Mina Velha quartz samples. The subtype comprises two-phase aqueous inclusions with the volumetric proportion of vapor H_2O varying between 1 and 20%. Their size ranges from 1 to 12 μm (mainly 3-8 μm), and with rounded to elongate, locally irregular shapes (Fig. 12D). They occur as secondary trails that usually intercept WC+We FIAs at Jaqueira. At Morro da Palmeirinha and Mina Velha these trails frequently intercept Wmp and Wmv FIAs, respectively (Fig. 12A).

Subtype Wh consists of three-phase (H_2OL+H_2OV+solid) aqueous inclusions as observed at Jaqueira *garimpo*. The volumetric proportion of vapor H_2O varies between 1 and 5%. The solid phase frequently shows a cubic shape and greenish coloration, and is thus assumed to be halite (Fig. 12E). The inclusions range from 7 to 12 μm in size and have oval to polygonal shapes. They occur spatially related to Wl FIAs and sometimes isolated and/or close to tourmaline crystals (Fig. 12F).

6.1.3. Type C

Type C consists of one-phase (CO_2V) or two phases (CO_2V+CO_2L) that formed CO_2-rich vapor bubbles during freezing (Fig. 13A). The inclusions display clear to predominantly dark color, have various shapes (subrounded, polygonal, irregular) and size ranging from 5 to 15 μm. At Maravilha, they occur as primary clusters or pseudosecondary trails and are usually spatially related to type WC. At Morro da Palmeirinha these inclusions occur as primary clusters and are frequently spatially related to type Wmp (Fig. 13B).

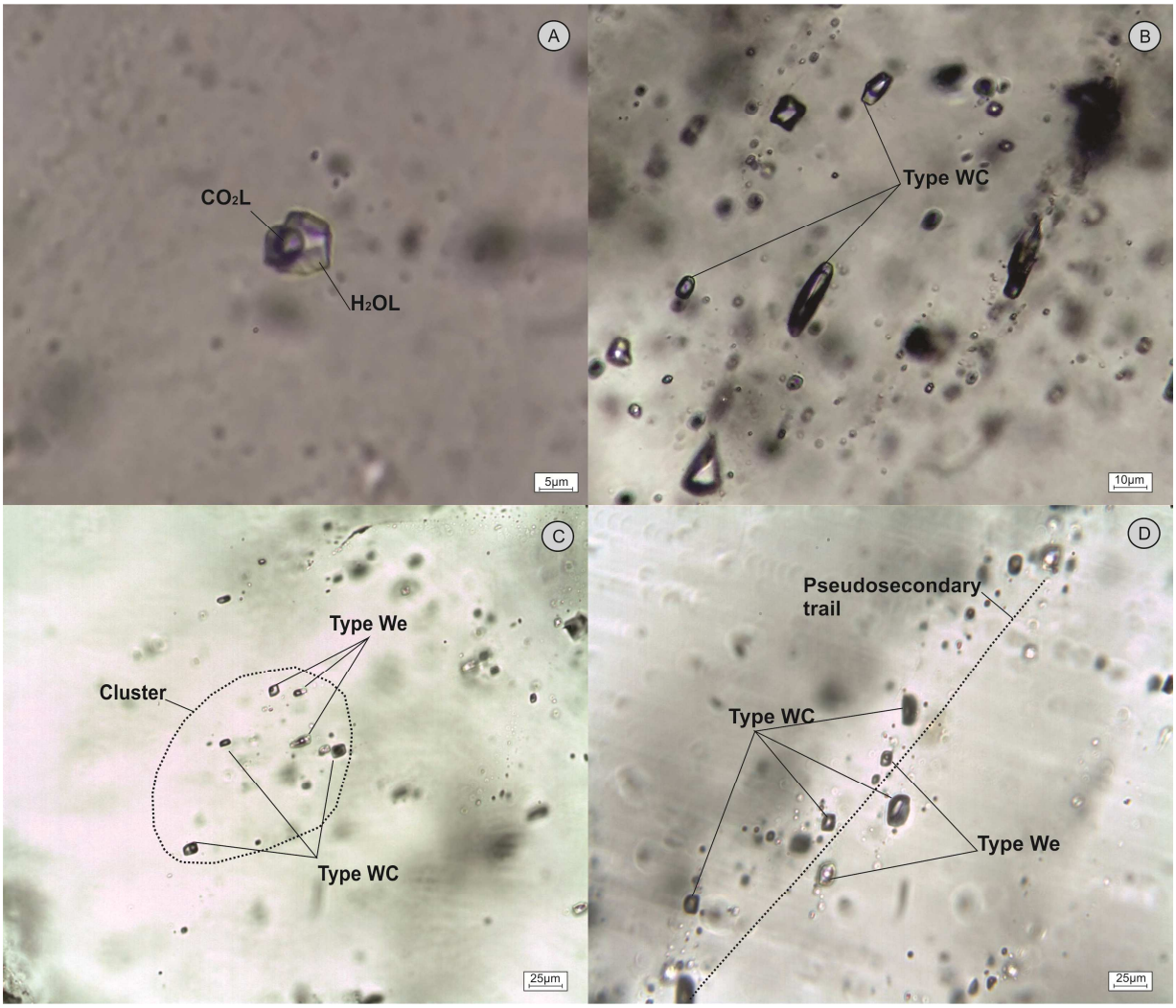

Fig. 11. Photomicrographs showing Type WC inclusions characteristics and distribution. (A) Two-phase subrounded inclusion. (B) Maravilha characteristic type WC FIA. (C-D) Jaqueira *garimpo* quartz cluster of FI and pseudosecondary FI trail respectively.

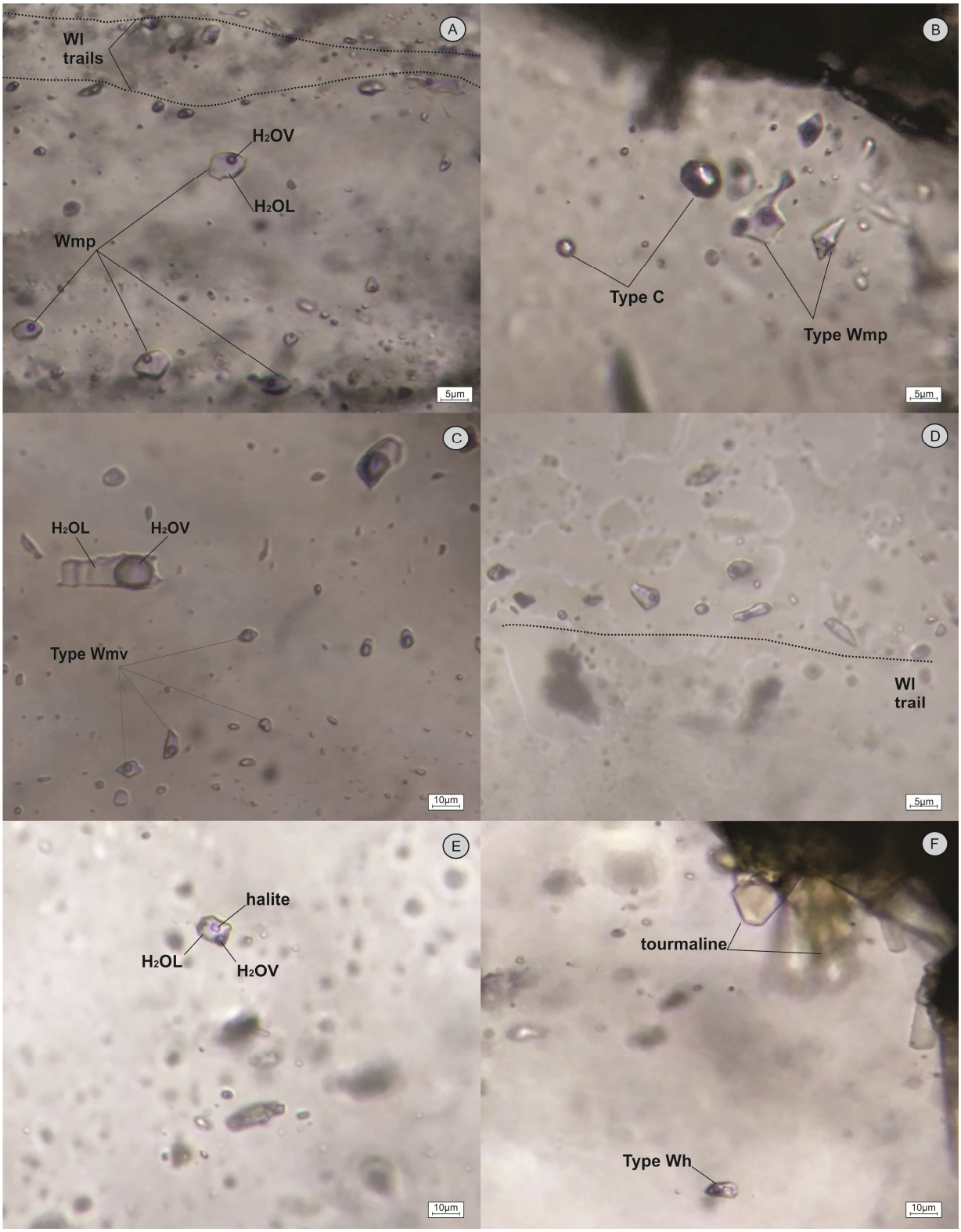
A
WI
trails
H₂OV
H₂OL
Wmp
5µm
B
Type C
Type Wmp
5µm
C
H₂OL
H₂OV
Type Wmv
10µm
D
WI
trail
5µm
E
halite
H₂OL
H₂OV
10µm
F
tourmaline
Type Wh
10µm

Fig. 12. Photomicrographs showing different Types W (aqueous) inclusions characteristics and distribution. (A) Isolated Wmp inclusions and Wl trail. (B) Wmp characteristic FIA. (C) Wmv inclusions. (D) Type Wl typical pseudosecondary trail. (E-F) Type Wh mains features and mode of occurrence.

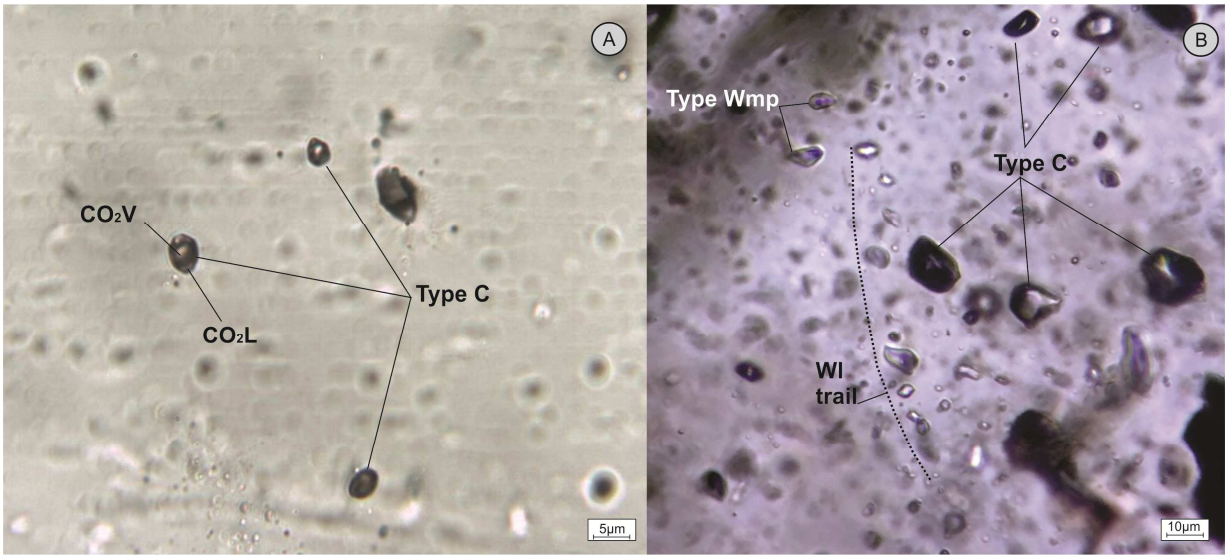

Fig. 13. Photomicrographs showing Type C FI characteristics and distribution. (A) Cluster at the Maravilha *garimpo*. (B) Characteristic FIA from Morro da Palmeirinha.

6.2. Microthermometry

A summary of microthermometric data obtained from fluid inclusion measurements are listed in Table 1. For statiscal analysis the data collected on each FIA were grouped according to the inclusion type.

GARIMPO	TYPE	N	T_m CO_2 (°C)	T_m cla (°C)	T_h CO_2 (°C)	T_m ice (°C)	T_m halite (°C)	T_h Total (°C)	Salinity (wt. % NaCl eq.)
Maravilha	WC	126	-58.6 to -57.1	3.7-9.7	7.3-23.8			215-398	0.6-11.1
	C	68	-58.2 to -57.4		4.0-24.2				
Jaqueira	WC	41	-59.0 to -57.5	1.2-9.0	4.2-23.0			265-395	2.0-14.2
	We	28				-14.1 to -0.5		251-412	0.8-17.9
	Wh	26					181-266	123-193	30.9-35.7
	Wl	103				-21.0 to -0.1		112-217	0.2-23.0
Morro da Palmeirinha	Wmp	68				-5.4 to -0.1		124-233	0.2-8.4
	Wl	80				-18.0 to -7.3		116-207	10.9-20.9
	C	42	-58.1 to -57.0		4.4-23.2				
Mina Velha	Wmv (V)	9				-16.9 to -9.5		301-495	13.4-21.1
	Wmv (L)	6				-15.6 to -12.1		289-365	16.1-19.1
	Wl	68				-13.6 to -0.2		151-281	0.3-17.4

Table 1. Fluid inclusions microthermometric data.

6.2.1. Type WC

At the Maravilha *garimpo*, FI in quartz exhibit $TmCO_2$ ranges from -58.6°C to -57.1°C (Fig. 14A). This indicates that CO_2 is the predominant volatile in the carbonic phase and that minor amounts of other volatiles (in general CH_4 and/or N_2) are present. The $ThCO_2$ ranges from 7.3°C to 23.8°C with all inclusion homogenizing to the liquid phase (Fig. 14B). The Tm cla ranges from 3.7°C to 9.7°C, which gives salinities between 0.6 and 11.1 wt.% NaCl eq. (Fig. 14C), and total homogenization temperature (Tht) varies between 215 and 398°C with mode at 245°C (Fig. 14D).

The FI in quartz from the Jaqueira *garimpo* have $TmCO_2$ ranges from -59.0°C to -57.5°C (Fig. 14A) also indicating that CO_2 is the predominant volatile in the carbonic phase and that minor amounts of other volatiles (in general CH_4 and/or N_2) are present. $ThCO_2$ ranges from 4.2°C to 23.0°, with all inclusion homogenizing to the liquid phase (Fig. 14B). Tm cla ranges from 1.2°C to 9.0°C, implying in salinities between 2.0 and 14.2 wt.% NaCl eq. (Fig. 14C). Tht varies between 265 and 395°C with temperature mode at 325°C (Fig. 14D).

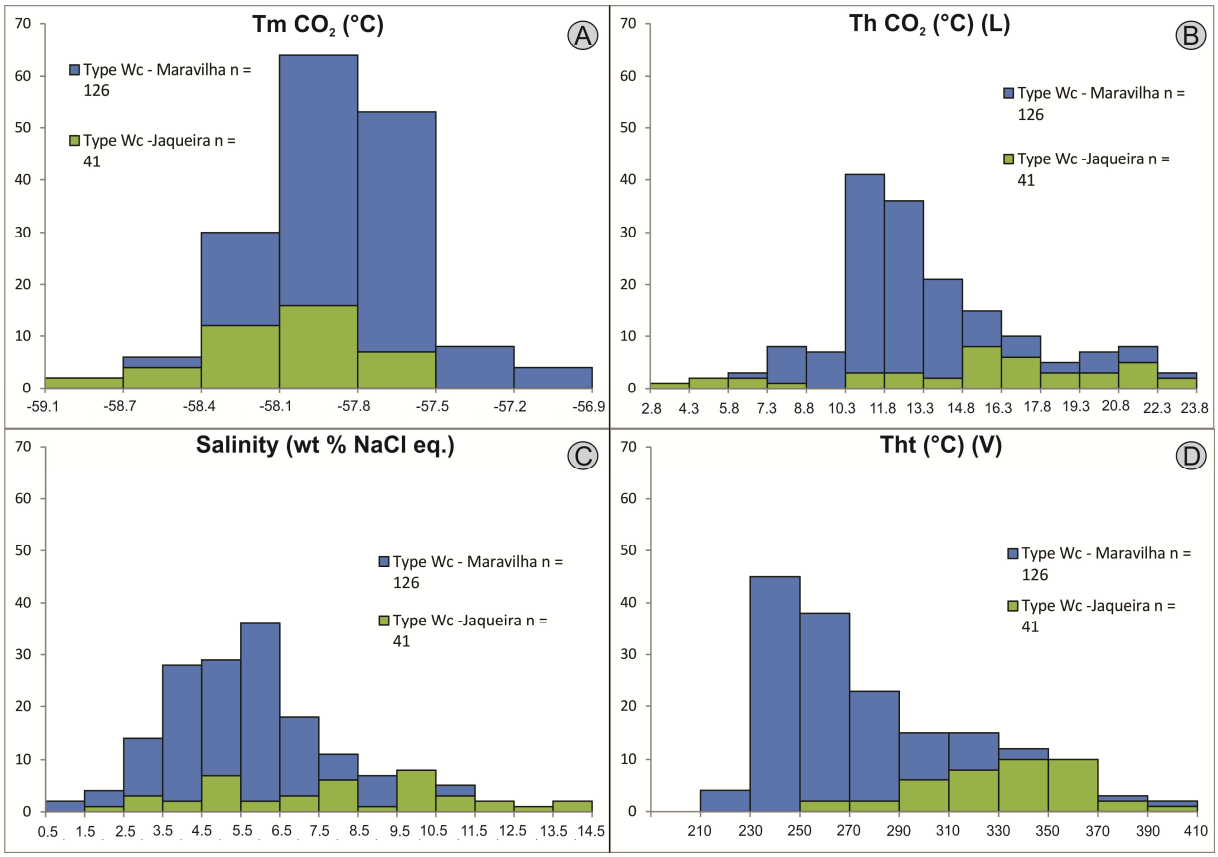

Fig. 14. Microthermometric data and calculated salinity histograms for Type WC inclusions from Maravilha and Jaqueira.

6.2.2. Type W

The FI subtype We from the Jaqueira *garimpo* has Tm ice varying between -14.1°C and -0.5°C, which gives salinities between 0.8 and 17.9 wt. % NaCl eq. (Fig. 15A). The Tht ranges from 251 to 412°C with temperature mode at 310°C (Fig. 15B). All inclusions homogenize to the liquid phase. In the subtype Wl inclusions Tm ice varies between -21.0°C and -0.1°C which implies salinity between 0.2 and 23.0 wt. % NaCl eq. (Fig. 15A). The Tht ranges from 112 to 217°C with temperature mode at 145°C (Fig. 15B). All Wl inclusions homogenize to the liquid phase. Tm halite in subtype Wh inclusions ranges from 181 to 266°C which implies salinity between 30.9 and 35.7 wt. % NaCl eq. Tht of these inclusions ranges from 123 to 193°C with mode at 179°C. In mostly of Wh inclusions, the vapor phase homogenizes to liquid before halite dissolution.

At the Morro da Palmeirinha *garimpo,* subtype Wmp inclusions Tm ice varies between -5.4°C and -0.1°C which gives salinities between 0.2 and 8.4 wt. % NaCl eq. (Fig. 15C). The Tht ranges from 124 to 233°C with temperature mode at 145°C (Fig. 15D). In the subtype Wl inclusions Tm ice varies between -18.0°C and -7.3°C which implies salinities between 10.9 and 20.9 wt. % NaCl eq. (Fig. 15C). All Wl inclusions homogenize to the liquid phase, and Tht ranges from 116 to 207°C with temperature mode at 134°C (Fig. 15D).

At the Mina Velha *garimpo,* subtype Wmv inclusions Tm ice varies between -16.9°C and -9.5°C which implies salinities between 13.4 and 21.1 wt. % NaCl eq. (Fig. 15E). This FI subtype homogenizes both to vapor Wmv (V) and liquid Wmv (L) states. Wmv (V) Tht ranges from 301 to 495°C with temperature mode at 490°C. Tht from Wmv (L) ranges from 289 to 365°C with mode at 320°C (Fig. 15F). In the subtype Wl inclusions Tm ice varies between -13.6°C and -0.2°C which gives salinities between 0.3 and 17.4 wt. % NaCl eq. (Fig. 15E). The Tht ranges from 151 to 281°C with mode at 194°C (Fig. 15F). All Wl inclusions homogenize to the liquid state.

6.2.3. Type C

The $TmCO_2$ of FI's from both Maravilha and Morro da Palmeirinha *garimpos* are quite similar, ranging from -58.2°C to -57.4°C at Maravilha and from -58.1°C to -57.0°C at Morro da Palmeirinha. These values indicate only minor amounts of other volatiles (in general CH_4 and/or N_2) are present. The same similarity occurs with $ThCO_2$. It ranges from 4.0 to 24.2°C at Maravilha and 4.4 to 23.2°C at Morro da Palmeirinha (Fig. 16A-B).

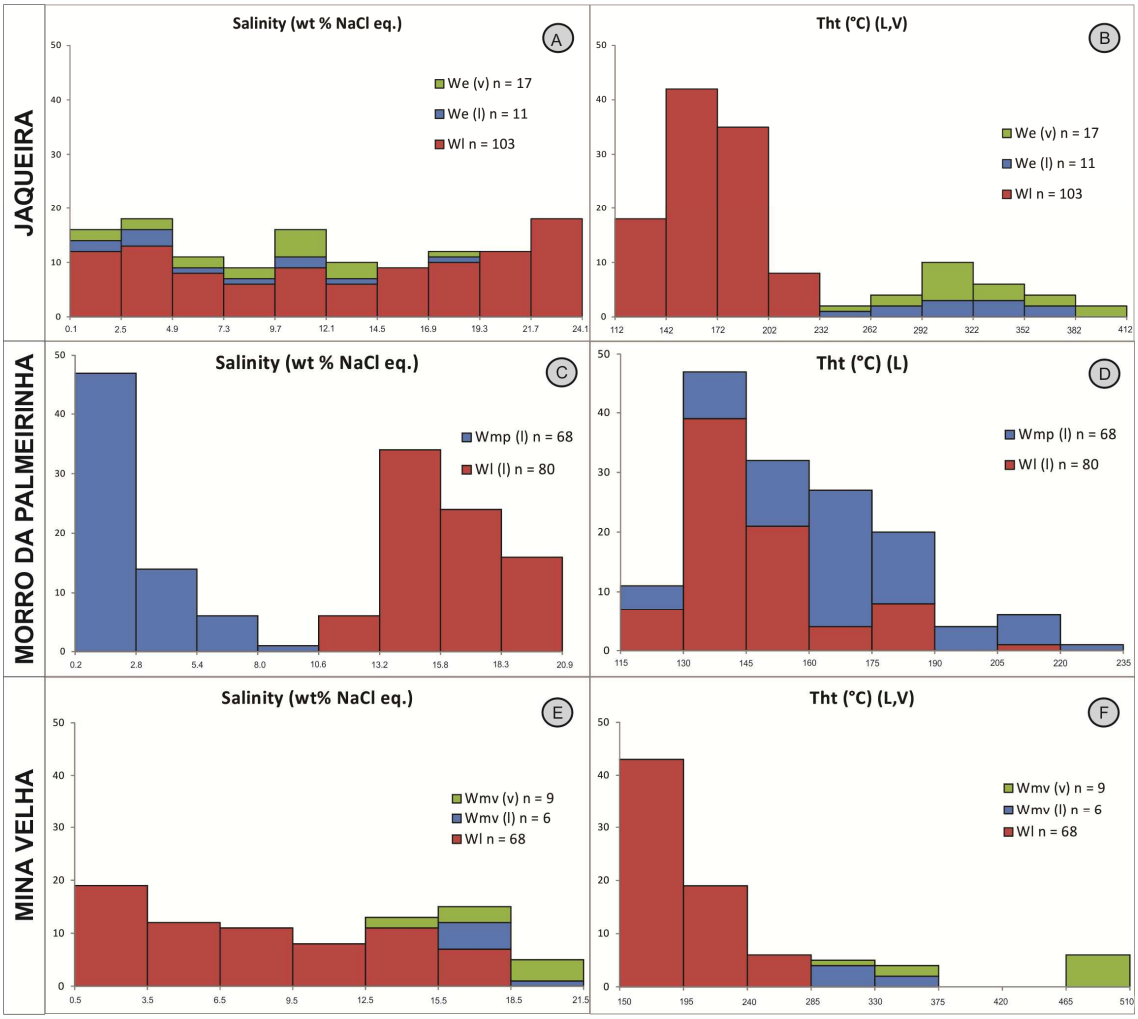

Fig. 15. Salinity and microthermometric data histograms for type W inclusions from Jaqueira (A-B), Morro da Palmeirinha (C-D) and Mina Velha (E-F).

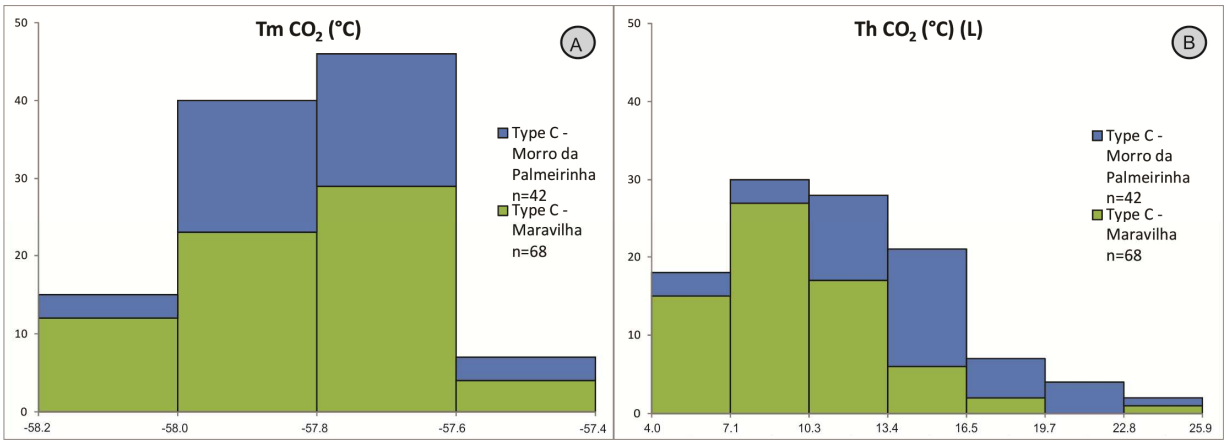

Fig. 16. (A) CO_2 final melting temperature and (B) CO_2 homogenization temperature histograms from FI type C.

6.3. Composition and density

A summary of FI composition and density obtained from microthermometric data calculations is presented in Table 2.

GARIMPO	TYPE	N	XCO_2 (mol. %)	XH_2O (mol. %)	XNaCl (mol. %)	CO_2 density (g/cm³)	Bulk density (g/cm³)
Maravilha	WC	126	0.13-0.87	0.12-0.86	0.00-0.02	0.7-0.9	0.7-1.0
	C	68					
Jaqueira	WC	41	0.06-0.87	0.12-0.92	0.00-0.04	0.7-0.9	0.8-1.0
	We	28					0.6-0.9
	Wh	26					1.1-1.2
	Wl	103					0.9-1.1
Morro da Palmeirinha	Wmp	68					0.8-1.0
	Wl	80					1.0-1.1
	C	42					
Mina Velha	Wmv (V)	9					0.6-0.9
	Wmv (L)	6					0.8-0.9
	Wl	68					0.8-1.0

Table 2. Fluid inclusions composition and density.

6.3.1. Type WC

For type WC inclusions composition, it is reasonable to assume that the presence of other volatiles in the carbonic phase, probably CH_4 and/or N_2 is minor and that it does not have affected significantly the microthermometric properties, specially $ThCO_2$ and Tm cla (e.g., Brown and Lamb, 1989).

At Maravilha, fluid composition ranges from: XCO_2: 0.13 to 0.87 mol%; XH_2O: 0.12 to 0.86 mol%; XNaCl: 0.00 to 0.02 mol%. The carbonic phase density ranges from 0.7 to 0.9 g/cm³ whereas the global density varies between 0.7 and 1.0 g/cm³.

The composition of Jaqueira inclusions ranges from: XCO_2: 0.06 to 0.87 mol%; XH_2O: 0.12 to 0.92 mol%; XNaCl: 0.00 to 0.04 mol%. The carbonic phase density ranges from 0.7 to 0.9 g/cm³ whereas the bulk density varies between 0.8 and 1.0 g/cm³.

6.3.2. Type W

At the Jaqueira *garimpo*, subtype We inclusions has bulk density ranging from 0.6 to 0.9 g/cm³. Subtype Wh inclusions has bulk density ranging from 1.1 to 1.2 g/cm³.

Subtype Wmp inclusions from Morro da Palmeirinha has bulk density ranging from 0.8 to 1.0 g/cm³.

At Mina Velha, the subtype Wmv (V) has bulk density ranging from 0.6 to 0.9 g/cm³ and the subtype Wmv (L) has bulk density ranging from 0.8 to 0.9 g/cm³.

Subtype Wl, which occurs at Jaqueira, Morro da Palmeirinha and Mina Velha *garimpos*, have bulk density similar ranges from 0.9 to 1.1g/cm³; 1.0 to 1.1g/cm³ and 0.8 to 1.0g/cm³ respectively.

6.4. Post-entrapment modifications versus fluid immiscibility characteristics

Petrographic investigation has shown that the mineralized host quartz shows wavy extinction and recrystallized portions, which indicates ductile deformation. Thus, post-entrapment modifications possibly occurred.

At the Maravilha and Jaqueira *garimpos* the variation of CO_2V volumetric proportion in the inclusions from type WC and their coexistence with type We may be indicative of either selective water leakage or inclusions formed by entrapment of immiscible fluids (Anderson et al., 1992). According to Huizenga and Touret (1999) water-rich H_2O-CO_2 fluid inclusions produced by fluid immiscibility must show lower densities when compared to water-poor (high CO_2V) inclusions. The opposite indicates that the inclusions were formed via selective water leakage.

Besides the wide variation of VCO_2 volumetric proportion (15-95%), type WC inclusions from Jaqueira VCO_2 x $ThCO_2$ diagram shows a trend that indicates inclusions produced by fluid immiscibility (Fig. 17A). Also the variation of $ThCO_2$ within the FIAs is mostly lower than 5°C (Fig. 17B). Further evidence for fluid immiscibility includes: (i) observation of subtype We and type WC within clusters and/or FIA, indicating that they formed contemporaneously; (ii) higher homogenization temperatures of type WC than subtype We (Roedder, 1984); (iii) lower salinities of type WC than subtype We (Coulibaly et al., 2008); (iv) asymmetric distribution of ThCO2 and Tht (Loucks, 2000).

On the other side Maravilha VCO_2 x $ThCO_2$ diagram shows no trend (Fig. 17C) and variations of $ThCO_2$ within some FIAs are higher than 15°C (Fig. 17D). Also type C inclusions $ThCO_2$ that coexists with type WC have different ranges. These characteristics suggest that Maravilha type WC inclusions have been submitted to post-entrapment modifications, and therefore, are not suitable for P-T calculations.

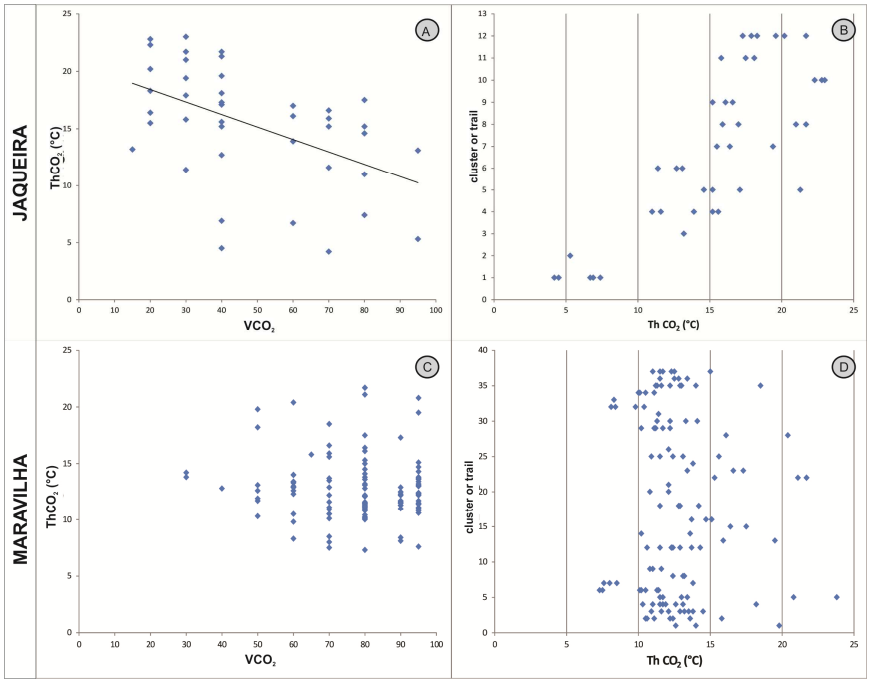

Fig. 17. (A, C) Type WC VCO_2 x $ThCO_2$ diagrams. (B, D) $ThCO_2$ variations within primary clusters or trails.

7. Mineral chemistry results

7.1. Chlorite chemistry

Petrographic analyses from ore mineralogy reveal chlorite as a common mineral, within mineralized quartz vein or meta-ultramafic host rocks. The EMPA analytical results have been recalculated on the basis of chlorite formula with 36 oxygen atoms (O, OH), 16 groups of OH, and 8 atoms of Si + Al IV, on the basis of 28 oxygen atoms per formula unit (a.p.f.u.). The total iron content obtained by the microprobe is considered as FeO, and H_2O was calculated by stoichiometry. Table 3 presents the composition range upper and lower limits of each chlorite a.p.f.u. which are Si, Al (total), Fe (total), Mn, Mg, Ca, Na, K, Al ^{IV} and Al ^{VI} from each one of the studied areas. It also contains the Si/Al and Fe/(Fe + Mg) ratios, the sum of the elements Ca+Na+K, total cations in the a.p.f.u. and sum of elements in the octahedral site. The EMPA complete results are presented in the Supplementary Tables 3.1 to 3.4.

In terms of Si and Al (total, IV, VI) the chlorites from four areas share similar compositions (Table 3). The Fe (total) contents from Jaqueira (4.000-4.610) are higher than Maravilha (2.416-3.227) and Mina Velha (2.210-2.673), while those from Morro da Palmeirinha (1.272-4.087) show a wider range of composition when compared to other areas. The Mg composition from Maravilha (5.471-6.489) and Mina Velha (5.696-6.861) chlorites are similar and show higher values than Jaqueira (3.978-4.711), while those from Morro da Palmeirinha (4.722-8.772) show a wider range of composition. The Mn, Ca, Na and K contents are close to zero as well as the sum Ca+Na+K. The Fe/Fe+Mg ratio from Jaqueira (0.475-0.526) chlorites showed higher values than Maravilha (0.300-0.366) and Mina Velha (0.252-0.309) while those from Morro da Palmeirinha (1.272-4.087) show a wider range of composition when compared to other areas. The total cations in the a.p.f.u. are close to twenty and sum of elements in the octahedral site is close to twelve.

Element (a.p.f.u.)	Maravilha	Jaqueira	Morro da Palmeirinha	Mina Velha
Si	5.475-5.977	5.261-5.678	5.534-6.040	5.251-5.929
Al (total)	4.620-5.330	5.160-5.710	4.111-5.310	4.660-5.700
Al (IV)	2.023-2.525	2.322-2.739	1.960-2.466	2.071-2.749
Al (VI)	2.395-3.291	2.680-3.283	2.108-3.011	2.548-3.339
Fe (total)	2.416-3.227	4.000-4.610	1.272-4.087	2.210-2.673
Mg	5.471-6.489	3.978-4.711	4.722-8.772	5.696-6.861
Mn	0.000-0.023	0.089-0.130	0.034-0.106	0.007-0.025
Ca	0.000-0.042	0.000-0.015	0.001-0.015	0.000-0.044
Na	0.009-0.118	0.000-0.026	0.006-0.063	0.000-0.050
K	0.002-0.027	0.000-0.019	0.006-0.198	0.001-0.156
Ca+Na+K	0.014-0.144	0.000-0.073	0.019-0.253	0.003-0.181
Fe/Fe+Mg	0.300-0.366	0.475-0.526	0.138-0.464	0.252-0.309
Si/Al	1.03-1.29	0.93-1.08	1.04-1.46	0.92-1.26
Total cations	19.383-19.932	19.538-19.921	19.563-19.967	19.387-19.906
Σ Octahedral	11.30-11.89	11.49-11.89	11.26-11.86	11.30-11.88

Table 3. Composition range of EMPA analytical results recalculated on the basis of chlorite formula presented in atoms per formula unit (a.p.f.u.) from each studied area.

According to Hey's (1954) classification (Fig. 18A) most of the Jaqueira and Mina Velha chlorites are picnochlorites, with minor occurrence of ripidolites. The opposite is observed at Maravilha and most of chlorites are ripidolites and only a few samples are picnochlorite. The chlorites from Morro da Palmeirinha are mostly distributed between the clinochlore and picnoclorite fields, with only three samples of ripidolite. In terms of Zane and Weiss (1998) ternary Al + □ (□ is octahedral vacancy); Mg and Fe classification (Fig. 18B) the chlorites from Maravilha, Morro da Palmeirinha and Mina Velha are type I (trioctahedral) Fe-chlorite (chamosite), while chlorite from Jaqueira are also of type I (trioctahedral), but plotted between the fields of Fe-chlorite (chamosite) and Mg-chlorite (clinochlore).

7.2. Chlorite geothermometry

The empirical chlorite thermometry is based on Al^{IV} variation content and Fe/(Fe+Mg) ratios of chlorites as a temperature function (Cathelineau, 1988; Zang and Fyfe, 1995). To avoid problems in the application of these empirical geothermometers some criteria must be investigated.

The first one regards Al^{IV} content saturation. According to Kranitoids and MacLean (1987) and Cathelineau (1988) only chlorites Al-saturated are suitable for geothermometry. Maravilha and Morro da Palmeirinha samples plotted below the Al-saturation line and are unsuitable for geothermometry (Fig. 18C). All samples from Jaqueira are Al-saturated and only three samples from Mina Velha plotted below the Al-saturation line.

According to Vidal et al. (2001) chlorites contaminated by submicroscopic inclusions or interlayers have typically variable amounts of Ca+Na+K, and only analyses with Ca+Na+K<0.5 a.p.f.u should be considered for geothermometry. Maximum values from Ca+Na+K were 0.054 and 0.181 at Jaqueira and Mina Velha samples respectively. Therefore, it is reasonable not to expect problems related to contaminated chlorites.

Klein et al. (2007) pointed out that covariance should be expected between Al^{IV} and Fe/(Fe+Mg) ratio. Both Jaqueira and Mina Velha samples presented positive correlations between Al^{IV} and Fe/(Fe+Mg) ratio (Fig. 18D).

De Caritat et al. (1993) suggested the consistency between chemical data from studied chlorites and of those chlorites used in empirical geothermometers should be employed. Considering three classical geothermometers from Cathelineau (1988), Kranitoids and MacLean (1987) and Zang and Fyfe (1995) as references, the Jaqueira and Mina Velha chlorite chemical composition (Fig. 18E-F) are consistent with those used in empirical geothermometer from Kranitoids and MacLean (1987), which is used here to estimate the formation temperature of chlorite at these *garimpos*.

At Jaqueira, temperatures range from 302 to 346°C with a mode at 331°C. At Mina Velha temperatures show a greater spread of the values, ranging from 258 to 332°C with mode at 317°C (Fig.19).

In addition to considerations previous discussed on application of empirical chlorite thermometers, Klein et al. (2007) recommends comparison of geothermometry results to another independent temperature estimation method as a basic principle for use of this type of data.

At Jaqueira chlorite temperatures have good consistency with types WC and We homogenization temperature ranges (Fig.20). This corroborates petrographic observations from chlorite replacing biotite and is reasonable to assume that chlorite belongs to the same hydrothermal system from types WC and We FI.

At Mina Velha chlorite temperatures have poor correlation with FI data of homogenization temperature (Fig.20). Some consistency is observed with chlorite mode (317°C) and Wmv (L) homogenization temperature (320°C). Therefore, chlorite formation temperature relationship with types Wmv or Wl FI is questionable.

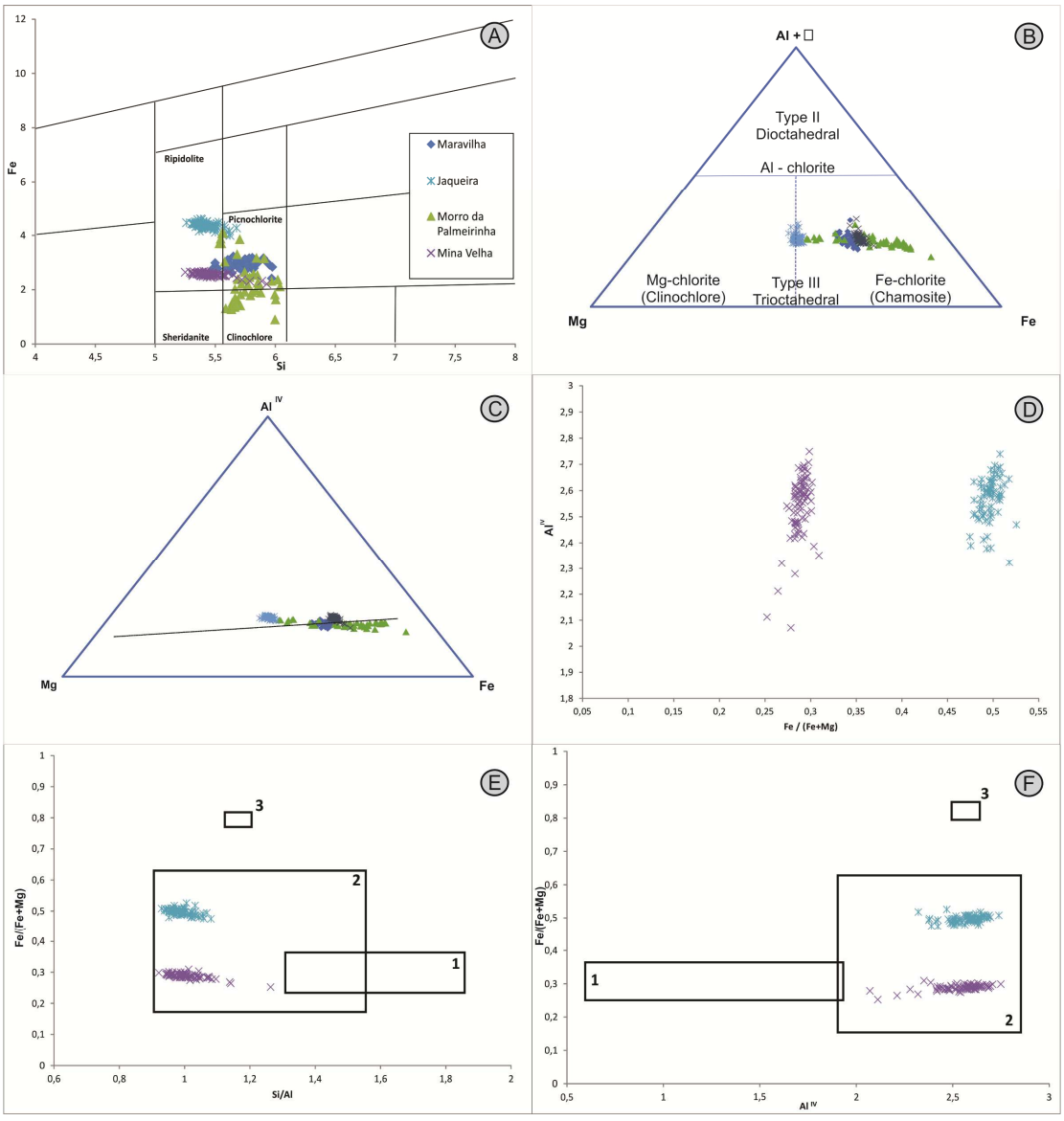

Fig. 18. Chlorite classifications according to: (A) Hey (1954) diagram and (B) Ternary Al + □ (□ is octahedral vacancy); Mg and Fe classification diagram of Zane and Weiss (1998). (C) Ternary diagram Al ^{IV} - Mg - Fe composition for chlorite from studied areas. Black line indicates boundary between Al-saturate (above) and Al-undersaturated chlorites. (D) Diagram showing covariance between the

Fe/(Fe+Mg) ratio and Al ^{IV} for Jaqueira and Mina Velha. (E-F) Composition fields of empirical geothermometers from 1: Cathelineau (1988), 2: Kranitoids and MacLean (1987), 3: Zang and Fyfe (1995) ploted in Fe/(Fe+Mg) vs Si/Al ratio and Fe/(Fe+Mg) vs Al^{IV} diagrams. The areas symbols are the same described in diagram (A).

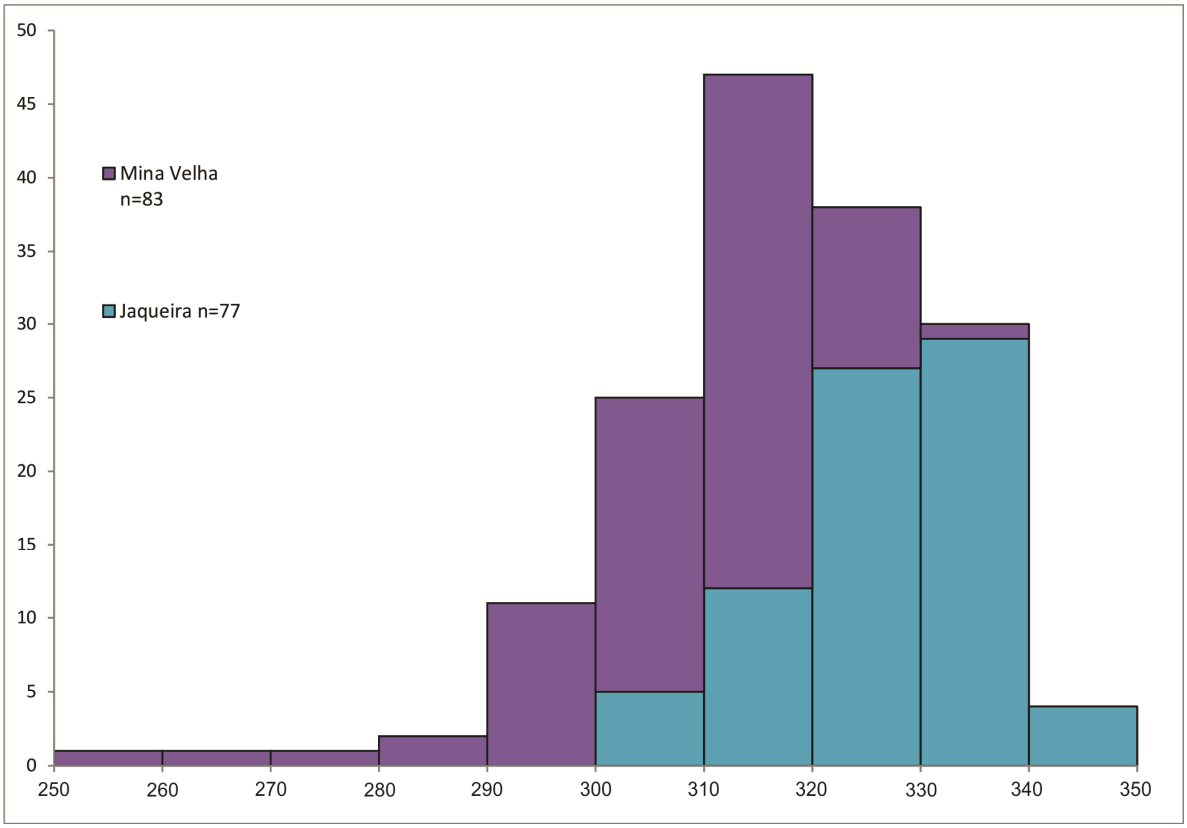

Fig. 19. Chlorite geothermometry frequency histogram from Jaqueira and Mina Velha.

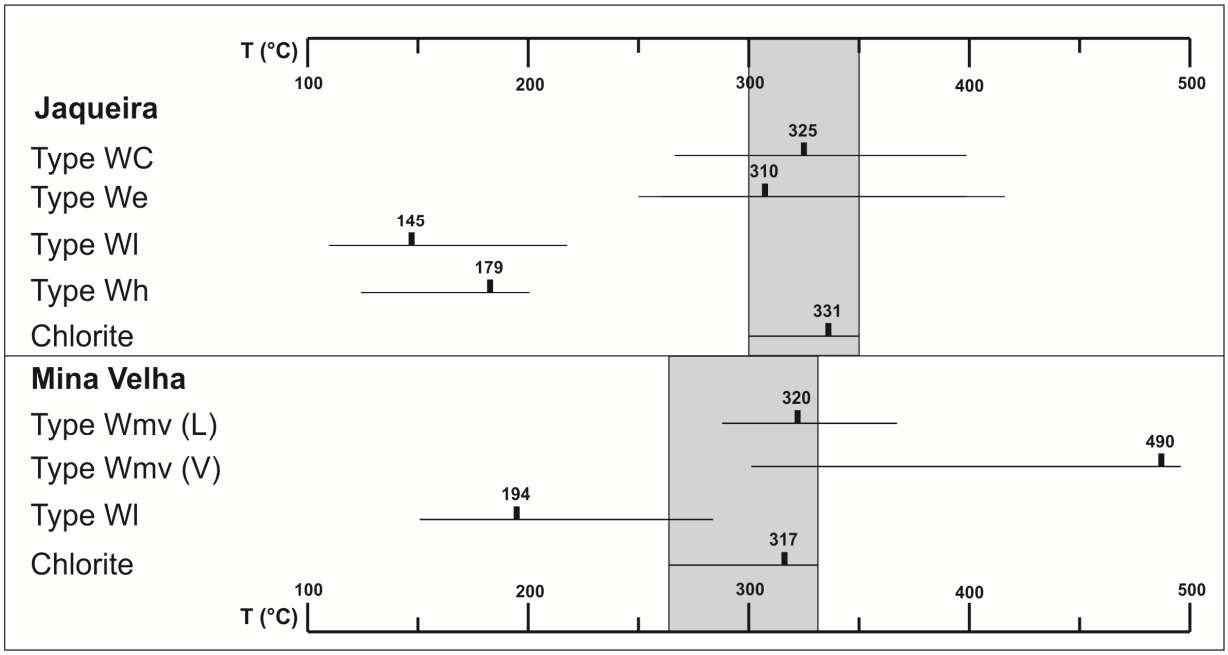

Fig. 20. Diagram comparing chlorite geothermometry and FI homogenization temperatures. The thin bar represents the range of temperatures and vertical thick bar is temperature mode. The grey shaded boxes highlight the chlorite temperature range.

8. Discussions

8.1. Hydrothermal alteration and whole rock geochemical composition

Optical microscopy analyses from both hosts Jacobina Group quartzites, Vale do Coxo Suite meta-ultramafic schists and mineralized quartz veins reveal the quartz + sericite + chlorite + pyrite + chalcopyrite as the main ore mineralogy indicating that sericitic is the hydrothermal alteration with sulfidation subordinated to it. The gangue minerals include the tourmaline + rutile + ilmenite assemblage, and the secondary minerals are leucoxene, covellite and chalcocite.

In the the Jacobina Group quartzites, the sericitic assemblage is widespread disseminated between quartz crystals and also occurs like anhedral crystals in a fissure-filling type. The sulfidation is represented by the pyrite + chalcopyrite assemblage who is subordinated to the two form of sericitic alteration. It seems to exist at least three pyrite generations: one composed of rounded to subrounded crystals with quartz grains stratifications which could be interpreted from sedimentary origin, and therefore from the pre-ore stage; another composed of euhedral to subhedral crystals related to fissure-filling sericitic assemblage from the ore stage; a third type represented by the disseminated subhedral to euhedral crystals which are interpreted from the post-ore stage. The major and trace elements geochemical composition from quartzites resembles the above mentioned hydrothermal mineralogy: the Al_2O_3, K_2O and Cr contents may be related to sericite and/or fuchsite composition; Fe_2O_3 and Cu should be related to sulfidation assemblage; TiO_2 content indicates rutile and ilmenite geochemical composition.

At the Vale do Coxo Suite meta-ultramafic schists the biotite is the mineral which represents the pre-ore stage. The sericitic assemblage is pervasive and replaces biotite during the ore stage. The sulfidation is represented by the pyrite + chalcopyrite assemblage and is subordinated to sericitic alteration. The rutile and ilmenite oxides are also subordinated to sericitic assemblage. The major and trace elements geochemical results are coherent with the observed mineralogy: the SiO_2, Al_2O_3 and K_2O contents probably reflect the sericitic assemblage; Fe_2O_3 indicates biotite and pyrite composition; Cr amount is probably from chalcopyrite; TiO_2 content is from rutile and/or ilmenite; MgO, Co, Ni and V amounts resembles the meta-ultramafic composition from host rocks.

In the quartz veins, sericitic assemblage occurs in two forms: a fissure-filling type when anhedral crystals are filling fractures from the ore stage; fine-grained crystals widely disseminated between quartz from the post-ore stage. The tourmaline is subordinated to sericitic alteration and seems to have at least two generations: one composed of anhedral to subhedral crystals related to sericitic assemblage from the ore stage; another composed of euhedral to subhedral crystals disseminated between quartz which could be related to the post-ore stage. The sulfidation is represented by the pyrite + chalcopyrite assemblage and is subordinated to sericitic alteration at Maravilha, Jaqueira and Morro da Palmeirinha. At Mina Velha the sulfidation is the main hydrothermal alteration and some veins are composed almost exclusively of massive pyrite. The geochemical results corroborate the petrographic observations: the Mina Velha samples showed lower SiO_2 and higher Fe_2O_3 contents than Maravilha, Jaqueira and Morro da Palmeirinha; the values for Co, Cr, Cu, Mo, Ni and V from Mina Velha are considerably higher than those of samples from the other areas.

8.2. Fluid inclusions

8.2.1. Constraints on fluid inclusions interpretation data

Nearly all of the Type WC fluid inclusions hosted on quartz from the Maravilha *garimpo* have post-entrapment features, which make them unsuitable to provide information on the physicochemical environment of ore formation.

Aqueous vapor-rich type Wmv fluid inclusions from Mina Velha are questionable. Because the relative few results (only 15 inclusions) are not enough to understand if they are a product of post entrapment modifications or are indeed primary inclusions. Besides this, such vapor-rich type may be related to type II from traditional classification from Nash (1976) which indicates inclusions from fluids of magmatic origin. Teixeira et al. (2001, 2010) have pointed out that the 2.08 to 1.88 Ga Rb-Sr age from granitoid intrusive suites (Barbosa et al., 2012 and references therein) have concordance with 1.988 to 1.918Ga $^{40}Ar/^{39}Ar$ ages of micas hosted by main fault systems (Ledru et al., 1997) and therefore the Au-bearing quartz veins may have some magmatic fluids influence.

Types WC and We inclusions from the Jaqueira *garimpo* are free of post-entrapment modifications and chlorite geothermometry concordance with homogenization temperatures permits interpretation of the evolution of the hydrothermal system and estimation of the pressure and temperature conditions of gold deposition.

8.2.2. Evolution of the hydrothermal system at the Jaqueira garimpo

The ore stage fluid is interpreted from Jaqueira types WC and We FIAs which indicates that the initial ore-forming fluids (Fig. 21) were a mixture of moderate temperatures (265-395°C) H_2O-CO_2-NaCl fluid with variable salinities (2.0-14.2 wt. % NaCl eq.) with a moderate to high temperature (251-412°C) H_2O-NaCl fluid also with variable salinities (0.8-17.9 wt. % NaCl eq.). Petrography showed that sericitic assemblage replaces biotite during the ore stage and chlorite geothermometry reveals temperatures ranging from 302 to 346°C. Thus the pressure and temperature conditions of the ore stage were estimated using the chlorite temperature formation data and isochores from types WC and We inclusions. Therefore, the estimated temperature for the ore stage ranges from 302 to 346°C and the pressure was lower than 1.98 kbar and higher than 1.62 kbar (Fig. 22).

After types WC and We inclusions entrapment a post-ore stage fluid interpreted from secondary type Wl FIA with low-medium temperatures (112-217°C) and wide range of salinity value (0.2-23.0 wt. % NaCl eq.) was mixed into the system (Fig. 21). There is no obvious interpretation about this late fluid nature. The homogenization temperature and salinity values fit into ranges proposed by Bodnar et al. (2014) for epithermal fluids but further studies are necessary to confirm this suggestion.

The halite-bearing (30.9-35.7 wt. % NaCl eq.) type Wh FIA may also be interpreted to be from the post-ore stage. They occur isolated or spatially related to Wl inclusions. Two hypotheses may be suggested for its origin. This inclusion type may have formed by large-scale fluid immiscibility, where solutes partitioned into the aqueous phase or from a fluid that was immiscible with the primary H_2O-CO_2-NaCl at elevated temperatures and percolated along the same structures (McCuaig and Kerrich, 1998 and references therein). A second hypothesis proposed by Wilkinson (2001) suggests that fluid immiscibility results in strong partition of salt into the residual liquid and continuous boiling in restricted fractures causes even more increases on salinity and possible formation of halite daughters bearing inclusions.

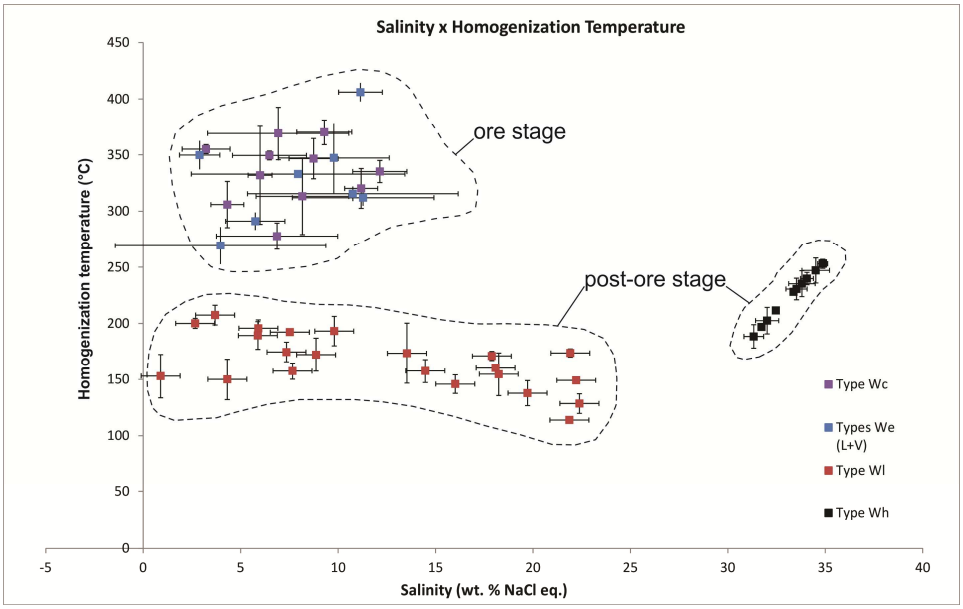

Fig. 21. Salinity versus total homogenization temperature plot of fluid inclusions from the Jaqueira *garimpo*. Each point represents a single FIA. The vertical and horizontal bars are standard deviation values within each FIA. The ore and post-ore stage interpretations are highlighted by black dashed line.

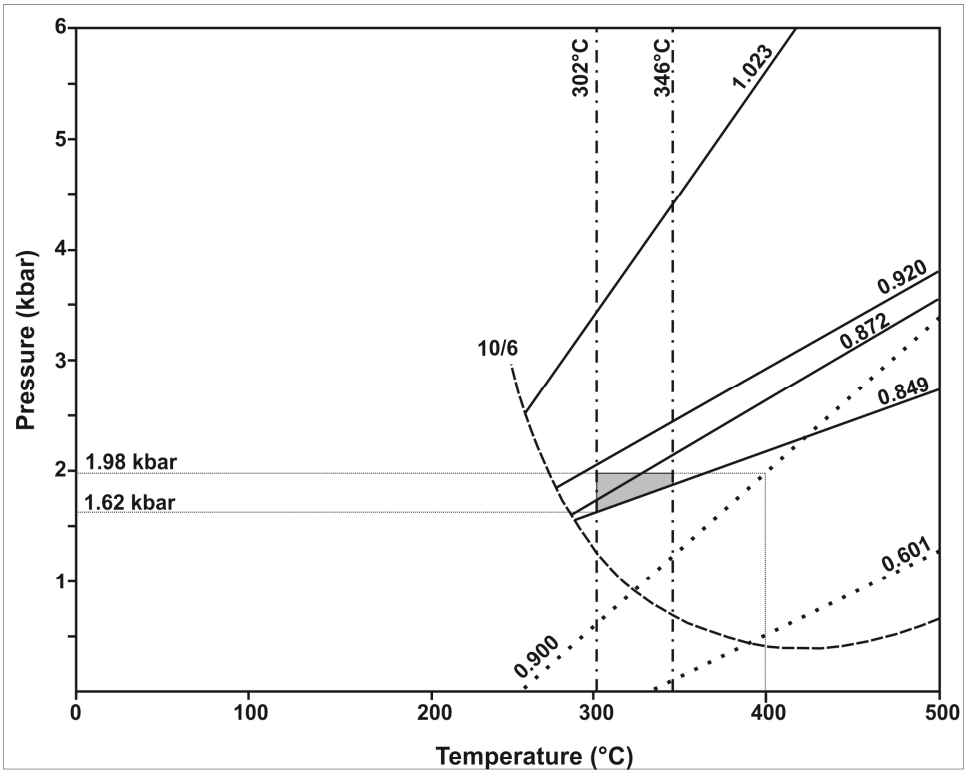

Fig. 22. Pressure-temperature diagram with isochores and covering the range of compositions and densities of types WC (thick solid lines) and We (dotted line). Isochores were calculated based on Bowers and Helgeson (1983). Vertical lines (dash dotted) are chlorite geothermometry range and dashed curve represents the solvus for XCO2 = 10 and 6 wt. % NaCl eq. from Bowers and Helgeson (1983). The grey shaded box highlights the temperature and pressure conditions for ore stage.

8.2.2. Gold transport and precipitation

The aqueous bisulfide and chloride complexes are considered to be the most likely species for gold transport in hydrothermal solutions because of their high thermodynamic stability and availability of reduced S and Cl ligands in most ore fluids (Mikucki, 1998). According to Pirajno (2009), at temperatures below 400°C the gold is transported in solution mainly as AuHS(aq.) at low pH and as $AuHS^-$ at neutral pH, and in the temperature range between 300 and 400°C these complexes are destabilized and Au is precipitated. At higher temperatures, Au tends to be transported as a chloride complex (Gammons et al., 1994). Fayek and Kyser (1995) present a diagram with the stability fields of chlorite, pyrite, pyrrhotite and hematite as a function of log $f\ O_2$ and log $f\ S_2$ at 300°C and 1.5 kbar for the quartz vein gold mineralization from Contact Lake deposit (Fig. 23). At Jaqueira the gold is typically associated with classic assemblage quartz + sericite + chlorite + pyrite from sericitic hydrothermal alteration at both host rocks and quartz vein. This assemblage suggests a near-neutral to slightly alkaline pH for the mineralized fluid (e.g., Mikucki, 1998). Microthermometric data and chlorite geothermometry showed P-T conditions of 1.62 to 1.98 kbar and temperature ranges from 302 to 346°C. Therefore, it is reasonable to suggest reduced conditions for the mineralizing fluid at Jaqueira and that gold was transported mainly by bisulfide complexes.

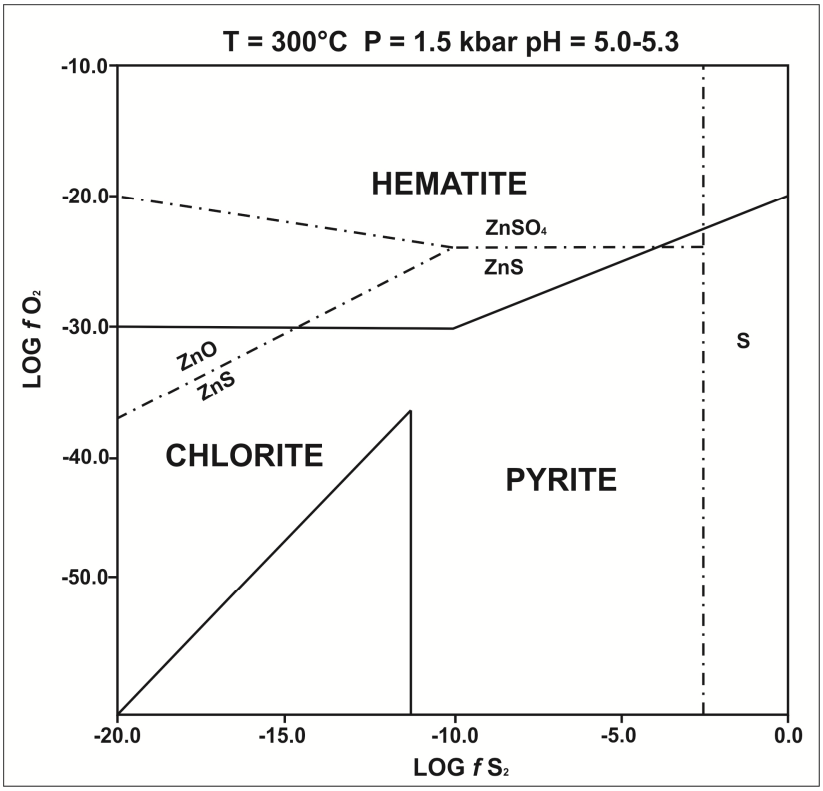

Fig. 23. Stability fields of selected mineral phases as a function of oxygen and sulfur fugacity. The hydrothermal assemblage with coexistence of pyrite + chlorite and physicochemical conditions suggests reduced conditions for the mineralizing fluid from Jaqueira. The diagram is modified from Fayek and Kyser (1995 and references therein).

Fluid immiscibility is an important process that causes gold precipitation and may be triggered by progressive cooling or a decrease in pressure (Wilkinson, 2001). Microthermometric investigations carried out at types WC and We inclusions and it is possible to assume that this FIA was formed by fluid immiscibility between H_2O-CO_2-NaCl and H_2O-NaCl fluids. The pressure conditions estimations showed a range of 1.62 to 1.98 kbar. During vein development, pressure decreases rapidly while the discontinuities are progressively opened. After fluid filling and mineral precipitation (sealing), pressure increases again in the discontinuities. This vein development, called fault-valve model (Sibson et al., 1988), may be responsible for such pressure variations. Therefore, the decrease in pressure may be the inductor of fluid immiscibility.

Fluid-rock interaction may also cause gold to precipitate, especially when sulfidation on host rocks and quartz veins is observed. The sulfur species, such as H_2S and S from bisulfide complexes are consumed by the reaction of Fe with silicates to form Fe-sulfides on the wall rock. The S decrease in fluid destabilizes bisulfide complexes causing gold to precipitate (McCuaig and Kerrich, 1998 and references therein). Petrographic observations from fluid-rock interaction were corroborated by the consistency between chlorite geothermometry and microthermometric FI data. Besides, gold is commonly related to sulfide assemblage both at host rock and quartz vein. Thus fluid-rock interaction also seems to be a trigger for gold deposition.

In summary, it appears that gold deposition at Jaqueira occurred in response to, at least, two mechanisms: fluid immiscibility and fluid-rock interaction. We interpret that the main phase of gold deposition was associated with hydrothermal mineral assemblage precipitation.

8.3. The Serra de Jacobina orogenic hydrothermal mineral system proposition

On their revision about mineral systems, Hagemann et al. (2016) suggest the description of trigger, source, conduit, driver, throttle, trap, dispersion and preservation, in order to provide consistent fundamentals on the elaboration of GIS predictive prospective maps.

Considering some consistent studies performed in the northeastern São Francisco Craton available in the literature (including the Serra de Jacobina), the present work gives support to a hydrothermal mineral system for the structurally-controlled Au-bearing quartz veins.

The trigger, also called critical window by Huston et al. (2016), which creates geological conditions that favor Au-bearing quartz veins development, was the Paleoproterozoic collision that occurred between the Gavião-Lençóis and the Mairi blocks. This collision zone defines the Contendas-Mirante-Jacobina Lineament and the Serra de Jacobina represents its northern segment (Barbosa et al., 2003; Cruz et al., 2016).

The source of the mineralized fluids was not the goal of this study, but some inferences can be made considering the geotectonic context. The H_2O-CO_2-NaCl and H_2O-NaCl mineralized fluids show temperature ranges, salinities and P-T formation conditions that resemble orogenic gold fluids (Bodnar et al., 2014). These orogenic fluids could be derived from devolatilization reactions during prograde metamorphism that occurred during Paleoproterozoic collision. Oxygen and deuterium isotope geochemistry results from sericite in the barren quartz veins hosted by the Serra do Córrego metaconglomerates, indicate composition close to those of magmatic fluids, associated with felsic melt, probably derived from several Paleoproterozoic granitic intrusions (Milesi et al., 2002). This diversity of fluid types is expected in a collisional context (McCuaig and Kerrich, 1998) and an effort on studies focused on this question is suggested.

The hydrothermal fluids at Serra de Jacobina flowed along the Pindobaçu and Maravilha fault systems, here considered the main conduits of the system. The Pindobaçu Fault System, or Pindobaçu Suture, is a deep mantle structure that sets the boundary between the Gavião-Lençóis and the Mairi blocks (Fig. 1). This structure allowed aqueous and aqueous carbonic “hotter” fluids upwards to the upper crust. The Maravilha fault system is a shallower structure restricted to the upper crust (Santos et al., 2019). This structure allowed fluid flow and, subsequently, fluid-rock interaction with the Jacobina Group and the Vale do Coxo ultramafic rocks. It also permitted circulation of a late, high salinity, cooler aqueous fluid that mixed with hotter aqueous and aqueous carbonic fluids. The structurally-controlled Au-bearing veins are hosted by second and locally third-order structures in all of these fault systems.

The lithospheric instabilities that initiate mineralizing events (the driver) at Serra de Jacobina orogenic context, is the compression-driven fluid flow type (Hagemann et al., 2016) and probably started when the Gavião-Lençóis and the Mairi blocks collided. The pressure variation during hydrothermal assemblage precipitation indicates a fault-valve behavior (Sibson et al., 1988) during development of the mineralized veins. This fluid flow focused in time and space, may be considered a throttle in hydrothermal structurally-controlled systems (Hagemann et al., 2016).

The trap for gold precipitation occurred in response to, at least, two mechanisms: fluid immiscibility and fluid-rock interaction. The sericitic alteration is widespread in the Jacobina Group and in some places the quartzite outcrops display green color. In the Vale do Coxo metaultramafic rocks sericitic alteration is pervasive and, within quartz veins, is filling-fracture type. Sulfidation is subordinated to the sericitic alteration in the Vale do Coxo rocks. Within quartz veins is filling-fracture type and at host quartzites is disseminated. Despite this wide hydrothermal assemblage variation, there was no gold dispersion, and the grades usually are higher within quartz veins.

Orogenic deposits formed within stable cratonic lithosphere that were exhumed and not completely eroded, are likely to have a high probability of long-term preservation (McCuaig and Hornsky, 2014). The Serra de Jacobina represents the northern segment of the Contendas-Mirante-Jacobina Lineament (Barbosa et al., 2003; Cruz et al., 2016), northeastern portion of São Francisco Craton (Almeida, 1977). Couto et al. (1978) made some considerations about the morphological evolution of the Serra de Jacobina. According to these authors the mountain chain, with altitudes higher than a thousand meters, represents a morphologic featured preserved from the Post-Gondwana Denudation Cycle developed during the Upper Cretaceous (King, 1956). Thus, the Serra de Jacobina is hosted by a stable cratonic lithosphere preserved from denudation cycle that eroded the São Francisco Craton landscape.

9. Conclusions

The Serra de Jacobina is a 250-km-long N-S mountain range with several Au-bearing structurally controlled quartz vein deposits locally called *garimpos*. Four of these deposits, named Maravilha, Jaqueira, Morro da Palmeirinha and Mina Velha, were studied in the present investigation. It was possible to conclude that:

- ✓ Sericitic alteration is widespread within the rocks of the Jacobina Group. In the Vale do Coxo meta-ultramafic rocks, this alteration is pervasive. In the quartz veins, it is of the filling-fracture type. Sulfidation is subordinated to sericitic alteration both at quartzites and schists from the Jacobina Group and from the Vale do Coxo, respectively. Within quartz veins, sulfidation is of massive filling-fracture type and disseminated between quartz crystals.
- ✓ Pindobaçu and Maravilha are the first-order structures, although the mineralized veins are preferentially hosted by second, and locally third, order structures of these systems.

Petrographic, fluid inclusion and microprobe studies at the Jaqueira *garimpo* indicate that:

- ✓ The initial ore-forming fluids were a mixture of medium-high temperatures H_2O-CO_2-NaCl and H_2O-NaCl fluids with variable salinities.
- ✓ Hydrothermal assemblage and gold P-T formation conditions were between 1.62 and 1.98 kbar, and between 302 and 346°C.
- ✓ Gold deposition occurred in response to two main mechanisms: fluid immiscibility and fluid-rock interaction.
- ✓ A late, high salinity H_2O-NaCl fluid with low-medium temperatures was mixed into the system.

AKNOWLEDGMENTS

This work is part of results from *Projeto Área de Relevante Interesse Mineral Serra de Jacobina (ARIM Serra de Jacobina)*. It was carried out and published with permission from Geological Survey of Brazil board. DAM thanks all geologists and staffs from both mine and exploration teams of the JMC - *Jacobina Mineração e Comércio* (Yamana Gold, Inc.) for constructive discussions during fieldwork. Special thanks go to *ARIM Serra de Jacobina* team members. ELK acknowledges the Brazilian *Conselho Nacional de Desenvolvimento Científico e Tecnológico* – CNPq for research grant #306798/2016-6. Authors are grateful to the Microscopy and Microanalysis Laboratory (LMic) of the *Universidade Federal de Ouro Preto*, a member of the Microscopy and Microanalysis Network of Minas Gerais State/Brazil/FAPEMIG. DAM also thanks Dr. Carlos Marques de Sá from Universidade Federal de Sergipe and Dr. Luiz César Correa Gomes from Universidade Federal da Bahia for their constructive suggestions on the pre-submission manuscript.

REFERENCES

ANDERSON, M.R.; RANKIN, A.H.; SPIRO, B. Fluid mixing in the generation of mesothermal gold mineralization in the Transvaal sequence, Transvaal, South Africa. **European Journal of Mineralogy**, v. 4, n. 5, p. 933-948, 1992.

ALMEIDA, F.F.M. O cráton do São Francisco. **Revista Brasileira de Geociências**, São Paulo, v. 7, n. 4, p. 349-367, 1977.

BAKKER, R.J.; DIAMOND, L.W. Estimation of volume fractions of liquid and vapor phases in fluid inclusions, and definition of inclusion shapes. **American Mineralogist**, v. 91, p. 635-657, 2006. DOI: 10.2138/am.2006.1845

BARBOSA, J.S.F. Terrenos Metamórficos do embasamento. **In**: BARBOSA, J.S.F. (Coord.). **Geologia da Bahia**: pesquisa e atualização. Salvador: CBPM, 2012. v.1, p. 101-201.

BARBOSA, J.S.F.; SABATÉ, P. Archean and Paleoproterozoic crust of the São Francisco Craton, Bahia, Brazil: geodynamic features. **Precambrian Research**, v. 133, p. 1-27, 2004. DOI: 10.1016/j.precamres.2004.03.001.

BARBOSA, J.S.F.; SABATÉ, P.; MOACYR, M.M. O cráton do São Francisco na Bahia: uma síntese. **Revista Brasileira de Geociências**, São Paulo, v. 33, n. 1, p. 3-6, 2003.

BATEMAN, J.D. Uranium-bearing auriferous reefs at Jacobina, Brazil. **Economic Geology**, Lancaster, v. 54, p. 417-425, 1958.

BODNAR, R.J.; LECUMBERRI-SANCHEZ, P.; MONCADA, D.; STEELE-MACINNIS, M. Fluid Inclusions in Hydrothermal Ore Deposits. *In*: HOLLAND, H.D.; TUREKIAN, K.K. (Ed.) **Treatise on Geochemistry**. 2.ed. Oxford: Elsevier, 2014. p.119-142.

BOWERS, T.S.; HELGESON, H.C. Calculation of the thermodynamic geochemical consequences of non-ideal mixing in the system H_2O-CO_2-NaCl on phase relations in geological systems: equation of state for H_2O-CO_2-NaCl fluids at high pressures and temperatures. **Geochimica et Cosmochimica Acta, v.** 47, n. 7, p. 1247-1275, 1983. DOI: 10.1016/0016-7037(83)90066-2

BROWN, P.E. FLINCOR: a computer program for the reduction and investigation of fluid inclusion-data. **American Mineralogist**, v. 74, n. 11-12, p. 1390-1393, 1989.

BROWN, P.E., LAMB, W.M. P-V-T properties of fluids in the system H2O+CO2+NaCl: new graphical presentations and implications for fluid inclusions studies. **Geochimica et Cosmochimica Acta**, v. 53, n. 6, p. 1209-1221, 1989. DOI: 10.1016/0016-7037(89)90057-4.

CARVALHO, E.R. **A imiscibilidade de fluidos em mineralizações auríferas do tipo lode na Bacia Paleoproterozoica de Jacobina-BA**. 2001. 89f. Dissertação (Mestrado) - Instituto de Geociências, Universidade Estadual de Campinas, Campinas, 2001.

CATHELINEAU, M. Cation site occupancy in chlorite and illites as a function of temperature. **Clay Minerals**, v. 23, p. 471-485, 1988. DOI: 10.1180/claymin.1988.023.4.13

COLLINS, P. L. F. Gas hydrates in CO2-bearing fluid inclusions and the use of freezing data for estimation of salinity. **Economic Geology**, Lancaster, v. 74, p. 1435-1444, 1979.

COULIBALY, Y.; BOIRON, M.C.; CATHELINEAU, M.; KOUAMELAN, A.N. Fluid immiscibility and gold deposition in the Birimian quartz veins of the Angovia deposit (Yaoure, Yvory Coast). Journal of African Earth Sciences, v. 50, n. 2–4, p. 234-254, 2008. DOI: 10.1016/j.jafrearsci.2007.09.014.

COUTO, P.A.; SAMPAIO, A.R.; GIL, C. A.A. *et al*. **Projeto Serra de Jacobina**: geologia e prospecção geoquímica. Relatório Final. Salvador: CPRM, 1978. 12v. Convênio DNPM/CPRM.

COX, D.P. Regional environment of the Jacobina auriferous conglomerate, Brazil. **Economic Geology**, Lancaster, v. 62, p. 773-780, 1967.

CRUZ, S. C. P., BARBOSA, J. S. F., ALVES, E. S., DAMASCENO, G. C., MACHADO, G. S., BORGES, J. O., GOMES, A. M., MESQUITA, L., PIMENTEL, I., LEAL, A. B. M., PALMEIRA, D. S. **Mapeamento geológico e levantamentos de recursos minerais da Folha Caetité (Escala 1:100.000)**. Salvador: CPRM, 2009. 175p. Programa de Levantamentos Geológicos Básicos, Convênio CPRM/UFBA-FAPEX.

CRUZ, S.C.P.; BARBOSA, J. S. F.; PINTO, M.S.; PEUCAT, J.J.; PAQUETTE, J.L.; SOUZA, J.S.; MARTINS, V.S.; CHEMALE JUNIOR, F.; CARNEIRO, M.A. The Siderian-Orosirian magmatism in the Gavião Paleoplate, Brazil: U-Pb geochronology, geochemistry and tectonic implications. **Journal of South American Earth Science**, v. 69, p. 43-79, 2016. DOI: 10.1016/j.jsames.2016.02.007.

DE CARITAT, P.; HUTCHEON, I.; WALSHE, J.L. Chlorite geothermometry: a review. **Clays and Clay Minerals**, v. 41, p. 219-239, 1993. DOI: 10.1346/CCMN.1993.0410210.

FAYEK, M.; KYSER, T.K. Characteristics of Auriferous and Barren Fluids Associated with the Proterozoic Contact Lake Deposit, Saskatchewan, Canada. **Economic Geology**, Lancaster, v.90, p.385-406, 1995.

GAMMONS, C.H.; WILLIAMS-JONES, A.E.; YU, Y. New data on the stability of gold chloride complexes at 300°C. **Mineralogical Magazine**, v.58A, p. 309-310, 1994.

GOLDSTEIN, R.H.; REYNOLDS, T.J. **Systematics of fluid inclusions in diagenetic minerals**. Oklahoma, USA: Society for Sedimentary Geology, 1994.

GROSS, W.H. Evidence for a modified placer origin for auriferous conglomerates, Canavieiras Mine, Jacobina, Brazil. **Economic Geology**, Lancaster, v.63, p.271-276, 1968.

GUIMARÃES, J.T. *et al*. Supergrupos Espinhaço e São Francisco. *In*: BARBOSA, J.S.F. (Coord.) **Geologia da Bahia**: pesquisa e atualização. Salvador: CBPM, 2012. v.2, p. 33-85.

HAGEMANN, S.G.; LISITSIN, V.A.; HUSTON, D.L. Mineral system analysis: quo vadis. **Ore Geology Review**, Perth, Austrália, v. 76, p. 504-522, 2016. DOI: 10.1016/j.oregeorev.2015.12.012

HEY, M.H. A new review of the chlorites. **Mineralogical Magazine**, v. 30, p. 277-292, 1954. DOI: 10.1180/minmag.1954.030.224.01.

HUIZENGA, J.M.; TOURET, J.L.R. Fluid inclusion in shear zones, the case fo Umwindsi shear zone in the Harare-Shamva-Bindura greenstone belt, NE Zimbabwe. **European Journal of Mineralogy**, v. 11, n. 6, p. 1079-1090, 1999. DOI: 10.1127/ejm/11/6/1079.

HUSTON, D.L.; MERNAGH, T.P.; HAGEMANN, S.G.; DOUBLIER, M.P.; FIORENTINI, M.; CHAMPION, D.C.; LYNTON, J.A.; CZARNOTA, K.; CAYLEY, R.; SKIRROW, R.; BASTRAKOV, E. Tectono-metallogenic systems - the place of mineral systems within tectonic evolution, with an emphasis on Australian examples. **Ore Geology Reviews**, v. 76, p. 168-210, 2016. DOI: 10.1016/j.oregeorev.2015.09.005.

KING, L.C. A geomorfologia do Brasil Oriental. **Revista Brasileira de Geografia**, v. 18, p. 147-265, 1956.

KLEIN, E.L.; HARRIS, C.; GIRET, A.; MOURA, C.A.V. The Cipoeiro gold deposit, Gurupi Belt, Brazil: Geology, chlorite geochemistry, and stable isotope study. **Journal South American Earth Sciences**, v. 23, p. 242-255, 2007. DOI: 10.1016/j.jsames.2006.09.002.

KRANITOIDS, P.; MACLEAN, W.H. Systematics of chlorite alteration at the Phelps Dodge massive sulfide deposit, Matagami, Quebec. **Economic Geology**, Lancaster, v. 82, p. 1898-1911, 1987.

LEDRU, P.; MILÉSI, J.P.; SABATÉ, P.; MALUSKI, H. Foreland basins and gold-bearing conglomerates: a new model for the Jacobina Basin (São Francisco Province, Brazil). **Precambrian Research**, v. 86, p. 155-176, 1997.

LEITE, C.M.M. *et al*. Nódulos de quartzo=simimanita em cinturões orogênicos:petrogênese e significado geodinâmico na evolução do orógeno Itabuna-Salvador-Curaçá na região de Mundo Novo, Bahia. *In*: SIMPÓSIO SOBRE O CRÁTON SÃO FRANCISCO, 3., 2005, Salvador, **Anais** [...] Salvador: CBPMUFBA, SBG, 2005. p. 235-238.

LEO, G.N.; COX, D.P.; CARVALHO, J.P.P. **Geologia da parte sul da Serra de Jacobina, Bahia, Brasil**. Rio de Janeiro: DNPM, 1964.

LORD, R.A.; PRICHARD, H.M.; SÁ, J.H.S.; NEARY, C.R. Chromitite Geochemistry and PGE Fractionation in the Campo Formoso Complex and Ipueira-Medrado Sill, Bahia State, Brazil. **Economic Geology**, Lancaster, v. 99, n. 2, p. 339-364, 2004. DOI: 10.2113/gsecongeo.99.2.339.

LOUCKS, R.R. Precise geothermometry on fluid inclusions populations that trapped mixtures of immiscible fluids. **American Journal of Science**, v. 300, p. 23-59, 2000.

MASCARENHAS, J.F. *et al*. Geologia e metalogenis de parte do greenstone belt de Mundo Novo e do Grupo Jacobina. *In*: CONGRESSO BRASILEIRO DE GEOLOGIA, 39., 1996, Salvador. **Roteiro da excursão** [...] Salvador: SBG, 1996. E-10.

MASCARENHAS, J.F. *et al*. **Geologia e recursos minerais do Grupo Jacobina e da parte sul do Greenstone Belt de Mundo Novo**. Salvador: CBPM, 1998. (Série Arquivos Abertos, 13).

MARTIN, H.; PEUCAT, J. J.; SABATE, P.; CUNHA, J. Crustal evolution of the early Archean of South America: example of the Sete Voltas Massif, Bahia State, Brazil. **Precambrian Research**, v. 82, p. 35-62, 1997. DOI: 10.1016/S0301-9268(96)00054-X.

McCUAIG, T.C.; KERRICH, R. P-T-t-deformation-fluid characteristics of lode gold deposits: evidence from alteration systematics. **Ore Geology Review**, Perth, Austrália, v. 12, p. 381-453, 1998. DOI: 10.1016/S0169-1368(98)80002-4.

McCUAIG, T.C.; BERESFORD, S.; HRONSKY, J. Translating the mineral system approach into an effective exploration targeting system. **Ore Geology Reviews**, Perth, Austrália, v. 38, p. 128-138, 2010. DOI: 10.1016/j.oregeorev.2010.05.008.

McCUAIG, T.C.; HRONSKY, J.M.A. **The mineral system concept**: the key to exploration targeting. Lancaster, PA: Society of Economic Geologists, 2014. p.153-176. (Special Publications, 18). DOI: 10.5382/SP.18.08

MENEZES, R.C.L., REIS, C., MIRANDA, D.A., SANTOS, F.P., BURGOS, C.M.C., RODRIGUES, J.B. Complexo Cromitífero de Campo Formoso: Evento Ultramáfico de 3,2 Ga no Cráton do São Francisco. *In*: CONGRESSO BRASILEIRO DE GEOLOGIA, 49., 2018, Rio de Janeiro. **Anais** [...] Rio de Janeiro: SBG, 2018.

MIKUCKI, E.J. Hydrothermal transport and depositional processes in Archean lode-gold systems: A review. **Ore Geology Review**, Perth, Austrália, v. 13, p. 307-321, 1998. DOI: 10.1016/S0169-1368(97)00025-5

MILESI, J.P.; LEDRU, P.; MARCOUX, E.; MOUGEOT, R.; JOHAN, V.; LEROUGE, C.; SABATÉ, P.; BAILLY, L.; RESPAUT, J.P.; SKIPWITH, P. The Jacobina Paleoproterozoic gold-bearing conglomerates, Bahia, Brazil: a “hydrothermal shear-reservoir” model. **Ore Geology Review**, Perth, Austrália, v. 19, p. 95-136, 2002. DOI: 10.1016/S0169-1368(01)00038-5.

MISI, A.; TEIXEIRA, J.B.G.; SÁ, J.H.S. (Coord.) **Mapa metalogenético digital do Estado da Bahia e principais províncias minerais**. Salvador: CBPM, 2012. 237p. (Série Publicações Especiais, 11). Convênio CBPM, DNPM, UFBA-CPGG.

NASH, J.T. **Fluid inclusions petrology**: data from porphyry copper deposits and applications to exploration. Washington: USGS, 1976. 16p. (Professional Paper, 907D).

PADILHA, A. L.; VITORELLO, I.; PÁDUA, M.B.; FUCK, R.A. Magnetotelluric images of Paleoproterozoic accretion and Mesoproterozoic to Neoproterozoic reworking processes in the northern São Francisco Craton, central-eastern Brazil. **Precambrian Research**, v. 333, 105416, 2019. DOI: 10.1016/j.precamres.2019.105416.

OLIVEIRA, E.P.; MCNAUGHTON, N.J.; ARMSTRONG, R. Mesoarchean to Paleoproterozoic growth of the northern segment of the Itabuna-Salvador orogen, São Francisco Craton, Brazil. *In*: KUSKY, T.M.; ZHAI, M.G.; XIAO, W. **The evolving continents**: understanding processes of continental growth. London: Geological Society, 2010. p. 263-286. (Geological Society. Special Publication, 338).

PEARSON, W.; MACÊDO, P.M., RÚBIO, A., LORENZO, C.L., KARPETA, P. Geology and gold mineralization of the Jacobina Mine and Bahia Gold Belt, Bahia, Brazil and a comparison to Tarkwa and Witwatersrand. *In*: RHODEN, H.N.; STEININGER, R.C.; VIKRE, P.G. (Ed.) **Geological Society of Nevada Symposium 2005**. Reno, Nevada: GSN, 2005. p.757-785.

PIRAJNO, FRANCO**. Hydrothermal Processes and Mineral Systems**. Perth, Austrália: Springer, 2009.

REIS, C.; OLIVEIRA, R.C.L.; MIRANDA, D.A.; SANTOS, F.P.; GUIMARÃES, J.T.; TELES, G. Estratigrafia do Grupo Jacobina. In: CONGRESSO BRASILEIRO DE GEOLOGIA, 49., 2018, Rio de Janeiro. **Anais** [...] Rio de Janeiro: SBG, 2018.

REIS, C.; MENEZES, R.C.L.; MIRANDA, D.A.; SANTOS, F.P.; LOUREIRO, H.S.C.; NEVES, J.P.; VIEIRA, R. **ARIM - Serra de Jacobina**: Mapa Geológico. Salvador : CPRM, 2019. 1 mapa color., 90,0 x 130,0 cm. Escala 1:250.000. Programa Gestão Estratégica da Geologia, da Mineração e da Transformação Mineral.

ROEDDER, E. **Fluid inclusions**. Reston, Virginia, USA: Mineralogical Society of America, 1984. 664p. (Reviews in Mineralogy, 12).

SABATÉ, P.; MARINHO, M.M.; VIDAL, P.; VACHETTE, M.C. The 2-Ga peraluminous magmatism of the Jacobina-Contendas Mirante belts (Bahia-Brazil): geologic and isotopic constraints on the sources. **Chemical Geology**, v. 83, p. 325-338, 1990. DOI: 10.1016/0009-2541(90)90288-I.

SANTO-PINTO, M.; PEUCAT, J. J.; MARTIN, H.; BARBOSA, J.S.F.; FANNING, M.; COCHERIE, A.; PAQUETTE, J.L. Crustal evolution between 2.0 and 3.5 Ga in the southern Gavião block (Umburanas-Brumado-Aracatu region), São Francisco Craton, Brazil: a 3.5-3.8 Ga proto-crust in the Gavião block? **Journal oh South American Earth Sciences**, v. 40, p. 129-142, 2012. DOI: 10.1016/j.jsames.2012.09.004.

SANTOS, F.P.; CHEMALE JUNIOR, F.; MENESES, A.R.A.S. The nature of the Paleoproterozoic orogen in the Serra de Jacobina Range and adjacent areas, northern São Francisco Craton, Brazil, based on structural geology and gravimetric modeling. **Precambrian Research**, v. 332, 105391, 2019. DOI: 10.1016/j.precamres.2019.105391.

SIBSON, R.H.; ROBERT, F.; POULSEN, K.H. High-angle reverse faults , fluid pressure cycling, and mesothermal gold-quartz deposits. **Economic Geology**, v. 16, p. 551-555, 1988. DOI: 10.1130/0091-7613(1988)016<0551:HARFFP>2.3.CO;2.

SILVA, L.C. *et al*. U-Pb SHRIMP ages in the Itabuna-Caraíba TTG high-grade complex: the first window beyond the paleoproterozoic overprint of the eastern Jequié craton, NE Brazil. *In*: ISGAM - INTERNATIONAL SYMPOSIUM ON GRANITES AND ASSOCIATED MINERALIZATION, 1997, Salvador. **Abstracts** […] Salvador: SBG, 1997, v.1, p. 282-283.

SILVA, L.C.; ARMSTRONG, R.; DELGADO, I.M.; PIMENTEL, M.; ARCANJO, J.B.; MELO, R.C.; TEIXEIRA, L.R.; JOST, H.; CARDOSO FILHO, J.M.; PEREIRA, L.H.M. Reavaliação da evolução geológica em terrenos pré-cambrianos brasileiros com base em novos dados U-Pb SHRIMP, parte I: limite centro-oriental do Cráton do São Francisco. **Revista Brasileira de Geociências**, São Paulo, v. 32, n. 4, p. 501-502, 2002.

SUN, S.S.; MCDONOUGH, W.F. **Chemical and isotopic systematics of oceanic basalts**: implications for mantle composition and processes. London: Geological Society, 1989. p. 313-345. (Special Publication,. 42). DOI: 10.1144/GSL.SP.1989.042.01.19.

TEIXEIRA, L.R. **O Complexo Caraíba e a Suíte São José do Jacuípe no cinturão Salvador-Curaçá (Bahia-Brasil)**: petrologia, geoquímica e potencial metalogenético. 1997. 202f. Tese (Doutorado) – Instituto de Geociências, Universidade Federal da Bahia, Salvador, 1997.

TEIXEIRA, J.B.G.; SOUZA, J.A.B.; SILVA, M.G.; LEITE, C.M.M.; BARBOSA, J.S.F.; COELHO, C.E.S.; ABRAM, M.B.; FILHO, V.M.C.; IYER, S.S.S. Gold mineralization in the Serra de Jacobina region, Bahia Brazil: tectonic framework and metallogenesis. **Mineralium Deposita**, Alemanha, v. 36, p. 332-344, 2001. DOI: 10.1007/s001260100174.

TEIXEIRA, J.B.G.; SILVA, M.G.; MISI, A.; CRUZ, S.C.P.; SÁ, J.H.S. Geotectonic setting and metallogeny of the northern São Francisco craton, Bahia, Brazil. **Journal of South American Earth Sciences**, v. 30, n. 2, p. 71-83, 2010. DOI: 10.1016/j.jsames.2010.02.001.

TEIXEIRA, J.B.G.; MISI, A.; SILVA, M.G.; BRITO, R.S.C. Reconstruction of Precambrian terranes of Northeastern Brazil along Cambrian strike-slip faults: A new model of geodynamic evolution and gold metallogeny in the State of Bahia. **Brazilian Journal of Geology**, São Paulo, v.49. n. 3, 2019. DOI: 10.1590/2317-4889201920190009

TELES, G.; CHEMALE, F.; OLIVEIRA, C.G. Paleoarchean record of the detrital pyrite-bearing, Jacobina Au-U deposits, Bahia, Brazil. **Precambrian Research**, v.256, p.289-313, 2015. DOI: 10.1016/j.precamres.2014.11.004.

TELES, G.; CHEMALE, F.; ÁVILA, J.N; IRELAND, T.R.; DIAS, A.N.C.; CRUZ, D.C.F.; CONSTANTINO, C.J.L. Textural and geochemical investigation of pyrite in Jacobina Basin, São Francisco Craton, Brazil: Implications for paleoenvironmental conditions and formation of pre-GOE metaconglomerate-hosted Au-(U) deposits. **Geochimica et Cosmochimica Acta**, v.273, p.331-353, 2020. DOI: https://doi.org/10.1016/j.gca.2020.01.035.

VIDAL, O.; PARRA, T.; TROTET, F. A thermodynamic model for Fe-Mg aluminous chlorite using data from phase equilibrium experiments and natural politic assemblages in the 100°C to 600°C and 1 to 25kb range. **American Journal of Science**, v. 301, p. 557-592, 2001. DOI:10.2475/ajs.301.6.557

WHITE, M.G. **Origin of uranium and gold in the quartzite-conglomerate of the Serra de Jacobina**. Washington: USGS, 1961. (Profissional Paper, 424-B).

WYBORN, L.A.I.; HEINRICH, C.A.; JAQUES, A.L. Australian proterozoic mineral systems: essential ingredients and mappable criteria. *In*: AUSTRALIAN INSTITUTE OF MINING AND METALLURGY ANNUAL CONFERENCE, 1994, Melbourne. **Procedings** […] Melbourne: Australian Institute of Mining and Metallurgy, 1994. p.109-115.

WILKINSON, J.J. Fluid inclusions in hydrothermal ore deposits. **Lithos**, v. 55, p. 229-272, 2001. DOI: 10.1016/S0024-4937(00)00047-5.

YAMANA ANNUAL REPORT. The beginning of what's next, 2018. 180p. Toronto, Canada. Available online at: www.yamana.com.

ZANE, A.; WEISS, Z. A procedure for classifying rock-forming chlorites based on microprobe data. **Rendiconti Lincei**, v. 9, n. 1, p. 51-56, 1988. DOI: 10.1007/BF02904455.

ZANG, W.; FYFE, W.S. Chloritization of the hydrothermally altered bedrock at the Igarapé Bahia gold deposit, Carajás, Brazil. **Mineralium Deposita**, v. 30, n. 1, p. 30-38, 1995. DOI: 10.1007/BF00208874.

ZINCONE, S.A.; BARBUENA, D.; OLIVEIRA, E.P.; BALDIM, M.R., 2017. Detrital zircon U-Pb ages as evidence for deposition of the Saúde Complex in a Paleoproterozoic foreland basin, northern São Francisco Craton, Brazil. **Journal of South American Earth Sciences**, v. 79, p. 537-548, 2017. DOI: 10.1016/j.jsames.2017.09.009

APPENDIX A. SUPPLEMENTARY DATA

Supplementary Table 1 - Chemical compositions of the quartz veins and host rocks from the Maravilha, Jaqueira, Morro da Palmeirinha and Mina Velha *garimpos*. Major elements results are presented in weight percent (wt. %), trace and rare earth elements (REE) in parts per million (ppm), Au, Pd and Pt in parts per billion (ppb).

GARIMPO	**Maravilha**				**Jaqueira**			
Sample ID	**HHI-282**	**HHI-283**	**HHI-287**	**HHI-288**	**HHI-295**	**HHI-296**	**HHI-297**	**HHI-298**
Rock	Quartz vein	Quartz vein	Quartz vein	Quartz vein	Quartz vein	Quartzite	Quartzite	Biotite Schist
Elements								
SiO_2	94,7	>99	94,7	96,5	98,3	75,4	66,2	63,2
TiO_2	0,1	0,03	0,32	0,19	0,03	1,55	2,13	1,73
Fe_2O_3	0,99	0,78	2,48	1,97	0,64	1,6	1,8	11,8
Al_2O_3	2,93	0,65	0,94	0,52	0,8	13,8	19,8	15,7
MgO	0,59	0,11	0,49	0,18	<0,1	0,37	0,58	0,18

GARIMPO	Maravilha				Jaqueira			
Sample ID	**HHI-282**	**HHI-283**	**HHI-287**	**HHI-288**	**HHI-295**	**HHI-296**	**HHI-297**	**HHI-298**
MnO	<0,01	<0,01	<0,01	0,01	<0,01	<0,01	<0,01	<0,01
CaO	<0,01	0,01	<0,01	0,01	<0,01	0,02	0,03	0,02
K_2O	0,02	<0,01	<0,01	<0,01	0,19	1,85	3,28	1,3
Na_2O	<0,1	<0,1	<0,1	<0,1	<0,1	0,11	0,24	<0,1
P_2O_5	0,049	<0,01	<0,01	0,01	0,012	0,076	0,135	0,064
Cr_2O_3	0,02	0,01	<0,01	0,01	0,01	0,02	0,02	<0,01
LOI	1	0,08	1,5	0,72	0,06	4,62	6,35	5,27
Ag	<0,02	0,11	<0,02	<0,02	0,07	<0,02	<0,02	<0,02
As	1	<1	5	2	1	15	19	6
Ba	5	<5	10	28	107	766	788	301
Be	0,5	0,2	0,3	0,3	0,3	3	2,9	2,1
Bi	0,14	<0,04	0,22	0,13	0,06	0,41	0,33	1
Cd	0,05	0,04	0,07	0,07	0,06	0,07	0,06	0,06
Co	41,4	3,3	25,9	12,5	0,8	6,6	6,5	11,9
Cr	24	8	23	13	9	23	48	37
Cs	<5	<5	<5	<5	<5	<5	<5	<5
Cu	3,7	2,5	50,1	22,9	2,6	19	9,8	31,8
Ga	4,6	1	3	2	1	24,2	34,9	29,8
Ge	<0,1	<0,1	0,2	0,1	<0,1	<0,1	0,3	<0,1
Hf	1,31	0,19	0,75	0,55	1,2	5,73	7,27	3,84
In	<0,02	<0,02	<0,02	<0,02	<0,02	0,07	0,08	0,06
Li	22	2	5	3	1	7	18	28
Mo	0,36	0,27	0,8	0,73	0,57	0,61	0,34	0,39
Nb	0,9	0,3	2,8	2,1	1,3	9	3,8	0,5
Ni	91,5	9,5	85,3	35,8	3,3	23,7	13,2	13,7
Pb	21,1	1,7	5,3	2,7	1,2	3,2	11,9	6,1
Rb	0,7	0,6	1	3,4	4,1	49,5	93,5	37,1
S	<0,01	<0,01	1,01	0,53	<0,01	0,1	0,06	<0,01
Sb	0,25	0,07	0,11	0,11	1,22	0,69	0,54	0,26
Sc	5,9	1,7	2,2	2,7	1,5	39	53,3	54
Se	<2	<2	<2	<2	<2	<2	<2	<2
Sn	0,7	0,5	0,9	0,9	1	2,2	2,6	2,7
Sr	74,7	15,1	4,2	23,3	10,8	90,7	197,5	40,7
Ta	0,18	<0,05	0,14	0,23	0,29	1,01	0,25	0,06
Te	<0,05	<0,05	0,11	0,07	0,36	0,23	0,09	0,06
Th	2,2	0,4	0,4	0,5	1,4	4,9	8,2	5
Ti	0,05	0,01	0,18	0,11	<0,01	0,88	0,95	0,69
Tl	<0,02	<0,02	<0,02	<0,02	0,17	0,16	0,24	0,09
U	0,5	<0,1	0,2	0,6	0,4	2,1	2,1	2
V	18	6	24	13	5	190	201	372
W	2,5	0,3	4,8	4,3	1,3	27,1	2,9	0,6
Y	3,2	0,7	2,2	2,4	2	111,3	41,6	25,7
Zn	7	2	38	29	3	4	5	14

GARIMPO	Maravilha				Jaqueira			
Sample ID	**HHI-282**	**HHI-283**	**HHI-287**	**HHI-288**	**HHI-295**	**HHI-296**	**HHI-297**	**HHI-298**
Zr	45,9	8,2	26,1	17,8	31,8	200,9	233,6	159,8
La	46,8	6,5	3,4	2,3	5,7	46,1	89,2	13
Ce	101,2	13,9	8	5,6	11,6	89,4	175,5	28,8
Pr	12,4	1,57	1	0,69	1,32	10,78	20,75	3,42
Nd	49,6	5,2	3,8	2,5	4,5	42,3	81,1	13,3
Sm	7,6	0,8	0,9	0,6	0,8	8,3	16,1	3,6
Eu	1,85	0,21	0,26	0,21	0,19	2,42	4,47	1,3
Gd	3,35	0,42	0,73	0,57	0,72	9,98	16,39	4,43
Tb	0,23	<0,05	0,08	0,07	0,07	1,69	2,07	0,74
Dy	0,7	0,13	0,41	0,3	0,36	12,67	10,54	4,49
Ho	0,11	<0,05	0,08	0,05	0,06	3,02	1,77	0,91
Er	0,34	0,07	0,18	0,13	0,24	9,42	4,55	2,67
Tm	0,05	<0,05	<0,05	<0,05	<0,05	1,23	0,6	0,39
Yb	0,3	<0,1	0,2	0,1	0,3	7,2	3,9	2,5
Lu	<0,05	<0,05	<0,05	<0,05	<0,05	1,11	0,57	0,41
Au	92	47	95	214	10	1343	51	82
Pd	<5	<5	<5	<5	<5	<5	<5	<5
Pt	<5	<5	<5	<5	<5	<5	<5	<5

GARIMPO	Jaqueira					Morro da Palmeirinha		
Sample ID	**HHI-300**	**HHI-301**	**HHI-302**	**HHI-303**	**HHI-304**	**HHI-255**	**HHI-256**	**HHI-257**
Rock	Quartz vein	Quartz vein	Quartz vein	Biotite Schist	Quartz vein	Quartz vein	Quartz vein	Quartz vein
Elements								
SiO_2	97,2	98,6	97,9	57,4	96,6	97,9	96,8	96,3
TiO_2	0,1	0,05	0,05	1,8	0,08	0,05	0,05	0,13
Fe_2O_3	0,98	0,91	0,95	10,7	1,16	0,78	0,88	1,1
Al_2O_3	1,13	0,83	0,87	15,8	1,28	0,97	0,95	1,66
MgO	0,12	<0,1	<0,1	2,81	0,3	0,22	0,24	0,43
MnO	<0,01	<0,01	<0,01	0,1	<0,01	<0,01	<0,01	0,01
CaO	<0,01	<0,01	<0,01	1,11	0,01	0,04	0,04	0,11
K_2O	0,26	0,22	0,25	2,35	0,19	0,02	0,01	0,03
Na_2O	<0,1	<0,1	<0,1	<0,1	<0,1	<0,1	<0,1	0,14
P_2O_5	0,015	0,012	0,016	0,067	0,01	<0,01	<0,01	<0,01
Cr_2O_3	<0,01	0,01	<0,01	<0,01	<0,01	0,01	<0,01	0,04
LOI	0,21	<0,01	0,08	7,67	0,56	0,05	0,07	0,21
Ag	0,99	<0,02	<0,02	<0,02	0,05	0,34	3,16	0,41
As	16	2	2	12	33	<1	<1	<1
Ba	113	88	128	1266	104	12	10	6
Be	0,3	0,2	0,3	2,5	0,3	7,1	3,9	5,9
Bi	0,24	0,06	0,15	0,6	0,95	1,09	1,4	0,46
Cd	0,05	0,04	0,05	0,1	0,08	0,06	0,05	0,05
Co	2,2	1,2	1,9	21,6	5,6	0,9	1,1	1,8
Cr	8	8	7	40	11	9	10	59
Cs	<5	<5	<5	<5	<5	<5	<5	<5
Cu	13,7	14,1	27,3	78,3	41	8,6	13,7	7,7

GARIMPO	Jaqueira					Morro da Palmeirinha		
Sample ID	**HHI-300**	**HHI-301**	**HHI-302**	**HHI-303**	**HHI-304**	**HHI-255**	**HHI-256**	**HHI-257**
Ga	2,3	1,7	1,8	30,9	2,5	1,5	1,6	2,5
Ge	<0,1	<0,1	<0,1	<0,1	<0,1	<0,1	<0,1	<0,1
Hf	1,83	1,21	1,1	4,56	1,64	1,06	1,09	1,04
In	<0,02	<0,02	<0,02	0,16	<0,02	<0,02	<0,02	<0,02
Li	2	1	1	34	4	2	2	2
Mo	2,27	0,6	0,59	1,1	1,25	0,21	0,32	0,32
Nb	1	0,5	0,8	8,7	1,2	0,5	0,5	0,5
Ni	2,8	2,4	2,3	10,4	10	3,8	4,4	7,6
Pb	4,2	1,8	2,2	8,8	3,2	1,3	1,4	0,8
Rb	5,1	4,6	4,5	68,9	6,6	1	1	1,2
S	0,15	0,1	0,18	0,71	0,08	<0,01	<0,01	<0,01
Sb	0,14	0,09	0,07	0,31	0,26	<0,05	<0,05	<0,05
Sc	3,2	1,7	1,9	54,8	4,7	1,6	1,9	4,3
Se	<2	<2	<2	<2	<2	<2	<2	<2
Sn	0,9	0,7	0,7	2,9	0,8	0,6	0,6	0,8
Sr	11,2	15	20,1	65,9	14,3	6,5	7,2	7
Ta	<0,05	<0,05	0,05	0,54	0,1	<0,05	<0,05	<0,05
Te	0,07	<0,05	<0,05	0,25	0,13	0,1	0,15	0,07
Th	1,7	1,1	1,1	4,5	2,7	0,9	1	0,5
Ti	0,05	0,02	0,02	1,01	0,04	0,01	0,01	0,04
Tl	0,03	<0,02	<0,02	0,19	<0,02	<0,02	<0,02	<0,02
U	0,6	0,3	0,3	1,2	0,8	0,4	0,4	0,5
V	15	10	10	364	17	5	5	16
W	1,2	0,9	1	2,1	4,7	0,8	1,1	1,2
Y	4,5	3,4	3,2	18,3	8,5	2,8	2,9	4,3
Zn	3	3	1	44	11	11	5	6
Zr	68,1	44,4	40,8	154	49,8	34,5	34,7	37,7
La	8,5	5,4	8,1	20,3	8,1	4,2	3,8	2
Ce	16,8	11,1	16,7	40,6	16	8,3	9,2	2,8
Pr	1,86	1,25	1,84	4,69	1,75	0,88	1,01	0,26
Nd	6,2	3,9	6	18,6	5,8	2,7	3,2	0,3
Sm	1,2	0,8	1,1	4,5	1,1	0,7	0,7	0,2
Eu	0,3	0,22	0,25	1,28	0,29	0,14	0,14	0,08
Gd	1,02	0,63	0,81	4,5	1,22	0,68	0,62	0,47
Tb	0,19	0,1	0,12	0,66	0,21	0,1	0,09	0,12
Dy	1,01	0,61	0,67	3,96	1,46	0,6	0,51	0,92
Ho	0,21	0,13	0,14	0,73	0,31	0,12	0,1	0,2
Er	0,66	0,41	0,46	1,99	0,88	0,39	0,32	0,59
Tm	0,12	0,06	0,07	0,29	0,12	0,06	<0,05	0,1
Yb	0,7	0,4	0,4	1,9	0,8	0,4	0,3	0,6
Lu	0,12	0,07	0,07	0,27	0,11	0,06	<0,05	0,08
Au	8922	628	137	538	1810	34118	98057	561
Pd	<5	<5	<5	<5	<5	<5	<5	<5
Pt	<5	<5	<5	<5	<5	6	<5	5

GARIMPO	Morro da Palmeirinha						
Sample ID	**HHI-258**	**HHI-260**	**HHI-261**	**HHI-263**	**HHI-264**	**HHI-265**	**HHI-266**
Rock Elements	Quartz vein	Quartz vein	Quartz vein	Quartz vein	Quartz vein	Quartz vein	Quartzite
SiO_2	96	72,2	60,9	92,3	91,5	87,5	66,4
TiO_2	0,05	0,02	0,02	0,13	0,16	0,26	0,8

GARIMPO	Morro da Palmeirinha						
Sample ID	**HHI-258**	**HHI-260**	**HHI-261**	**HHI-263**	**HHI-264**	**HHI-265**	**HHI-266**
Fe_2O_3	2,55	23,5	32,2	3,37	2,64	3,67	8,26
Al_2O_3	1,01	1,51	2	2,75	3,32	5,56	14,4
MgO	0,19	0,13	0,1	0,61	0,75	1,23	2,99
MnO	<0,01	0,02	0,02	<0,01	<0,01	<0,01	0,01
CaO	0,01	0,01	0,01	0,02	0,02	0,04	0,12
K_2O	0,02	0,02	0,02	0,01	<0,01	0,03	0,01
Na_2O	<0,1	<0,1	<0,1	0,18	0,21	0,5	0,74
P_2O_5	0,028	0,464	0,677	0,036	0,024	0,048	0,116
Cr_2O_3	0,02	0,04	0,05	0,06	0,03	0,04	0,14
LOI	0,2	2,89	3,88	0,55	0,39	0,81	2,53
Ag	2,13	3,77	<0,02	0,93	0,94	1,48	0,35
As	40	150	204	50	27	36	82
Ba	15	100	181	15	13	11	24
Be	2,7	3,3	4,6	1,7	1,5	1,8	2,6
Bi	38,85	95,98	100,48	50,59	57,19	94,92	175,2
Cd	0,07	0,08	0,19	0,06	0,05	0,05	0,07
Co	2	42,4	46,5	2,8	1	1,3	2,7
Cr	27	195	262	142	68	101	329
Cs	<5	<5	<5	<5	<5	<5	<5
Cu	35,2	513,6	443,7	39	21,5	19,8	35,5
Ga	1,4	2,3	3,6	4,9	5,6	10,4	23
Ge	<0,1	<0,1	0,2	<0,1	<0,1	<0,1	<0,1
Hf	0,96	0,97	1,51	4,74	3,31	1,7	8,24
In	<0,02	0,04	0,05	<0,02	<0,02	0,02	0,06
Li	1	1	2	2	2	3	6
Mo	0,49	6,52	7,5	0,99	1,39	1,44	4,19
Nb	0,2	0,8	0,7	1,2	1,3	1,2	2,5
Ni	6,3	222,1	277,9	11,3	10,1	11,4	14,4
Pb	4,2	25,2	34,9	5,3	5,3	8,8	17,1
Rb	0,7	1,1	1,3	2,1	0,5	0,3	0,6
S	0,03	0,05	0,04	0,11	0,01	0,03	0,03
Sb	1,68	4,42	4,75	0,95	0,94	0,78	1,89
Sc	2,3	9,6	15,2	6,4	6,3	9,5	23,6
Se	<2	4	2	<2	<2	<2	<2
Sn	0,6	0,8	0,8	0,7	0,6	0,7	0,9
Sr	2,8	39,2	75	14	6,8	11,6	27,7
Ta	<0,05	0,12	0,14	0,17	0,11	0,08	0,15
Te	1,96	8,44	7,68	3,36	3,3	4,35	10,09
Th	1,3	2,8	4,4	3,8	4,4	6,9	25,8
Ti	<0,01	<0,01	<0,01	0,04	0,05	0,08	0,19
Tl	<0,02	<0,02	<0,02	<0,02	<0,02	<0,02	<0,02
U	0,4	7,9	10,4	2,8	2,7	3,8	11,4
V	6	17	20	25	21	46	89
W	0,8	7,4	10,4	1,9	1,7	2,3	3,7
Y	18,9	16,8	28,2	8,7	8,1	13,5	49,4
Zn	12	77	121	10	10	9	25
Zr	31,9	38,5	54,2	142,4	107,7	84,2	345,5
La	6,9	137,4	297,5	10,7	20	12,2	84,2

GARIMPO	Morro da Palmeirinha						
Sample ID	**HHI-258**	**HHI-260**	**HHI-261**	**HHI-263**	**HHI-264**	**HHI-265**	**HHI-266**
Ce	8,5	90,8	192,9	15,5	34,1	19,2	147,5
Pr	0,98	32,46	67,06	2,01	3,65	1,81	15,68
Nd	3,2	120,3	247,6	6,7	13,1	5,9	55,9
Sm	1,9	19	39,9	1,4	2,6	1,4	10,1
Eu	1,39	4,08	8,21	0,38	0,64	0,4	2,34
Gd	8,7	12,53	24,69	1,74	2,47	2,09	9,79
Tb	2,15	1,22	2,34	0,28	0,33	0,39	1,52
Dy	14,91	4,72	8,73	1,74	1,8	2,59	9,08
Ho	2,95	0,7	1,24	0,36	0,32	0,52	1,79
Er	8,57	1,79	2,82	1,04	0,92	1,59	5,59
Tm	1,25	0,21	0,34	0,16	0,14	0,23	0,84
Yb	7,9	1,4	2,1	1,1	1	1,6	6
Lu	1,09	0,19	0,3	0,17	0,15	0,25	0,98
Au	31790	42787	36209	7098	7220	14966	17763
Pd	<5	<5	<5	<5	<5	<5	<5
Pt	<5	7	<5	<5	<5	<5	7

GARIMPO	Mina Velha							
Sample ID	**HHI-269**	**HHI-270**	**HHI-271**	**HHI-272**	**HHJ-695**	**HHJ-696**	**HHJ-697**	**HHJ-698**
Rock	Chlorite Schist	Chlorite Schist	Chlorite Schist	Chlorite Schist	Chlorite Schist	Chlorite Schist	Chlorite Schist	Chlorite Schist
Elements								
SiO_2	45,1	46,9	48,1	48,2	47	57,9	53,5	45,4
TiO_2	0,44	0,52	0,56	0,53	0,46	0,34	0,44	0,47
Fe_2O_3	19,5	18,1	15	14,9	19,2	17,5	16,1	21,4
Al_2O_3	11,5	13,1	14,8	14,4	12,6	10,7	14,5	13,5
MgO	9,02	9,12	13,7	13,4	10,5	6,16	8,7	10,4
MnO	0,03	0,03	0,06	0,06	0,04	0,02	0,03	0,04
CaO	<0,01	<0,01	0,03	0,02	0,01	0,01	0,02	0,01
K_2O	0,49	0,74	0,12	0,11	0,16	0,04	0,1	0,12
Na_2O	<0,1	<0,1	<0,1	<0,1	<0,1	<0,1	<0,1	<0,1
P_2O_5	0,014	0,013	0,042	0,031	0,01	0,011	<0,01	<0,01
Cr_2O_3	0,12	0,09	0,08	0,08	0,18	0,2	0,17	0,21
LOI	11,99	10,39	8,05	7,97	10,01	6,51	7,58	9,09
Ag	<0,02	<0,02	<0,02	<0,02	1,27	0,69	0,78	1,38
As	15	10	4	3	18	19	20	2
Ba	10	14	<5	7	16	9	5	7
Be	0,7	1	0,6	0,6	0,4	1	0,4	0,5
Bi	2,79	1,9	1,49	1,59	3,85	4,48	2,75	2,72
Cd	0,06	0,06	0,05	0,05	<0.02	<0.02	<0.02	<0.02
Co	138,7	58,5	114,4	124,6	67,8	52,2	41	67
Cr	358	374	221	201	450	516	446	585
Cs	<5	<5	<5	<5	<5	<5	<5	<5
Cu	388,6	403,7	98	243,3	300,1	873,6	358,2	570,7
Ga	20	20,8	20,1	21,5	19,4	13,4	15,5	17,9
Ge	<0,1	<0,1	<0,1	<0,1	0,2	0,2	0,2	0,3
Hf	1,24	1,49	1,81	1,44	1,87	1,05	1,29	1,66
In	0,06	0,08	<0,02	<0,02	0,05	0,05	0,05	0,06
Li	56	68	69	67	56	34	51	64
Mo	3,71	3,51	0,41	0,47	23,64	10,86	3,54	2,68
Nb	0,7	1	3,9	2,1	0,8	0,9	0,8	1

GARIMPO	Mina Velha							
Sample ID	**HHI-269**	**HHI-270**	**HHI-271**	**HHI-272**	**HHJ-695**	**HHJ-696**	**HHJ-697**	**HHJ-698**
Ni	177,3	157,9	246,3	241,6	199,8	195	253,8	279,1
Pb	10,5	8,6	8,3	7,2	8,8	11,5	8,4	11,5
Rb	10,9	17,7	2,3	2,8	10,4	5,5	4,1	3,7
S	2,82	1,03	1,99	2,39	1,22	0,11	0,24	0,44
Sb	0,28	0,39	0,17	0,2	0,94	0,83	0,56	0,57
Sc	39,6	41,3	50,9	50,5	29,1	22,7	24,8	27,7
Se	<2	<2	<2	<2	7	6	6	7
Sn	0,7	0,9	0,6	0,7	0,7	0,6	0,5	0,7
Sr	7,1	15,4	9	11,3	9,4	5,6	4,6	4,1
Ta	0,14	0,11	2,13	0,7	0,71	0,4	0,4	0,74
Te	0,35	0,18	0,1	0,07	0,35	0,3	0,25	0,32
Th	0,8	1	1,1	0,9	2,3	3	2,2	2,3
Ti	0,07	0,11	0,17	0,17	0,06	0,05	0,07	0,06
Tl	0,04	0,05	<0,02	<0,02	0,02	<0.02	<0.02	<0.02
U	0,9	1,3	0,5	0,6	1,6	2,1	2,2	2,9
V	158	169	198	194	172	124	145	162
W	1	1,2	1,8	1,7	0,5	0,4	0,5	0,6
Y	4,7	5,8	5,2	5,5	4,9	4,2	3,4	4,8
Zn	60	60	102	101	52	43	47	58
Zr	41,5	49,3	49,6	46,2	68,7	39,5	47,9	60,6
La	4,1	3,9	9,4	3,3	6,9	5,8	5,4	6,8
Ce	10,4	8,5	12,4	12	11,3	10,3	8,4	8,8
Pr	1,27	0,96	1,4	1,42	1,31	1,1	0,9	0,95
Nd	4,8	3,2	5,1	5,2	5	4,1	3,4	3,7
Sm	0,9	0,8	1,5	1,5	0,9	0,7	0,7	0,7
Eu	0,22	0,24	0,38	0,35	0,26	0,2	0,24	0,21
Gd	1,05	1,41	2,01	1,92	1,27	0,9	1,08	1,04
Tb	0,2	0,27	0,34	0,34	0,24	0,16	0,21	0,2
Dy	1,43	2,06	2,43	2,33	1,8	1,19	1,58	1,46
Ho	0,32	0,46	0,51	0,53	0,39	0,26	0,35	0,33
Er	1,04	1,39	1,64	1,56	1,24	0,91	1,15	1,05
Tm	0,15	0,22	0,24	0,23	0,2	0,13	0,17	0,15
Yb	1	1,4	1,6	1,5	1,4	0,8	1,1	1,1
Lu	0,14	0,2	0,23	0,22	0,2	0,13	0,15	0,16
Au	246	71	1164	2901	221	112	69	132
Pd	26	8	15	16	18	18	16	31
Pt	<5	<5	<5	11	<5	6	<5	<5

Supplementary Table 3.1 - Complete results of electron microprobe analysis of chlorites from the Maravilha *garimpo*.

Analysis	1	2	3	4	5	6	7	8	9	10
SiO2 (wt%)	29.51	27.87	29.23	27.78	27.12	27.97	27.20	28.35	28.39	28.44
Al2O3	19.43	21.53	21.68	22.07	22.31	22.15	21.01	21.11	20.68	20.59
Cr2O3	0.104	0.177	0.104	0.115	0.127	0.126	0.171	0.067	0.135	0.157
FeO	17.25	19.03	17.85	16.47	17.61	15.48	17.79	17.88	18.15	18.61
MnO	0.091	0.038	0.044	0.082	0.094	0.056	0.008	0.000	0.071	0.026
MgO	20.53	18.71	18.54	20.22	19.50	20.24	19.18	18.42	17.87	18.43
CaO	0.039	0.022	0.007	0.09	0.017	0.015	0.021	0.191	0.029	0.016
Na2O	0.057	0.077	0.088	0.14	0.055	0.105	0.054	0.231	0.06	0.08

Analysis	1	2	3	4	5	6	7	8	9	10
K2O	0.027	0.044	0.023	0.015	0.02	0.028	0.032	0.044	0.02	0.045
H2O (c)	11.85	11.89	11.85	11.66	12.08	11.51	11.73	11.89	11.78	11.43
Total	98.89	99.39	99.42	98.64	98.93	97.68	97.20	98.18	97.19	97.82
Si (a.p.f.u.)	5.954	5.651	5.855	5.591	5.499	5.64	5.599	5.769	5.839	5.809
Al	4.62	5.14	5.11	5.23	5.33	5.26	5.09	5.06	5.01	4.95
Fe (total)	2.911	3.227	2.991	2.772	2.987	2.611	3.063	3.043	3.121	3.179
Mn	0.016	0.007	0.007	0.014	0.016	0.01	0.001	0	0.012	0.004
Mg	6.174	5.657	5.534	6.065	5.894	6.084	5.887	5.587	5.478	5.612
Ca	0.008	0.005	0.002	0.019	0.004	0.003	0.005	0.042	0.006	0.004
Na	0.022	0.03	0.034	0.055	0.022	0.041	0.022	0.091	0.024	0.032
K	0.007	0.011	0.006	0.004	0.005	0.007	0.008	0.011	0.005	0.012
Al (IV)	2.046	2.349	2.145	2.409	2.501	2.36	2.401	2.231	2.161	2.191
Al (VI)	2.574	2.791	2.965	2.821	2.829	2.9	2.689	2.829	2.849	2.759
Fe/Fe+Mg	0.320	0.363	0.351	0.314	0.336	0.300	0.342	0.353	0.363	0.362
Si/Al	1.29	1.10	1.15	1.07	1.03	1.07	1.10	1.14	1.17	1.17
Ca+Na+K	0.037	0.046	0.042	0.078	0.031	0.051	0.035	0.144	0.035	0.048
Total cations	19.736	19.765	19.572	19.787	19.804	19.707	19.773	19.676	19.584	19.67
Σ Octaedral	11.675	11.682	11.497	11.672	11.726	11.605	11.64	11.459	11.46	11.554

Analysis	11	12	13	14	15	16	17	18	19	20
SiO2 (wt%)	28.97	28.96	28.55	27.68	27.06	28.83	28.15	27.24	30.08	27.57
Al2O3	20.67	21.24	20.39	20.84	20.63	21.41	20.22	20.66	22.74	20.05
Cr2O3	0.151	0.157	0.13	0.064	0.086	0.045	0.026	0.041	0.05	0.071
FeO	18.56	17.26	18.67	18.70	16.27	16.63	16.91	18.03	14.56	17.96
MnO	0.019	0.024	0.036	0.071	0.05	0.068	0.072	0.061	0.055	0.086
MgO	18.01	19.49	19.49	19.39	20.64	19.51	21.32	19.91	18.87	18.91
CaO	0.028	0.023	0.019	0.051	0.023	0.027	0.018	0.048	0.029	0.057
Na2O	0.048	0.059	0.061	0.05	0.111	0.028	0.112	0.054	0.108	0.129
K2O	0.014	0.029	0.025	0.052	0.073	0.025	0.077	0.055	0.073	0.103
H2O (c)	11.48	11.80	11.79	11.89	11.83	11.98	11.92	11.83	11.90	11.65
Total	97.95	99.04	99.16	98.79	96.77	98.55	98.83	97.93	98.47	96.59
Si (a.p.f.u.)	5.903	5.811	5.783	5.653	5.475	5.816	5.697	5.605	5.971	5.748
Al	4.96	5.02	4.86	5.01	4.92	5.09	4.82	5.01	5.32	4.92
Fe (total)	3.164	2.897	3.162	3.194	2.753	2.805	2.861	3.103	2.416	3.131
Mn	0.003	0.004	0.006	0.012	0.009	0.012	0.012	0.011	0.009	0.015
Mg	5.471	5.83	5.885	5.902	6.226	5.87	6.43	6.107	5.583	5.876
Ca	0.006	0.005	0.004	0.011	0.005	0.006	0.004	0.011	0.006	0.013
Na	0.019	0.023	0.024	0.02	0.044	0.011	0.044	0.022	0.042	0.052

Analysis	11	12	13	14	15	16	17	18	19	20
K	0.004	0.007	0.006	0.014	0.019	0.006	0.02	0.014	0.018	0.027
Al (IV)	2.097	2.189	2.217	2.347	2.525	2.184	2.303	2.395	2.029	2.252
Al (VI)	2.863	2.831	2.643	2.663	2.395	2.906	2.517	2.615	3.291	2.668
Fe/Fe+Mg	0.366	0.332	0.350	0.351	0.307	0.323	0.308	0.337	0.302	0.348
Si/Al	1.19	1.16	1.19	1.13	1.11	1.14	1.18	1.12	1.12	1.17
Ca+Na+K	0.029	0.035	0.034	0.045	0.068	0.023	0.068	0.047	0.066	0.092
Total cations	19.579	19.648	19.766	19.835	19.777	19.633	19.905	19.897	19.383	19.804
Σ Octaedral	11.501	11.562	11.696	11.771	11.383	11.593	11.82	11.836	11.299	11.69

Analysis	21	22	23	24	25	26	27	28	29	30
SiO2 (wt%)	28.06	28.5	27.86	27.43	27.26	29.09	28.42	27.24	28.41	28.28
Al2O3	20.29	20.57	20.77	20.32	20.95	19.53	20.53	21.82	20.04	20.10
Cr2O3	0.087	0.055	0.119	0.042	0.056	0.048	0.04	0.056	0.01	0.048
FeO	16.80	17.68	17.60	17.68	17.28	18.12	17.56	16.39	16.28	16.92
MnO	0.093	0.082	0.092	0.057	0.067	0.056	0.025	0.135	0.064	0.063
MgO	20.39	20.28	19.99	18.45	18.59	19.81	19.71	20.69	20.41	20.74
CaO	0.076	0.02	0.058	0.012	0.02	0.021	0.049	0.031	0.026	0.011
Na2O	0.123	0.054	0.127	0.144	0.044	0.083	0.058	0.12	0.079	0.044
K2O	0.059	0.058	0.06	0.082	0.055	0.068	0.041	0.077	0.033	0.034
H2O (c)	11.79	11.66	11.74	11.77	11.95	11.84	11.75	11.83	11.70	11.78
Total	97.77	98.96	98.42	95.99	96.27	98.67	98.18	98.39	97.05	98.02
Si (a.p.f.u.)	5.736	5.751	5.674	5.755	5.695	5.915	5.781	5.523	5.824	5.76
Al	4.88	4.89	4.98	5.02	5.15	4.68	4.92	5.21	4.84	4.82
Fe (total)	2.872	2.985	2.998	3.102	3.019	3.082	2.987	2.779	2.792	2.883
Mn	0.016	0.014	0.016	0.01	0.012	0.01	0.004	0.023	0.011	0.011
Mg	6.212	6.102	6.068	5.769	5.789	6.003	5.977	6.255	6.237	6.298
Ca	0.017	0.004	0.013	0.003	0.004	0.005	0.011	0.007	0.006	0.002
Na	0.049	0.021	0.05	0.059	0.018	0.033	0.023	0.047	0.031	0.017
K	0.015	0.015	0.016	0.022	0.015	0.018	0.011	0.02	0.009	0.009
Al (IV)	2.264	2.249	2.326	2.245	2.305	2.085	2.219	2.477	2.176	2.24
Al (VI)	2.616	2.641	2.654	2.775	2.845	2.595	2.701	2.733	2.664	2.58
Fe/Fe+Mg	0.316	0.328	0.331	0.350	0.343	0.339	0.333	0.308	0.309	0.314
Si/Al	1.18	1.18	1.14	1.15	1.11	1.26	1.18	1.06	1.20	1.20
Ca+Na+K	0.081	0.04	0.079	0.084	0.037	0.056	0.045	0.074	0.046	0.028
Total cations	19.823	19.802	19.842	19.754	19.719	19.759	19.743	19.882	19.761	19.82
Σ Octaedral	11.716	11.742	11.736	11.656	11.665	11.69	11.669	11.79	11.704	11.772

Analysis	31	32	33	34	35	36	37	38	39	40

Analysis	31	32	33	34	35	36	37	38	39	40
SiO2 (wt%)	28.22	28.59	28.55	27.46	28.72	28.54	28.73	28.38	28.49	28.27
Al2O3	20.23	21.28	20.18	20.32	20.55	20.33	20.81	19.37	19.99	21.06
Cr2O3	0.028	0.041	0.057	0.011	0.017	0.033	0.015	0.07	0.026	0.037
FeO	17.13	16.27	17.13	16.79	16.53	16.5	16.99	17.33	17.27	16.67
MnO	0.051	0.067	0.063	0.034	0.107	0.015	0.051	0.094	0.114	0.095
MgO	21.12	19.53	20.59	21.26	21.27	20.97	20.04	20.75	20.93	20.74
CaO	0.036	0	0.018	0.008	0.009	0.034	0.027	0.022	0.024	0.035
Na2O	0.301	0.076	0.076	0.022	0.031	0.116	0.148	0.088	0.077	0.08
K2O	0.056	0.031	0.031	0.012	0.008	0.052	0.059	0.048	0.074	0.045
H2O (c)	11.87	11.81	11.83	11.71	11.96	11.86	11.88	11.72	11.85	11.91
Total	99.04	97.7	98.53	97.63	99.2	98.45	98.75	97.87	98.85	98.94
Si (a.p.f.u.)	5.701	5.808	5.786	5.622	5.761	5.772	5.799	5.806	5.765	5.694
Al	4.81	5.09	4.82	4.9	4.86	4.84	4.95	4.67	4.76	4.99
Fe (total)	2.894	2.764	2.903	2.875	2.773	2.791	2.868	2.965	2.922	2.807
Mn	0.009	0.012	0.011	0.006	0.018	0.003	0.009	0.016	0.02	0.016
Mg	6.362	5.914	6.222	6.489	6.36	6.322	6.03	6.33	6.314	6.227
Ca	0.008	0	0.004	0.002	0.002	0.007	0.006	0.005	0.005	0.008
Na	0.118	0.03	0.03	0.009	0.012	0.045	0.058	0.035	0.03	0.031
K	0.014	0.008	0.008	0.003	0.002	0.013	0.015	0.013	0.019	0.012
Al (IV)	2.299	2.192	2.214	2.378	2.239	2.228	2.201	2.194	2.235	2.306
Al (VI)	2.511	2.898	2.606	2.522	2.621	2.612	2.749	2.476	2.525	2.684
Fe/Fe+Mg	0.313	0.319	0.318	0.307	0.304	0.306	0.322	0.319	0.316	0.311
Si/Al	1.19	1.14	1.20	1.15	1.19	1.19	1.17	1.24	1.21	1.14
Ca+Na+K	0.14	0.038	0.042	0.014	0.016	0.065	0.079	0.053	0.054	0.051
Total cations	19.932	19.644	19.805	19.917	19.802	19.81	19.747	19.864	19.85	19.804
Σ Octaedral	11.776	11.588	11.742	11.892	11.772	11.728	11.656	11.787	11.781	11.734

Supplementary Table 3.2 - Complete results of electron microprobe analysis of chlorites from the Jaqueira *garimpo*.

Analysis	1	2	3	4	5	6	7	8	9	10
SiO2 (wt%)	25.66	24.92	24.97	25.87	25.45	25.23	25.02	25.53	25.39	25.19
Al2O3	22.60	22.40	22.26	21.03	22.68	22.10	22.63	22.03	21.76	22.19
Cr2O3	0.015	0.019	0	0.046	0.007	0.01	0	0.01	0.008	0.011
FeO	24.79	24.88	24.69	24.12	24.04	24.69	24.20	24.81	24.61	24.51
MnO	0.616	0.602	0.498	0.641	0.633	0.644	0.67	0.724	0.674	0.657
MgO	13.40	13.86	13.99	14.74	13.62	13.90	13.53	13.88	14.15	13.76
CaO	0.023	0.009	0	0.008	0.012	0.013	0.021	0.02	0.014	0.003
Na2O	0.003	0	0	0.005	0.03	0.04	0	0	0.032	0.055
K2O	0.011	0.017	0.016	0.011	0.011	0.009	0.027	0.027	0.006	0.03
H2O (c)	11.37	11.27	11.25	11.30	11.31	11.27	11.24	11.33	11.28	11.25

Total	98.49	97.98	97.67	97.77	97.79	97.91	97.34	98.36	97.92	97.66
Si (a.p.f.u.)	5.415	5.304	5.321	5.494	5.396	5.368	5.339	5.404	5.401	5.37
Al	5.62	5.62	5.59	5.26	5.66	5.54	5.69	5.49	5.45	5.57
Fe (total)	4.374	4.429	4.401	4.282	4.263	4.394	4.319	4.392	4.376	4.371
Mn	0.11	0.109	0.09	0.115	0.114	0.116	0.121	0.13	0.121	0.119
Mg	4.216	4.397	4.444	4.666	4.304	4.408	4.305	4.381	4.486	4.372
Ca	0.005	0.002	0	0.002	0.003	0.003	0.005	0.005	0.003	0.001
Na	0.001	0	0	0.002	0.012	0.017	0	0	0.013	0.023
K	0.003	0.005	0.004	0.003	0.003	0.002	0.007	0.007	0.002	0.008
Al (IV)	2.585	2.696	2.679	2.506	2.604	2.632	2.661	2.596	2.599	2.63
Al (VI)	3.035	2.924	2.911	2.754	3.056	2.908	3.029	2.894	2.851	2.94
Fe/Fe+Mg	0.509	0.502	0.498	0.479	0.498	0.499	0.501	0.501	0.494	0.500
Si/Al	0.96	0.94	0.05	1.04	1.04	0.97	0.94	0.98	0.99	0.96
Ca+Na+K	0,009	0,007	0,004	0,007	0,018	0,022	0,012	0,012	0,018	0,032
Total cations	19,759	19,877	19,866	19,851	19,761	19,859	19,801	19,825	19,862	19,842
Σ Octaedral	11.735	11.859	11.846	11.817	11.737	11.826	11.774	11.797	11.834	11.802
Cath (℃)a	770	806	801	745	777	786	795	774	775	785
K&M (℃)a	330	341	339	319	331	334	337	330	330	334
Z&F (℃)a	276	289	287	271	279	282	285	278	279	282

a: Cath, Cathelineau (1988); K&M, Kranitoids and MacLean (1987); Z&F, Zang and Fyfe (1995)

Analysis	11	12	13	14	15	16	17	18	19	20
SiO2 (wt%)	25.39	25.18	25.61	25.30	26.09	25.75	26.27	25.20	25.68	26.22
Al2O3	22.42	22.24	22.17	21.98	21.59	21.90	21.86	21.38	22.14	20.58
Cr2O3	0.016	0.013	0.004	0	0.014	0.028	0.017	0.033	0.016	0.02
FeO	24.55	24.78	24.72	24.41	24.62	25.39	24.78	24.79	24.71	23.92
MnO	0.579	0.639	0.63	0.617	0.616	0.585	0.633	0.676	0.511	0.6
MgO	14.00	13.87	13.51	13.67	14.36	13.94	15.12	14.21	14.05	14.85
CaO	0.006	0.021	0.054	0.012	0.014	0.027	0.016	0.011	0.024	0.017
Na2O	0.048	0.022	0.011	0	0.027	0.015	0.061	0.015	0.019	0.021
K2O	0.016	0.012	0.033	0.016	0.032	0.027	0.055	0.018	0.028	0.012
H2O (c)	11.35	11.29	11.30	11.21	11.40	11.39	11.59	11.21	11.37	11.28
Total	98.38	98.07	98.07	97.22	98.76	99.09	100.40	97.54	98.55	97.52
Si (a.p.f.u.)	5.365	5.351	5.433	5.412	5.488	5.421	5.437	5.391	5.419	5.577
Al	5.58	5.57	5.54	5.54	5.35	5.43	5.33	5.39	5.5	5.16
Fe (total)	4.339	4.404	4.386	4.367	4.331	4.471	4.29	4.435	4.361	4.255
Mn	0.104	0.115	0.113	0.112	0.11	0.104	0.111	0.122	0.091	0.108
Mg	4.41	4.394	4.275	4.358	4.502	4.374	4.664	4.53	4.42	4.711
Ca	0.001	0.005	0.012	0.003	0.003	0.006	0.004	0.003	0.005	0.004
Na	0.02	0.009	0.005	0	0.011	0.006	0.024	0.006	0.008	0.009
K	0.004	0.003	0.009	0.004	0.009	0.007	0.015	0.005	0.008	0.003
Al (IV)	2.635	2.649	2.567	2.588	2.512	2.579	2.563	2.609	2.581	2.423
Al (VI)	2.945	2.921	2.973	2.952	2.838	2.851	2.767	2.781	2.919	2.737
Fe/Fe+Mg	0.496	0.501	0.506	0.501	0.490	0.505	0.479	0.495	0.497	0.475
Si/Al	0.96	0.96	0.98	0.98	1.03	1.00	1.02	1.00	0.99	1.08
Ca+Na+K	0,025	0,017	0,026	0,007	0,023	0,019	0,043	0,014	0,021	0,016
Total cations	19,837	19,859	19,784	19,806	19,823	19,842	19,895	19,902	19,82	19,838

Σ Octaedral	11.798	11.834	11.747	11.789	11.781	11.8	11.832	11.868	11.791	11.811
Cath (℃)a	786	791	765	771	747	768	763	778	769	718
K&M (℃)a	334	336	328	329	321	329	325	331	328	310
Z&F (℃)a	283	284	275	277	270	276	277	280	277	262

a: Cath, Cathelineau (1988); K&M, Kranitoids and MacLean (1987); Z&F, Zang and Fyfe (1995)

Analysis	21	22	23	24	25	26	27	28	29	30
SiO2 (wt%)	25.50	25.83	25.02	25.20	25.42	25.66	25.80	24.96	25.24	25.80
Al2O3	21.87	21.55	22.50	22.46	21.60	22.35	21.80	21.89	20.73	21.42
Cr2O3	0.021	0.01	0.029	0	0.009	0.006	0.004	0	0.038	0.022
FeO	24.77	24.84	24.99	24.97	25.20	24.98	25.02	25.52	25.04	23.67
MnO	0.622	0.645	0.629	0.67	0.604	0.63	0.571	0.595	0.641	0.646
MgO	14.67	14.71	13.70	13.74	13.73	13.64	12.68	13.35	14.09	14.39
CaO	0.006	0.002	0.007	0.001	0.022	0.015	0.026	0.015	0.032	0.018
Na2O	0.029	0.045	0	0.012	0.019	0.031	0.035	0.023	0.027	0.007
K2O	0	0.009	0.013	0.001	0.005	0	0.01	0.01	0.032	0.026
H2O (c)	11.38	11.41	11.29	11.32	11.24	11.37	11.19	11.18	11.15	11.27
Total	98.87	99.05	98.18	98.37	97.85	98.68	97.14	97.54	97.02	97.27
Si (a.p.f.u.)	5.373	5.431	5.315	5.339	5.425	5.414	5.531	5.356	5.43	5.489
Al	5.43	5.34	5.63	5.6	5.43	5.55	5.5	5.53	5.25	5.37
Fe (total)	4.365	4.368	4.44	4.425	4.498	4.409	4.487	4.579	4.506	4.211
Mn	0.111	0.115	0.113	0.12	0.109	0.113	0.104	0.108	0.117	0.116
Mg	4.607	4.611	4.338	4.34	4.368	4.292	4.051	4.271	4.52	4.563
Ca	0.001	0	0.002	0	0.005	0.003	0.006	0.003	0.007	0.004
Na	0.012	0.018	0	0.005	0.008	0.013	0.015	0.01	0.011	0.003
K	0	0.002	0.004	0	0.001	0	0.003	0.003	0.009	0.007
Al (IV)	2.627	2.569	2.685	2.661	2.575	2.586	2.469	2.644	2.57	2.511
Al (VI)	2.803	2.771	2.945	2.939	2.855	2.964	3.031	2.886	2.68	2.859
Fe/Fe+Mg	0.487	0.486	0.506	0.505	0.507	0.507	0.526	0.517	0.499	0.480
Si/Al	0.99	1.02	0.94	0.95	1.00	0.98	1.01	0.97	1.03	1.02
Ca+Na+K	0,013	0,02	0,006	0,005	0,014	0,016	0,024	0,016	0,027	0,014
Total cations	19,908	19,896	19,855	19,839	19,85	19,799	19,706	19,867	19,897	19,796
Σ Octaedral	11.886	11.865	11.836	11.824	11.83	11.778	11.673	11.844	11.823	11.749
Cath (℃)a	784	765	803	795	767	771	733	789	766	747
K&M (℃)a	333	326	340	338	329	330	319	337	327	320
Z&F (℃)a	283	277	287	285	275	277	262	282	276	271

a: Cath, Cathelineau (1988); K&M, Kranitoids and MacLean (1987); Z&F, Zang and Fyfe (1995)

Analysis	31	32	33	34	35	36	37	38	39	40
SiO2 (wt%)	25.64	25.64	25.56	25.90	25.93	25.37	24.98	26.15	26.42	26.74
Al2O3	21.10	21.26	22.22	22.95	22.17	22.28	21.27	22.40	22.38	22.26
Cr2O3	0.001	0.005	0.005	0.008	0.008	0	0	0	0.016	0
FeO	24.48	24.62	24.63	24.47	24.53	25.43	25.58	24.52	24.36	23.72
MnO	0.554	0.565	0.641	0.629	0.642	0.606	0.658	0.62	0.519	0.539
MgO	14.42	13.97	14.14	13.76	13.47	13.85	13.65	13.99	13.87	13.43
CaO	0.018	0.024	0.01	0.017	0.026	0.026	0.018	0.022	0	0.011
Na2O	0.016	0.033	0.008	0.04	0.004	0.056	0.055	0	0	0
K2O	0.043	0.013	0.004	0.012	0.012	0.035	0.034	0.038	0.004	0.009

H2O (c)	11.24	11.21	11.37	11.49	11.34	11.37	11.14	11.47	11.47	11.41
Total	97.51	97.34	98.59	99.28	98.13	99.02	97.39	99.21	99.04	98.12
Si (a.p.f.u.)	5.471	5.484	5.391	5.409	5.483	5.351	5.379	5.468	5.523	5.62
Al	5.3	5.36	5.52	5.64	5.52	5.53	5.39	5.51	5.51	5.51
Fe (total)	4.368	4.404	4.344	4.274	4.338	4.484	4.607	4.287	4.259	4.169
Mn	0.1	0.102	0.115	0.111	0.115	0.108	0.12	0.11	0.092	0.096
Mg	4.588	4.456	4.446	4.283	4.246	4.353	4.381	4.361	4.324	4.207
Ca	0.004	0.005	0.002	0.004	0.006	0.006	0.004	0.005	0	0.002
Na	0.007	0.014	0.003	0.016	0.002	0.023	0.023	0	0	0
K	0.012	0.004	0.001	0.003	0.003	0.009	0.009	0.01	0.001	0.002
Al (IV)	2.529	2.516	2.609	2.591	2.517	2.649	2.621	2.532	2.477	2.38
Al (VI)	2.771	2.844	2.911	3.049	3.003	2.881	2.769	2.978	3.033	3.13
Fe/Fe+Mg	0.488	0.497	0.494	0.499	0.505	0.507	0.513	0.496	0.496	0.498
Si/Al	1.03	1.02	0.98	0.96	0.99	0.97	1.00	0.99	1.00	1.02
Ca+Na+K	0,023	0,023	0,006	0,023	0,011	0,038	0,036	0,015	0,001	0,004
Total cations	19,864	19,836	19,833	19,753	19,731	19,875	19,919	19,759	19,712	19,611
Σ Octaedral	11.827	11.806	11.816	11.717	11.702	11.826	11.877	11.736	11.708	11.602
Cath (℃)a	752	748	778	772	749	791	782	753	736	704
K&M (℃)a	322	322	331	330	322	336	334	323	317	307
Z&F (℃)a	272	270	280	278	269	283	280	272	266	256

a: Cath, Cathelineau (1988); K&M, Kranitoids and MacLean (1987); Z&F, Zang and Fyfe (1995)

Analysis	41	42	43	44	45	46	47	48	49	50
SiO2 (wt%)	24.83	26.92	26.01	25.75	25.29	26.68	25.38	26.00	25.83	25.69
Al2O3	22.01	21.60	21.90	21.92	22.19	21.96	21.63	21.39	20.79	21.33
Cr2O3	0.005	0.027	0.016	0.004	0.019	0	0.004	0.016	0.034	0.034
FeO	25.02	23.64	23.99	24.42	23.80	24.01	24.98	24.64	24.43	24.43
MnO	0.625	0.572	0.596	0.653	0.581	0.588	0.6	0.63	0.607	0.611
MgO	13.51	14.63	14.08	13.81	14.08	12.54	14.15	14.69	14.64	14.53
CaO	0.011	0.032	0.009	0.01	0.037	0.005	0.022	0.008	0.015	0.02
Na2O	0.016	0.04	0.039	0.026	0.063	0.01	0.026	0	0.046	0
K2O	0.029	0.015	0.024	0.025	0.056	0.042	0.008	0.002	0	0.024
H2O (c)	11.16	11.51	11.35	11.31	11.26	11.27	11.28	11.39	11.26	11.30
Total	97.22	98.99	98.01	97.93	97.38	97.11	98.08	98.77	97.65	97.97
Si (a.p.f.u.)	5.335	5.611	5.496	5.461	5.386	5.678	5.399	5.474	5.504	5.452
Al	5.57	5.3	5.45	5.48	5.57	5.5	5.42	5.3	5.22	5.33
Fe (total)	4.497	4.121	4.24	4.331	4.24	4.273	4.443	4.338	4.353	4.337
Mn	0.114	0.101	0.107	0.117	0.105	0.106	0.108	0.112	0.11	0.11
Mg	4.329	4.545	4.434	4.365	4.47	3.978	4.486	4.61	4.651	4.596
Ca	0.003	0.007	0.002	0.002	0.008	0.001	0.005	0.002	0.003	0.005
Na	0.007	0.016	0.016	0.011	0.026	0.004	0.011	0	0.019	0
K	0.008	0.004	0.006	0.007	0.015	0.011	0.002	0.001	0	0.006
Al (IV)	2.665	2.389	2.504	2.539	2.614	2.322	2.601	2.526	2.496	2.548
Al (VI)	2.905	2.911	2.946	2.941	2.956	3.178	2.819	2.774	2.724	2.782
Fe/Fe+Mg	0.510	0.476	0.489	0.498	0.487	0.518	0.498	0.485	0.483	0.486

Analysis	41	42	43	44	45	46	47	48	49	50
Si/Al	0.96	1.06	1.01	1.00	0.97	1.03	1.00	1.03	1.05	1.02
Ca+Na+K	0,018	0,027	0,024	0,02	0,049	0,016	0,018	0,003	0,022	0,011
Total cations	19,871	19,722	19,768	19,79	19,835	19,56	19,884	19,852	19,878	19,858
Σ Octaedral	11.845	11.678	11.727	11.754	11.771	11.535	11.856	11.834	11.838	11.825
Cath (℃)a	796	707	744	756	780	686	776	751	742	758
K&M (℃)a	338	307	320	324	331	303	331	322	318	324
Z&F (℃)a	285	259	270	272	281	248	279	272	269	275

a: Cath, Cathelineau (1988); K&M, Kranitoids and MacLean (1987); Z&F, Zang and Fyfe (1995)

Analysis	51	52	53	54	55	56	57	58	59	60
SiO2 (wt%)	25.75	25.63	25.22	25.49	26.74	26.01	25.08	25.68	25.49	24.56
Al2O3	20.46	21.77	21.40	22.17	22.83	21.67	22.35	22.89	22.29	22.44
Cr2O3	0.004	0.023	0.016	0.023	0.021	0.023	0.013	0.003	0.015	0.019
FeO	24.13	24.59	24.55	24.72	23.09	24.22	24.92	24.20	24.21	24.91
MnO	0.529	0.511	0.677	0.623	0.581	0.597	0.661	0.668	0.544	0.673
MgO	13.87	14.34	14.03	14.58	13.51	14.21	13.90	13.76	14.13	13.56
CaO	0.013	0.008	0.016	0.003	0.015	0.002	0.002	0.015	0.064	0.016
Na2O	0.013	0.002	0	0.009	0.032	0.025	0.017	0.006	0.052	0.019
K2O	0.031	0.012	0.018	0.012	0.021	0.015	0.031	0.025	0.068	0.015
H2O (c)	11.07	11.34	11.17	11.41	11.48	11.35	11.30	11.42	11.34	11.20
Total	95.87	98.23	97.10	99.04	98.32	98.12	98.27	98.67	98.20	97.40
Si (a.p.f.u.)	5.577	5.423	5.413	5.357	5.588	5.498	5.323	5.395	5.391	5.261
Al	5.22	5.43	5.41	5.49	5.62	5.4	5.58	5.66	5.55	5.66
Fe (total)	4.371	4.35	4.408	4.345	4.036	4.282	4.423	4.252	4.282	4.463
Mn	0.097	0.092	0.123	0.111	0.103	0.107	0.119	0.119	0.097	0.122
Mg	4.48	4.522	4.49	4.568	4.209	4.477	4.398	4.311	4.455	4.33
Ca	0.003	0.002	0.004	0.001	0.003	0	0	0.003	0.015	0.004
Na	0.005	0.001	0	0.004	0.013	0.01	0.007	0.002	0.021	0.008
K	0.009	0.003	0.005	0.003	0.006	0.004	0.008	0.007	0.018	0.004
Al (IV)	2.423	2.577	2.587	2.643	2.412	2.502	2.677	2.605	2.609	2.739
Al (VI)	2.797	2.853	2.823	2.847	3.208	2.898	2.903	3.055	2.941	2.921
Fe/Fe+Mg	0.494	0.490	0.495	0.487	0.490	0.489	0.501	0.497	0.490	0.508
Si/Al	1.07	1.00	1.00	0.98	0.99	1.02	0.95	0.95	0.97	0.93
Ca+Na+K	0,017	0,006	0,009	0,008	0,022	0,014	0,015	0,012	0,054	0,016
Total cations	19,788	19,845	19,866	19,89	19,591	19,794	19,869	19,758	19,838	19,88
Σ Octaedral	11.745	11.817	11.844	11.871	11.556	11.764	11.843	11.737	11.775	11.836
Cath (℃)a	718	768	771	789	715	744	800	777	778	820
K&M (℃)a	311	328	329	334	310	319	339	331	331	346
Z&F (℃)a	260	277	278	284	260	269	287	280	281	293

a: Cath, Cathelineau (1988); K&M, Kranitoids and MacLean (1987); Z&F, Zang and Fyfe (1995)

Analysis	61	62	63	64	65	66	67	68	69	70
SiO2 (wt%)	25.22	25.51	25.26	25.95	25.93	25.79	25.41	24.98	25.09	26.77
Al2O3	21.83	22.01	22.65	22.29	22.15	22.11	22.66	21.20	21.32	22.90
Cr2O3	0.009	0	0.02	0.02	0.006	0.009	0.028	0.022	0.026	0
FeO	24.99	24.50	25.08	24.16	24.12	24.72	23.55	25.38	24.70	22.70

Analysis	41	42	43	44	45	46	47	48	49	50
MnO	0.621	0.64	0.685	0.564	0.658	0.657	0.541	0.554	0.642	0.532
MgO	14.13	14.06	14.28	14.16	13.64	14.38	14.37	13.79	13.98	13.13
CaO	0.005	0.015	0.024	0.002	0.002	0.007	0.009	0.014	0.004	0.003
Na2O	0.034	0.003	0.034	0	0	0.05	0.016	0.048	0.041	0.065
K2O	0.021	0.014	0.036	0	0	0.03	0.02	0.056	0.068	0.035
H2O (c)	11.29	11.31	11.45	11.41	11.32	11.44	11.36	11.12	11.15	11.41
Total	98.15	98.06	99.52	98.56	97.83	99.19	97.96	97.16	97.02	97.55
Si (a.p.f.u.)	5.359	5.408	5.363	5.454	5.493	5.409	5.367	5.387	5.396	5.623
Al	5.46	5.5	5.41	5.52	5.53	5.46	5.64	5.38	5.4	5.66
Fe (total)	4.441	4.344	4.453	4.246	4.273	4.336	4.159	4.576	4.444	3.999
Mn	0.112	0.115	0.123	0.1	0.118	0.117	0.097	0.101	0.117	0.095
Mg	4.478	4.443	4.52	4.437	4.307	4.496	4.523	4.432	4.483	4.112
Ca	0.001	0.003	0.005	0	0	0.002	0.002	0.003	0.001	0.001
Na	0.014	0.001	0.014	0	0	0.02	0.007	0.02	0.017	0.026
K	0.006	0.004	0.01	0	0	0.008	0.005	0.015	0.019	0.009
Al (IV)	2.641	2.592	2.637	2.546	2.507	2.591	2.633	2.613	2.604	2.377
Al (VI)	2.819	2.908	2.773	2.974	3.023	2.869	3.007	2.767	2.796	3.283
Fe/Fe+Mg	0.498	0.494	0.496	0.489	0.498	04.91	0.479	0.508	0.498	0.493
Si/Al	0.98	0.98	0.99	0.99	0.99	0.99	0.95	1.00	1.00	0.99
Ca+Na+K	0,021	0,008	0,029	0	0	0,03	0,014	0,038	0,037	0,036
Total cations	19,89	19,83	19,914	19,77	19,731	19,857	19,809	19,921	19,895	19,538
Σ Octaedral	11.85	11.81	11.869	11.757	11.721	11.818	11.786	11.876	11.84	11.489
Cath (℃)a	788	773	787	758	745	772	786	779	777	703
K&M (℃)a	335	329	334	324	321	329	333	333	331	307
Z&F (℃)a	283	278	283	274	269	279	284	279	279	256

a: Cath, Cathelineau (1988); K&M, Kranitoids and MacLean (1987); Z&F, Zang and Fyfe (1995)

Supplementary Table 3.3 - Complete results of electron microprobe analysis of chlorites from the Morro da Palmeirinha *garimpo*.

Analysis	1	2	3	4	5	6	7	8	9	10
SiO2 (wt%)	29.09	29.83	29.11	28.64	28.72	28.38	27.39	26.64	28.72	30.80
Al2O3	20.26	20.70	20.26	21.34	20.75	21.28	20.38	21.40	20.10	20.22
Cr2O3	0.082	0.095	0.162	0.206	0.467	0.285	0.84	0.64	0.255	0.117
FeO	10.71	13.84	11.44	9.24	15.80	12.11	22.11	21.23	12.91	11.17
MnO	0.47	0.352	0.462	0.622	0.333	0.517	0.375	0.344	0.434	0.415
MgO	24.69	21.06	24.03	25.79	21.18	23.34	15.80	16.27	23.15	24.40
CaO	0.057	0.051	0.035	0.018	0.02	0.021	0.02	0.009	0.029	0.011
Na2O	0.058	0.08	0.077	0.028	0.053	0.055	0.119	0.067	0.05	0.067
K2O	0.061	0.057	0.08	0.037	0.048	0.062	0.123	0.085	0.123	0.114
H2O (c)	12.04	11.98	12.03	12.17	11.99	12.01	11.52	11.51	11.93	12.32
Total	97.52	98.05	97.69	98.08	99.36	98.06	98.68	98.20	97.70	99.63
Si (a.p.f.u.)	5.793	5.97	5.806	5.643	5.746	5.665	5.704	5.551	5.772	5.997
Al	4.75	4.88	4.76	4.95	4.89	5	5	5.25	4.76	4.63

Analysis	1	2	3	4	5	6	7	8	9	10
Fe (total)	1.783	2.316	1.908	1.523	2.644	2.022	3.851	3.701	2.171	1.818
Mn	0.079	0.06	0.078	0.104	0.056	0.087	0.066	0.061	0.074	0.068
Mg	7.331	6.284	7.145	7.574	6.317	6.948	4.904	5.055	6.937	7.08
Ca	0.012	0.011	0.007	0.004	0.004	0.004	0.004	0.002	0.006	0.002
Na	0.022	0.031	0.03	0.011	0.021	0.021	0.048	0.027	0.019	0.025
K	0.015	0.015	0.02	0.009	0.012	0.016	0.033	0.023	0.032	0.028
Al (IV)	2.207	2.03	2.194	2.357	2.254	2.335	2.296	2.449	2.228	2.003
Al (VI)	2.543	2.85	2.566	2.593	2.636	2.665	2.704	2.801	2.532	2.627
Fe/Fe+Mg	0.196	0.269	0.211	0.167	0.295	0.225	0.440	0.423	0.238	0.204
Si/Al	1.22	1.22	1.22	1.14	1.18	1.13	1.14	1.06	1.21	1.30
Ca+Na+K	0.049	0.057	0.057	0.024	0.037	0.041	0.085	0.052	0.057	0.055
Total cations	19.815	19.591	19.801	19.858	19.772	19.813	19.754	19.779	19.83	19.678
Σ Octaedral	11.736	11.51	11.697	11.794	11.653	11.722	11.525	11.618	11.714	11.593

Analysis	11	12	13	14	15	16	17	18	19	20
SiO2 (wt%)	29.23	28.89	29.29	28.80	27.52	29.42	28.62	28.51	28.43	26.44
Al2O3	22.04	21.80	21.71	20.48	20.65	19.82	21.24	20.53	22.63	21.54
Cr2O3	0.228	0.193	0.264	0.326	0.421	0.34	0.252	0.473	0.082	0.081
FeO	9.10	8.28	8.39	10.95	19.09	11.27	13.19	13.98	18.44	21.12
MnO	0.644	0.541	0.528	0.411	0.228	0.394	0.4	0.397	0.386	0.407
MgO	25.25	26.04	26.96	24.98	18.24	24.01	22.45	21.91	19.98	16.38
CaO	0.017	0.011	0.017	0.012	0.027	0.03	0.072	0.041	0.01	0.01
Na2O	0.04	0.033	0.016	0.101	0.068	0.045	0.04	0.061	0.082	0.155
K2O	0.057	0.062	0.038	0.055	0.08	0.069	0.033	0.094	0.088	0.15
H2O (c)	12.30	12.24	12.42	12.09	11.62	12.00	12.00	11.89	12.22	11.46
Total	98.91	98.09	99.63	98.21	97.94	97.40	98.30	97.89	102.35	97.74
Si (a.p.f.u.)	5.699	5.663	5.655	5.711	5.683	5.88	5.718	5.753	5.58	5.534
Al	5.06	5.03	4.94	4.78	5.02	4.66	5	4.88	5.23	5.31
Fe (total)	1.484	1.358	1.354	1.817	3.296	1.884	2.205	2.359	3.026	3.698
Mn	0.106	0.09	0.086	0.069	0.04	0.067	0.068	0.068	0.064	0.072
Mg	7.338	7.607	7.76	7.384	5.615	7.153	6.688	6.591	5.846	5.113
Ca	0.004	0.002	0.004	0.003	0.006	0.006	0.015	0.009	0.002	0.002
Na	0.015	0.013	0.006	0.039	0.027	0.017	0.015	0.024	0.031	0.063
K	0.014	0.016	0.009	0.014	0.021	0.018	0.008	0.024	0.022	0.04
Al (IV)	2.301	2.337	2.345	2.289	2.317	2.12	2.282	2.247	2.42	2.466
Al (VI)	2.759	2.693	2.595	2.491	2.703	2.54	2.718	2.633	2.81	2.844
Fe/Fe+Mg	0.168	0.151	0.149	0.197	0.370	0.208	0.248	0.264	0.341	0.420
Si/Al	1.13	1.13	1.4	1.19	1.13	1.26	1.14	1.18	1.07	1.04
Ca+Na+K	0.033	0.031	0.019	0.056	0.054	0.041	0.038	0.057	0.055	0.105
Total cations	19.757	19.812	19.857	19.878	19.783	19.753	19.764	19.786	19.816	19.847
Σ Octaedral	11.687	11.748	11.795	11.761	11.654	11.644	11.679	11.651	11.746	11.727

Analysis	21	22	23	24	25	26	27	28	29	30
SiO2 (wt%)	29.38	30.22	29.50	26.65	29.06	28.63	25.98	28.79	29.37	29.11

Analysis	21	22	23	24	25	26	27	28	29	30
Al2O3	20.18	19.93	21.82	21.42	21.56	21.05	20.90	21.49	21.50	21.84
Cr2O3	0.457	0.248	0.281	0.098	0.13	0.026	0.154	0.026	0.215	0.478
FeO	13.07	12.64	10.54	23.36	7.85	8.50	21.69	8.64	8.69	9.13
MnO	0.309	0.289	0.496	0.393	0.469	0.463	0.265	0.546	0.584	0.47
MgO	22.66	22.10	25.77	15.39	27.40	26.74	15.80	26.52	26.24	25.80
CaO	0.013	0.041	0.035	0.011	0.024	0.018	0.011	0.012	0.009	0.036
Na2O	0.037	0.06	0.065	0.117	0.081	0.125	0.1	0.048	0.077	0.133
K2O	0.065	0.133	0.065	0.07	0.035	0.068	0.056	0.024	0.035	0.063
H2O (c)	12.01	12.00	12.49	11.51	12.37	12.17	11.24	12.25	12.34	12.35
Total	98.18	97.66	101.06	99.02	98.98	97.79	96.20	98.35	99.06	99.41
Si (a.p.f.u.)	5.868	6.04	5.666	5.556	5.635	5.641	5.545	5.639	5.709	5.654
Al	4.75	4.69	4.93	5.26	4.92	4.89	5.25	4.96	4.92	5
Fe (total)	2.183	2.112	1.693	4.073	1.272	1.401	3.872	1.415	1.413	1.484
Mn	0.052	0.049	0.081	0.069	0.077	0.077	0.048	0.091	0.096	0.077
Mg	6.746	6.585	7.378	4.783	7.92	7.855	5.027	7.743	7.603	7.47
Ca	0.003	0.009	0.007	0.002	0.005	0.004	0.003	0.003	0.002	0.007
Na	0.014	0.023	0.024	0.047	0.03	0.048	0.041	0.018	0.029	0.05
K	0.017	0.034	0.016	0.019	0.009	0.017	0.015	0.006	0.009	0.016
Al (IV)	2.132	1.96	2.334	2.444	2.365	2.359	2.455	2.361	2.291	2.346
Al (VI)	2.618	2.73	2.596	2.816	2.555	2.531	2.795	2.599	2.629	2.654
Fe/Fe+Mg	0.244	0.243	0.187	0.460	0.138	0.151	0.435	0.155	0.157	0.166
Si/Al	1.24	1.29	1.15	1.06	1.15	1.15	1.06	1.14	1.16	1.13
Ca+Na+K	0.034	0.066	0.047	0.068	0.044	0.069	0.059	0.027	0.04	0.073
Total cations	19.719	19.599	19.847	19.829	19.895	19.941	19.831	19.884	19.818	19.836
Σ Octaedral	11.599	11.476	11.748	11.741	11.824	11.864	11.742	11.848	11.741	11.685

Analysis	31	32	33	34	35	36	37	38	39	40
SiO2 (wt%)	28.68	26.17	30.92	29.27	28.87	28.37	29.22	29.09	29.05	28.48
Al2O3	21.21	21.12	17.98	20.79	20.64	19.52	21.50	21.04	20.55	20.28
Cr2O3	0.373	0.069	0.385	0.194	0.226	0.217	0.305	0.276	0.17	0.149
FeO	8.00	22.98	5.54	13.46	18.38	14.41	9.24	8.73	15.08	18.42
MnO	0.542	0.346	0.285	0.308	0.246	0.382	0.566	0.54	0.198	0.24
MgO	27.47	14.89	30.33	21.86	17.84	22.17	26.08	26.66	21.95	18.60
CaO	0.056	0.004	0.032	0.021	0.063	0.052	0.053	0.016	0.008	0.034
Na2O	0.12	0.087	0.049	0.083	0.03	0.13	0.063	0.073	0.067	0.04
K2O	0.067	0.06	0.054	0.072	0.044	0.156	0.072	0.046	0.09	0.054
H2O (c)	12.31	11.28	12.36	11.99	11.72	11.76	12.35	12.28	12.02	11.69
Total	98.83	97.01	97.94	98.05	98.06	97.17	99.45	98.75	99.18	97.99
Si (a.p.f.u.)	5.588	5.566	5.998	5.855	5.909	5.787	5.678	5.682	5.852	5.844
Al	4.87	5.29	4.11	4.9	4.97	4.69	4.92	4.84	4.87	4.9
Fe (total)	1.303	4.087	0.898	2.251	3.145	2.458	1.501	1.425	2.54	3.161
Mn	0.089	0.062	0.047	0.052	0.043	0.066	0.093	0.089	0.034	0.042
Mg	7.977	4.722	8.772	6.52	5.443	6.743	7.553	7.762	6.321	5.689
Ca	0.012	0.001	0.007	0.005	0.014	0.011	0.011	0.003	0.002	0.007
Na	0.045	0.036	0.018	0.032	0.012	0.051	0.024	0.028	0.026	0.016

Analysis	31	32	33	34	35	36	37	38	39	40
K	0.017	0.016	0.013	0.018	0.011	0.041	0.018	0.011	0.023	0.014
Al (IV)	2.412	2.434	2.002	2.145	2.091	2.213	2.322	2.318	2.148	2.156
Al (VI)	2.458	2.856	2.108	2.755	2.879	2.477	2.598	2.522	2.722	2.744
Fe/Fe+Mg	0.140	0.464	0.093	0.257	0.366	0.267	0.166	0.155	0.287	0.357
Si/Al	1.15	1.05	1.46	1.19	1.19	1.23	1.15	1.17	1.20	1.19
Ca+Na+K	0.074	0.053	0.038	0.055	0.037	0.103	0.053	0.042	0.051	0.037
Total cations	19.967	19.797	19.925	19.682	19.585	19.886	19.85	19.887	19.702	19.7
Σ Octaedral	11.827	11.727	11.825	11.578	11.51	11.744	11.745	11.798	11.617	11.636

Supplementary Table 3.4 - Complete results of electron microprobe analysis of chlorites from the Mina Velha *garimpo*.

Analysis	1	2	3	4	5	6	7	8	9	10
SiO2 (wt%)	26.65	27.32	27.87	26.50	26.75	26.75	27.51	26.77	28.95	27.29
Al2O3	23.28	22.77	21.99	22.85	22.60	23.26	22.37	22.67	22.96	22.07
Cr2O3	0.079	0.068	0.102	0.055	0.067	0.061	0.052	0.095	0.103	0.08
FeO	15.32	15.42	15.08	15.44	15.73	15.72	15.11	15.66	14.35	15.12
MnO	0.109	0.107	0.128	0.111	0.133	0.124	0.096	0.082	0.11	0.108
MgO	21.08	21.57	21.48	20.94	20.92	20.71	21.36	20.91	20.40	21.22
CaO	0.013	0.002	0.004	0.008	0.016	0.026	0.003	0.019	0.016	0.011
Na2O	0.042	0.037	0.000	0.03	0.008	0.002	0.044	0.029	0.057	0.000
K2O	0.026	0.055	0.18	0.054	0.002	0.025	0.021	0.024	0.619	0.153
H2O (c)	11.91	12.02	11.97	11.81	11.83	11.90	11.94	11.84	12.14	11.85
Total	98.51	99.37	98.80	97.80	98.06	98.58	98.51	98.10	99.71	97.90
Si (a.p.f.u.)	5.368	5.452	5.584	5.383	5.424	5.39	5.526	5.424	5.721	5.525
Al	5.52	5.35	5.19	5.47	5.4	5.52	5.29	5.41	5.34	5.26
Fe (total)	2.58	2.574	2.526	2.622	2.668	2.65	2.539	2.653	2.371	2.56
Mn	0.019	0.018	0.022	0.019	0.023	0.021	0.016	0.014	0.018	0.019
Mg	6.328	6.417	6.415	6.341	6.322	6.221	6.397	6.314	6.01	6.404
Ca	0.003	0.000	0.001	0.002	0.003	0.006	0.001	0.004	0.003	0.002
Na	0.016	0.014	0.000	0.012	0.003	0.001	0.017	0.011	0.022	0
K	0.007	0.014	0.046	0.014	0.001	0.006	0.005	0.006	0.156	0.04
Al (IV)	2.632	2.548	2.416	2.617	2.576	2.61	2.474	2.576	2.279	2.475
Al (VI)	2.888	2.802	2.774	2.853	2.824	2.91	2.816	2.834	3.061	2.785
Fe/Fe+Mg	0.290	0.286	0.283	0.293	0.297	0.299	0.284	0.296	0.283	0.286
Si/Al	0.97	1.02	1.08	0.98	1.00	0.98	1.04	1.00	1.07	1.05
Ca+Na+K	0.026	0.028	0.047	0.028	0.007	0.013	0.023	0.021	0.181	0.042
Total cations	19.862	19.86	19.815	19.879	19.863	19.833	19.812	19.859	19.667	19.836
Σ Octaedral	11.815	11.811	11.737	11.835	11.837	11.802	11.768	11.815	11.46	11.768
Cath (℃)a	786	758	716	781	768	778	735	768	672	735
K&M (℃)a	318	309	295	317	313	317	301	313	281	302
Z&F (℃)a	302	293	279	300	295	299	285	295	265	285

a: Cath, Cathelineau (1988); K&M, Kranitoids and MacLean (1987); Z&F, Zang and Fyfe (1995)

Analysis	11	12	13	14	15	16	17	18	19	20
SiO2 (wt%)	27.56	26.18	30.07	27.58	26.86	26.50	28.09	27.73	26.40	26.12
Al2O3	21.79	23.11	23.29	23.28	23.04	23.20	22.00	21.97	22.58	21.47
Cr2O3	0.093	0.092	0.078	0.14	0.08	0.055	0.104	0.1	0.104	0.053
FeO	15.26	15.63	13.41	15.30	15.59	15.25	15.08	15.10	15.13	14.36
MnO	0.113	0.1	0.099	0.081	0.068	0.064	0.047	0.124	0.086	0.117
MgO	21.37	20.78	19.50	20.60	21.27	21.02	22.01	21.49	20.57	20.56
CaO	0.019	0.017	0.002	0.014	0.012	0.015	0.01	0.025	0.005	0.082
Na2O	0.019	0.045	0.016	0.027	0.043	0.028	0.033	0.021	0.006	0.077
K2O	0.079	0.019	0.262	0.038	0.021	0.027	0.122	0.115	0.035	0.069
H2O (c)	11.88	11.79	12.17	12.01	11.95	11.86	12.07	11.94	11.68	11.42
Total	98.18	97.76	98.90	99.07	98.93	98.02	99.57	98.62	96.60	94.33
Si (a.p.f.u.)	5.564	5.325	5.929	5.509	5.394	5.36	5.582	5.569	5.421	5.485
Al	5.18	5.54	5.41	5.48	5.45	5.53	5.15	5.2	5.46	5.31
Fe (total)	2.576	2.659	2.21	2.555	2.619	2.579	2.506	2.536	2.599	2.522
Mn	0.019	0.017	0.017	0.014	0.012	0.011	0.008	0.021	0.015	0.021
Mg	6.43	6.302	5.73	6.133	6.34	6.338	6.522	6.432	6.297	6.438
Ca	0.004	0.004	0	0.003	0.003	0.003	0.002	0.005	0.001	0.018
Na	0.007	0.018	0.006	0.01	0.017	0.011	0.013	0.008	0.002	0.031
K	0.02	0.005	0.066	0.01	0.005	0.007	0.031	0.029	0.009	0.018
Al (IV)	2.436	2.675	2.071	2.491	2.606	2.64	2.418	2.431	2.579	2.515
Al (VI)	2.744	2.865	3.339	2.989	2.844	2.89	2.732	2.769	2.881	2.795
Fe/Fe+Mg	0.286	0.297	0.278	0.294	0.292	0.289	0.278	0.283	0.292	0.281
Si/Al	1.07	0.96	1.10	1.01	0.99	0.97	1.08	1.07	0.99	1.03
Ca+Na+K	0.031	0.027	0.072	0.023	0.025	0.021	0.046	0.042	0.012	0.067
Total cations	19.829	19.896	19.387	19.742	19.866	19.863	19.841	19.828	19.829	19.862
Σ Octaedral	11.769	11.843	11.296	11.691	11.815	11.818	11.768	11.758	11.792	11.776
Cath (℃)a	722	799	605	740	777	788	717	721	768	748
K&M (℃)a	297	324	258	304	316	319	295	297	313	305
Z&F (℃)a	281	306	243	286	299	303	280	281	296	290

a: Cath, Cathelineau (1988); K&M, Kranitoids and MacLean (1987); Z&F, Zang and Fyfe (1995)

Analysis	21	22	23	24	25	26	27	28	29	30
SiO2 (wt%)	26.79	26.92	26.86	27.11	26.63	26.69	26.95	27.27	27.25	26.42
Al2O3	22.49	22.80	22.89	23.98	23.26	22.81	23.15	24.03	22.35	23.24
Cr2O3	0.027	0.041	0.07	0.026	0.022	0.032	0.062	0.04	0.008	0.02
FeO	15.13	15.16	15.60	15.22	14.89	15.47	15.93	15.50	14.98	15.24
MnO	0.1	0.116	0.132	0.078	0.107	0.078	0.126	0.051	0.12	0.067
MgO	21.39	21.54	21.00	20.62	21.26	20.92	20.84	20.24	22.00	21.05
CaO	0.017	0	0.02	0.01	0.002	0.05	0.06	0.008	0.006	0
Na2O	0.017	0.036	0.029	0	0.005	0.013	0.012	0.027	0.014	0.049
K2O	0.025	0.031	0.024	0.012	0.013	0.018	0.019	0.025	0.018	0.009
H2O (c)	11.83	11.93	11.90	12.02	11.88	11.83	11.96	12.02	11.95	11.84
Total	97.82	98.57	98.53	99.08	98.07	97.91	99.11	99.21	98.70	97.94
Si (a.p.f.u.)	5.43	5.414	5.414	5.412	5.38	5.412	5.406	5.44	5.468	5.35

Analysis	21	22	23	24	25	26	27	28	29	30
Al	5.37	5.4	5.43	5.64	5.53	5.45	5.47	5.65	5.28	5.54
Fe (total)	2.565	2.549	2.63	2.541	2.516	2.622	2.673	2.585	2.513	2.581
Mn	0.017	0.02	0.023	0.013	0.018	0.013	0.021	0.009	0.02	0.011
Mg	6.464	6.457	6.312	6.137	6.374	6.323	6.232	6.019	6.582	6.354
Ca	0.004	0	0.004	0.002	0	0.011	0.013	0.002	0.001	0
Na	0.007	0.014	0.011	0	0.002	0.005	0.005	0.01	0.005	0.019
K	0.006	0.008	0.006	0.003	0.003	0.005	0.005	0.006	0.005	0.002
Al (IV)	2.57	2.586	2.586	2.588	2.62	2.588	2.594	2.56	2.532	2.65
Al (VI)	2.8	2.814	2.844	3.052	2.91	2.862	2.876	3.09	2.748	2.89
Fe/Fe+Mg	0.284	0.283	0.284	0.293	0.283	0.300	0.300	0.300	0.276	0.289
Si/Al	1.01	1.00	1.00	0.96	0.97	0.99	0.99	0.96	1.04	0.97
Ca+Na+K	0.017	0.022	0.021	0.005	0.005	0.021	0.023	0.018	0.011	0.021
Total cations	19.875	19.879	19.85	19.758	19.834	19.854	19.844	19.733	19.879	19.868
Σ Octaedral	11.846	11.84	11.809	11.743	11.818	11.82	11.802	11.703	11.863	11.836
Cath (℃)a	766	771	771	771	782	771	773	762	753	791
K&M (℃)a	311	313	314	314	317	314	315	312	307	320
Z&F (℃)a	296	297	296	297	301	297	297	293	292	304

a: Cath, Cathelineau (1988); K&M, Kranitoids and MacLean (1987); Z&F, Zang and Fyfe (1995)

Analysis	31	32	33	34	35	36	37	38	39	40
SiO2 (wt%)	26.97	27.82	26.62	27.52	29.55	28.91	27.38	28.50	27.09	26.95
Al2O3	23.89	22.78	22.89	21.86	19.84	21.50	22.20	21.26	23.28	23.06
Cr2O3	0.031	0.017	0.066	0.03	0.007	0.008	0.019	0.066	0.071	0.089
FeO	15.34	14.98	15.75	15.24	13.89	13.81	14.95	14.60	15.02	15.03
MnO	0.08	0.107	0.116	0.08	0.066	0.08	0.118	0.089	0.094	0.113
MgO	20.70	20.94	21.36	21.69	23.10	22.57	21.62	22.33	21.29	21.35
CaO	0.013	0.007	0.013	0.022	0.02	0.009	0.007	0.008	0.015	0.019
Na2O	0.044	0.036	0	0.028	0.029	0.024	0.004	0.042	0.004	0.128
K2O	0.032	0.038	0.015	0.031	0.142	0.152	0.021	0.114	0.012	0.15
H2O (c)	12.00	11.99	11.91	11.91	12.04	12.11	11.91	12.04	11.99	11.96
Total	99.10	98.72	98.74	98.41	98.68	99.17	98.23	99.05	98.87	98.85
Si (a.p.f.u.)	5.389	5.565	5.363	5.542	5.888	5.788	5.516	5.68	5.422	5.403
Al	5.62	5.37	5.43	5.19	4.66	5.07	5.27	4.99	5.49	5.44
Fe (total)	2.564	2.507	2.654	2.568	2.314	2.312	2.518	2.433	2.514	2.52
Mn	0.014	0.018	0.02	0.014	0.011	0.014	0.02	0.015	0.016	0.019
Mg	6.167	6.246	6.416	6.512	6.861	6.439	6.494	6.633	6.351	6.38
Ca	0.003	0.002	0.003	0.005	0.004	0.002	0.002	0.002	0.003	0.004
Na	0.017	0.014	0	0.011	0.011	0.009	0.002	0.016	0.002	0.05
K	0.008	0.01	0.004	0.008	0.036	0.039	0.005	0.029	0.003	0.038
Al (IV)	2.611	2.435	2.637	2.458	2.112	2.212	2.484	2.32	2.578	2.597
Al (VI)	3.009	2.935	2.793	2.732	2.548	2.858	2.786	2.67	2.912	2.843
Fe/Fe+Mg	0.294	0.286	0.293	0.283	0.252	0.264	0.279	0.286	0.284	0.283
Si/Al	0.96	1.04	0.99	1.07	1.26	1.14	1.05	1.14	0.99	0.99
Ca+Na+K	0.028	0.026	0.007	0.024	0.051	0.05	0.009	0.047	0.008	0.092
Total cations	19.793	19.748	19.906	19.863	19.795	19.683	19.84	19.821	19.82	19.884

Analysis	31	32	33	34	35	36	37	38	39	40
Σ Octaedral	11.754	11.706	11.883	11.826	11.734	11.623	11.818	11.751	11.793	11.762
Cath (℃)a	779	722	787	730	618	650	738	685	768	774
K&M (℃)a	317	297	319	300	261	272	302	284	312	314
Z&F (℃)a	299	281	302	284	250	260	287	271	297	299

a: Cath, Cathelineau (1988); K&M, Kranitoids and MacLean (1987); Z&F, Zang and Fyfe (1995)

Analysis	41	42	43	44	45	46	47	48	49	50
SiO2 (wt%)	27.02	27.32	28.09	27.19	27.92	26.24	26.15	26.21	26.95	26.78
Al2O3	23.99	23.21	23.55	23.98	23.73	23.42	23.44	23.60	23.41	23.72
Cr2O3	0.073	0.047	0.083	0.068	0.037	0.12	0.089	0.08	0.093	0.063
FeO	15.18	15.66	15.15	15.05	14.76	15.15	15.24	15.30	15.06	14.79
MnO	0.075	0.089	0.124	0.101	0.077	0.049	0.054	0.05	0.108	0.139
MgO	20.74	20.41	19.00	20.33	20.75	20.74	20.81	20.64	21.33	20.30
CaO	0.014	0.11	0.009	0.007	0	0.005	0.004	0.011	0.003	0.023
Na2O	0.008	0.009	0.032	0	0	0	0	0.014	0.007	0.029
K2O	0.03	0.142	0.218	0.028	0.025	0.017	0.008	0.012	0.02	0.022
H2O (c)	12.04	11.96	11.93	11.99	12.10	11.82	11.81	11.82	12.00	11.89
Total	99.17	98.96	98.19	98.74	99.40	97.56	97.61	97.74	98.98	97.76
Si (a.p.f.u.)	5.383	5.478	5.649	5.441	5.534	5.323	5.312	5.318	5.385	5.401
Al	5.63	5.48	5.58	5.65	5.54	5.59	5.61	5.64	5.51	5.63
Fe (total)	2.528	2.626	2.548	2.519	2.446	2.57	2.589	2.596	2.517	2.494
Mn	0.013	0.015	0.021	0.017	0.013	0.008	0.009	0.009	0.018	0.024
Mg	6.16	6.101	5.696	6.063	6.131	6.272	6.303	6.242	6.354	6.105
Ca	0.003	0.024	0.002	0.002	0	0.001	0.001	0.002	0.001	0.005
Na	0.003	0.003	0.012	0	0	0	0	0.006	0.003	0.011
K	0.008	0.036	0.056	0.007	0.006	0.004	0.002	0.003	0.005	0.006
Al (IV)	2.617	2.522	2.351	2.559	2.466	2.677	2.688	2.682	2.615	2.599
Al (VI)	3.013	2.958	3.229	3.091	3.074	2.913	2.922	2.958	2.895	3.031
Fe/Fe+Mg	0.291	0.301	0.309	0.294	0.285	0.291	0.291	0.294	0.284	0.290
Si/Al	0.96	1.00	1.01	0.96	1.00	0.95	0.95	0.94	0.98	0.96
Ca+Na+K	0.014	0.063	0.07	0.009	0.006	0.005	0.003	0.011	0.009	0.022
Total cations	19.768	19.779	19.581	19.718	19.684	19.822	19.856	19.842	19.83	19.728
Σ Octaedral	11.714	11.7	11.494	11.69	11.664	11.763	11.823	11.805	11.784	11.654
Cath (℃)a	781	750	695	762	732	800	804	802	780	775
K&M (℃)a	317	308	290	311	301	323	325	324	316	315
Z&F (℃)a	300	289	270	294	285	306	307	307	300	298

a: Cath, Cathelineau (1988); K&M, Kranitoids and MacLean (1987); Z&F, Zang and Fyfe (1995)

Analysis	51	52	53	54	55	56	57	58	59	60
SiO2 (wt%)	26.55	26.75	27.09	27.25	27.47	27.31	26.67	26.60	26.46	27.87
Al2O3	23.68	23.01	23.10	23.84	23.20	23.37	23.00	22.80	23.33	23.15
Cr2O3	0.093	0.1	0.06	0.066	0.069	0.072	0.056	0.051	0.059	0.053
FeO	15.50	15.01	15.17	14.85	14.91	14.97	15.15	15.49	15.48	15.15

Analysis	51	52	53	54	55	56	57	58	59	60
MnO	0.116	0.085	0.095	0.091	0.058	0.075	0.09	0.087	0.099	0.126
MgO	20.14	20.98	20.24	20.76	20.95	20.74	21.00	21.26	20.74	21.21
CaO	0.022	0.013	0.014	0.012	0.015	0.015	0.016	0.006	0.012	0.017
Na2O	0.034	0.018	0.013	0.008	0.054	0.046	0.001	0.036	0.043	0.002
K2O	0.035	0.013	0.098	0.11	0.138	0.014	0.03	0.049	0.047	0.15
H2O (c)	11.86	11.86	11.85	12.03	12.01	11.99	11.84	11.86	11.86	12.11
Total	98.03	97.84	97.73	99.02	98.87	98.60	97.85	98.24	98.13	99.84
Si (a.p.f.u.)	5.369	5.41	5.485	5.432	5.486	5.463	5.401	5.379	5.352	5.52
Al	5.64	5.48	5.51	5.6	5.46	5.51	5.48	5.43	5.56	5.4
Fe (total)	2.621	2.539	2.568	2.475	2.491	2.504	2.566	2.619	2.618	2.51
Mn	0.02	0.015	0.016	0.015	0.01	0.013	0.015	0.015	0.017	0.021
Mg	6.07	6.325	6.107	6.169	6.236	6.183	6.339	6.408	6.255	6.262
Ca	0.005	0.003	0.003	0.003	0.003	0.003	0.003	0.001	0.003	0.004
Na	0.013	0.007	0.005	0.003	0.021	0.018	0	0.014	0.017	0.001
K	0.009	0.003	0.025	0.028	0.035	0.004	0.008	0.013	0.012	0.038
Al (IV)	2.631	2.59	2.515	2.568	2.514	2.537	2.599	2.621	2.648	2.48
Al (VI)	3.009	2.89	2.995	3.032	2.946	2.973	2.881	2.809	2.912	2.92
Fe/Fe+Mg	0.302	0.286	0.296	0.286	0.285	0.288	0.288	0.290	0.295	0.286
Si/Al	0.95	0.99	1.00	0.97	1.00	0.99	0.99	0.99	0.96	1.02
Ca+Na+K	0.027	0.013	0.033	0.034	0.059	0.025	0.011	0.028	0.032	0.043
Total cations	19.785	19.819	19.747	19.754	19.778	19.747	19.832	19.897	19.859	19.777
Σ Octaedral	11.72	11.769	11.686	11.691	11.683	11.673	11.801	11.851	11.802	11.713
Cath (℃)a	785	772	748	765	748	755	775	782	791	737
K&M (℃)a	319	314	307	311	306	308	315	317	321	302
Z&F (℃)a	300	298	289	295	290	292	298	300	303	286

a: Cath, Cathelineau (1988); K&M, Kranitoids and MacLean (1987); Z&F, Zang and Fyfe (1995)

Analysis	61	62	63	64	65	66	67	68	69	70
SiO2 (wt%)	27.08	26.89	27.98	27.16	27.76	27.24	27.88	26.81	26.97	27.23
Al2O3	23.34	22.68	22.77	23.31	23.41	22.15	22.73	23.62	22.52	22.73
Cr2O3	0.044	0.029	0.057	0.066	0.031	0.13	0.104	0.081	0.137	0.014
FeO	15.24	15.18	15.62	15.54	15.30	14.90	15.17	15.63	15.10	14.68
MnO	0.137	0.106	0.039	0.085	0.076	0.08	0.096	0.046	0.103	0.079
MgO	21.62	21.12	20.11	21.09	20.93	21.16	20.76	21.16	20.86	21.82
CaO	0.02	0.012	0.012	0.006	0.016	0.03	0.021	0.012	0.035	0.002
Na2O	0.056	0	0.054	0.013	0.04	0.021	0.017	0	0.015	0.007
K2O	0.021	0.037	0.04	0.03	0.044	0.119	0.021	0.025	0.041	0.014
H2O (c)	12.06	11.85	11.95	12.01	12.09	11.83	11.99	12.02	11.81	11.96
Total	99.62	97.90	98.63	99.31	99.70	97.66	98.79	99.40	97.59	98.54
Si (a.p.f.u.)	5.388	5.443	5.614	5.423	5.506	5.523	5.579	5.352	5.475	5.459
Al	5.47	5.41	5.38	5.48	5.47	5.29	5.36	5.55	5.38	5.37
Fe (total)	2.536	2.57	2.621	2.594	2.538	2.526	2.539	2.61	2.564	2.461
Mn	0.023	0.018	0.007	0.014	0.013	0.014	0.016	0.008	0.018	0.013
Mg	6.412	6.375	6.016	6.277	6.188	6.397	6.194	6.297	6.314	6.521

Analysis	61	62	63	64	65	66	67	68	69	70
Ca	0.004	0.003	0.003	0.001	0.003	0.007	0.005	0.003	0.008	0
Na	0.022	0	0.021	0.005	0.015	0.008	0.007	0	0.006	0.003
K	0.005	0.01	0.01	0.008	0.011	0.031	0.005	0.006	0.011	0.004
Al (IV)	2.612	2.557	2.386	2.577	2.494	2.477	2.421	2.648	2.525	2.541
Al (VI)	2.858	2.853	2.994	2.903	2.976	2.813	2.939	2.902	2.855	2.829
Fe/Fe+Mg	0.283	0.287	0.303	0.292	0.291	0.283	0.291	0.293	0.289	0.274
Si/Al	0.99	1.01	1.04	0.99	1.01	1.04	1.04	0.96	1.02	1.02
Ca+Na+K	0.031	0.013	0.034	0.014	0.029	0.046	0.017	0.009	0.025	0.007
Total cations	19.874	19.843	19.69	19.82	19.756	19.827	19.729	19.849	19.808	19.844
Σ Octaedral	11.829	11.816	11.638	11.788	11.715	11.75	11.688	11.817	11.751	11.824
Cath (℃)a	779	761	706	768	741	736	718	791	751	756
K&M (℃)a	316	310	293	313	304	302	296	320	307	308
Z&F (℃)a	300	294	274	296	287	286	279	303	290	294

a: Cath, Cathelineau (1988); K&M, Kranitoids and MacLean (1987); Z&F, Zang and Fyfe (1995)

Analysis	71	72	73	74	75	76	77	78	79	80
SiO2 (wt%)	26.27	27.06	27.54	27.21	27.42	27.60	27.54	26.45	26.52	26.02
Al2O3	23.60	22.74	22.40	22.65	22.73	22.70	22.50	23.60	23.82	23.98
Cr2O3	0.077	0.027	0.036	0.096	0.037	0.084	0.026	0.112	0.098	0.027
FeO	15.46	15.22	15.12	15.08	15.89	15.15	14.93	15.04	15.84	15.63
MnO	0.079	0.098	0.083	0.059	0.086	0.039	0.105	0.084	0.079	0.144
MgO	20.97	21.73	21.46	21.45	21.71	20.57	20.84	20.99	20.95	20.60
CaO	0	0.017	0.027	0.04	0.018	0.018	0.206	0.007	0.004	0.011
Na2O	0	0.014	0.008	0.01	0.028	0	0.031	0.033	0.011	0.032
K2O	0.013	0.026	0.023	0.09	0.024	0.022	0.089	0.055	0.038	0.026
H2O (c)	11.88	11.97	11.95	11.95	12.07	11.90	11.90	11.94	12.02	11.88
Total	98.35	98.90	98.65	98.64	100.01	98.08	98.17	98.31	99.38	98.35
Si (a.p.f.u.)	5.304	5.423	5.525	5.462	5.447	5.565	5.551	5.314	5.293	5.251
Al	5.61	5.37	5.29	5.36	5.32	5.39	5.34	5.58	5.6	5.7
Fe (total)	2.61	2.551	2.536	2.532	2.64	2.555	2.517	2.527	2.644	2.638
Mn	0.014	0.017	0.014	0.01	0.014	0.007	0.018	0.014	0.013	0.025
Mg	6.312	6.492	6.419	6.418	6.43	6.182	6.262	6.286	6.234	6.198
Ca	0	0.004	0.006	0.009	0.004	0.004	0.044	0.002	0.001	0.002
Na	0	0.005	0.003	0.004	0.011	0	0.012	0.013	0.004	0.013
K	0.003	0.007	0.006	0.023	0.006	0.006	0.023	0.014	0.01	0.007
Al (IV)	2.696	2.577	2.475	2.538	2.553	2.435	2.449	2.686	2.707	2.749
Al (VI)	2.914	2.793	2.815	2.822	2.767	2.955	2.891	2.894	2.893	2.951
Fe/Fe+Mg	0.293	0.282	0.283	0.283	0.291	0.292	0.287	0.287	0.298	0.299
Si/Al	0.95	1.01	1.04	1.02	1.02	1.03	1.04	0.95	0.95	0.92
Ca+Na+K	0.003	0.016	0.015	0.036	0.021	0.01	0.079	0.029	0.015	0.022
Total cations	19.871	19.883	19.812	19.848	19.886	19.727	19.777	19.828	19.856	19.869
Σ Octaedral	11.85	11.853	11.784	11.782	11.851	11.699	11.688	11.721	11.784	11.812
Cath (℃)a	806	768	735	755	760	722	727	803	810	823

Analysis	71	72	73	74	75	76	77	78	79	80
K&M (℃)a	325	312	301	308	310	298	299	324	327	332
Z&F (℃)a	308	297	286	292	293	281	283	308	309	313

a: Cath, Cathelineau (1988); K&M, Kranitoids and MacLean (1987); Z&F, Zang and Fyfe (1995)

CAPÍTULO 3
CONCLUSÕES

A Serra de Jacobina é uma cadeia de montanhas de direção Norte-Sul com duzentos e cinquenta quilômetros de extensão. Nela ocorrem diversos depósitos de ouro em veios de quartzo, estruturalmente controlados, localmente chamados de garimpos. Quatro destes garimpos, denominados Maravilha, Jaqueira, Morro da Palmeirinha e Mina Velha, foram alvo de estudo no presente trabalho. Foi possível concluir que:

- ✓ Os sistemas de falhas Pindobaçu e Maravilha são as estruturas de primeira ordem que controlam a mineralização, embora os veios de quartzo estejam hospedados preferencialmente nas estruturas de segunda e terceira ordens desses sistemas.
- ✓ A alteração sericítica é disseminada nas rochas do Grupo Jacobina. Nas rochas metaultramáficas da Suíte Vale do Coxo a alteração sericítica é pervasiva e nos veios de quartzo ocorre preenchendo fraturas. A sulfetação é subordinada à alteração sericítica tanto nas rochas do Grupo Jacobina quanto nas da Suíte Vale do Coxo e nos veios de quartzo.

Os estudos de petrografia, inclusões fluidas e microssonda eletrônica no garimpo da Jaqueira indicaram que:

- ✓ O fluido mineralizador inicial era uma mistura de dois fluidos inicialmente imiscíveis, um aqua-carbônico e outro aquoso, com temperaturas moderadas a altas e salinidades variadas.
- ✓ Para as condições de formação da assembleia hidrotermal e da mineralização aurífera foram calculados valores de pressão entre 1,62 e 1,98 kbar e temperatura entre 302 e 346°C.
- ✓ A precipitação do ouro ocorreu em resposta a, pelo menos, dois mecanismos principais: imiscibilidade de fluidos e interação fluido-rocha.
- ✓ Um fluido aquoso tardio, de alta salinidade e temperaturas baixas foi misturado adicionado neste sistema.
- ✓ Gold deposition occurred in response to two main mechanisms: fluid immiscibility and fluid-rock interaction.
- ✓ A late, high salinity H_2O-NaCl fluid with lower temperatures (112-217°C) was mixed into the system.

APÊNDICE A – JUSTIFICATIVA DA PARTICIPAÇÃO DOS CO-AUTORES

Além do aluno Daniel Augusto de Miranda e seu orientador, doutor Aroldo Misi, participaram deste estudo outros três colaboradores cujos nomes foram incluídos na co-autoria da publicação.

O geólogo Evandro Luiz Klein é doutor em Geologia e Geoquímica pela Universidade Federal do Pará e *Université Jean Monnet* (2004). Membro concursado da CPRM - Serviço Geológico do Brasil desde 1994 e docente do Programa de Pós-Graduação em Geologia e Geoquímica da Universidade Federal do Pará desde 2007. Tem vasta experiência na área de estudos de inclusões fluidas em ambientes de ouro orogênico como Cinturão Gurupi e Província Aurífera do Tapajós. Sua participação no estudo se deu nos seguintes itens da publicação: 6. Fluid Inclusions results; 7. Mineral Chemistry results, subitem 7.2 Chlorite Geothermometry; 8. Discussions. O professor ensinou a sistemática da coleta dos dados microtermométricos em inclusões fluidas; os fundamentos básicos para o uso da geotermometria de cloritas, além de contribui nas discussões sobre a evolução do sistema mineral hidrotermal e condições P-T de deposição do ouro.

A geóloga Gláucia Queiroga é doutora em Geologia Regional pela Universidade Federal de Minas Gerais (2010). É professora permanente do Programa de Pós-Graduação em Evolução Crustal e Recursos Naturais do Departamento de Geologia da Universidade Federal de Ouro Preto e coordenadora do setor de microssonda eletrônica do Laboratório de Microscopia e Microanálises (LMic) do DEGEO. Sua participação no estudo se deu no item 7. Mineral Chemistry results. A professora ensinou teoria e prática no cálculo da fórmula química das cloritas analisadas no LMic.

O geólogo Marco Paulo de Castro é doutor em Geologia Regional pela Universidade Federal de Ouro Preto (2019). É responsável permanente pelo setor de microssonda do Laboratório de Microscopia e Microanálises (LMic) do Departamento de Geologia da Universidade Federal de Ouro Preto. Tem experiência em trabalhos de evolução crustal em ambientes orogênicos e microanálises. Sua participação no estudo se deu nos seguintes itens da publicação: 4. Analytical Procedures, subitem 4.4 Electron microprobe analysis; 7. Mineral Chemistry results, subitem 7.1 Chlorite chemistry. Ensinou ao aluno a estruturação dos procedimentos de microanálise utilizados no trabalho, teoria e prática durante a execução das análises de microssonda eletrônica executadas no LMic, além de contribuir nas discussões sobre a petrografia e química das cloritas.

ANEXO A – REGRAS DE FORMATAÇÃO DA REVISTA JOURNAL OF SOUTH AMERICAN EARTH SCIENCES

AUTHOR INFORMATION PACK 6 Sep 2019 www.elsevier.com/locate/jsames

PREPARATION

Paper length

The maximum number of words per article is 19,000.

NEW SUBMISSIONS

Submission to this journal proceeds totally online and you will be guided stepwise through the creation and uploading of your files. The system automatically converts your files to a single PDF file, which is used in the peer-review process. As part of the Your Paper Your Way service, you may choose to submit your manuscript as a single file to be used in the refereeing process. This can be a PDF file or a Word document, in any format or layout that can be used by referees to evaluate your manuscript. It should contain high enough quality figures for refereeing. If you prefer to do so, you may still provide all or some of the source files at the initial submission. Please note that individual figure files larger than 10 MB must be uploaded separately.

References

There are no strict requirements on reference formatting at submission. References can be in any style or format as long as the style is consistent. Where applicable, author(s) name(s), journal title/book title, chapter title/article title, year of publication, volume number/book chapter and the article number or pagination must be present. Use of DOI is highly encouraged. The reference style used by the journal will be applied to the accepted article by Elsevier at the proof stage. Note that missing data will be highlighted at proof stage for the author to correct.

Formatting requirements

There are no strict formatting requirements but all manuscripts must contain the essential elements needed to convey your manuscript, for example Abstract, Keywords, Introduction, Materials and Methods, Results, Conclusions, Artwork and Tables with Captions. If your article includes any Videos and/or other Supplementary material, this should be included in your initial submission for peer review purposes. Divide the article into clearly defined sections.

Figures and tables embedded in text

Please ensure the figures and the tables included in the single file are placed next to the relevant text in the manuscript, rather than at the bottom or the top of the file. The corresponding caption should be placed directly below the figure or table.

Peer review

This journal operates a single blind review process. All contributions will be initially assessed by the editor for suitability for the journal. Papers deemed suitable are then typically sent to a minimum of two independent expert reviewers to assess the scientific quality of the paper. The Editor is responsible for the final decision regarding acceptance or rejection of articles. The Editor's decision is final. More information on types of peer review.

REVISED SUBMISSIONS

Use of word processing software

Regardless of the file format of the original submission, at revision you must provide us with an editable file of the entire article. Keep the layout of the text as simple as possible. Most formatting codes will be removed and replaced on processing the article. The electronic text should be prepared in a way very similar to that of conventional manuscripts (see also the Guide to Publishing with Elsevier). See also the section on Electronic artwork.

To avoid unnecessary errors you are strongly advised to use the 'spell-check' and 'grammar-check' functions of your word processor.

LaTeX

You are recommended to use the Elsevier article class elsarticle.cls to prepare your manuscript and
BibTeX to generate your bibliography.
Our LaTeX site has detailed submission instructions, templates and other information.

Article structure

Subdivision - numbered sections

Divide your article into clearly defined and numbered sections. Subsections should be numbered
1.1 (then 1.1.1, 1.1.2, ...), 1.2, etc. (the abstract is not included in section numbering). Use this numbering also for internal cross-referencing: do not just refer to 'the text'. Any subsection may be given a brief heading. Each heading should appear on its own separate line.

Introduction

State the objectives of the work and provide an adequate background, avoiding a detailed literature survey or a summary of the results.

Material and methods

Provide sufficient details to allow the work to be reproduced by an independent researcher. Methods that are already published should be summarized, and indicated by a reference. If quoting directly from a previously published method, use quotation marks and also cite the source. Any modifications to existing methods should also be described.

Theory/calculation

A Theory section should extend, not repeat, the background to the article already dealt with in the Introduction and lay the foundation for further work. In contrast, a Calculation section represents a practical development from a theoretical basis.

Results

Results should be clear and concise.

Discussion

This should explore the significance of the results of the work, not repeat them. A combined Results and Discussion section is often appropriate. Avoid extensive citations and discussion of published literature.

Conclusions

The main conclusions of the study may be presented in a short Conclusions section, which may stand alone or form a subsection of a Discussion or Results and Discussion section.

Data Availability

Authors are encouraged to include a 'Data Availability' section in their manuscript which is visible in ALL reading formats and may refer to data hosted in ANY repository. It should be placed before the references to provide readers with information about where they can obtain the research data required to reproduce the work reported in the manuscript, and typically consists of a simple sentence giving the URL(s) of and citation(s) to the dataset(s). Full information can be found here.

If there is more than one appendix, they should be identified as A, B, etc. Formulae and equations in appendices should be given separate numbering: Eq. (A.1), Eq. (A.2), etc.; in a subsequent appendix, Eq. (B.1) and so on. Similarly for tables and figures: Table A.1; Fig. A.1, etc.

Essential title page information

• ***Title.*** Concise and informative. Titles are often used in information-retrieval systems. Avoid
abbreviations and formulae where possible.

• ***Author names and affiliations.*** Please clearly indicate the given name(s) and family name(s)
of each author and check that all names are accurately spelled. You can add your name between parentheses in your own script behind the English transliteration. Present the

authors' affiliation addresses (where the actual work was done) below the names. Indicate all affiliations with a lowercase superscript letter immediately after the author's name and in front of the appropriate address.
Provide the full postal address of each affiliation, including the country name and, if available, the e-mail address of each author.
• ***Corresponding author.*** Clearly indicate who will handle correspondence at all stages of refereeing
and publication, also post-publication. This responsibility includes answering any future queries about
Methodology and Materials. **Ensure that the e-mail address is given and that contact details**
are kept up to date by the corresponding author.
• ***Present/permanent address.*** If an author has moved since the work described in the article was done, or was visiting at the time, a 'Present address' (or 'Permanent address') may be indicated as a footnote to that author's name. The address at which the author actually did the work must be retained as the main, affiliation address. Superscript Arabic numerals are used for such footnotes.

Highlights

Highlights are mandatory for this journal. They consist of a short collection of bullet points that convey the core findings of the article and should be submitted in a separate editable file in the online submission system. Please use 'Highlights' in the file name and include 3 to 5 bullet points (maximum 85 characters, including spaces, per bullet point). You can view example Highlights on our information site.

Abstract

A concise and factual abstract is required. The abstract should state briefly the purpose of the research, the principal results and major conclusions. An abstract is often presented separately from the article, so it must be able to stand alone. For this reason, References should be avoided, but if essential, then cite the author(s) and year(s). Also, non-standard or uncommon abbreviations should be avoided, but if essential they must be defined at their first mention in the abstract itself.

Graphical abstract

Although a graphical abstract is optional, its use is encouraged as it draws more attention to the online article. The graphical abstract should summarize the contents of the article in a concise, pictorial form designed to capture the attention of a wide readership. Graphical abstracts should be submitted as a separate file in the online submission system. Image size: Please provide an image with a minimum of 531 × 1328 pixels (h × w) or proportionally more. The image should be readable at a size of 5 × 13 cm using a regular screen resolution of 96 dpi. Preferred file types: TIFF, EPS, PDF or MS Office files. You can view Example Graphical Abstracts on our information site. Authors can make use of Elsevier's Illustration Services to ensure the best presentation of their images and in accordance with all technical requirements.

Keywords

Immediately after the abstract, provide a maximum of 6 keywords, using American spelling]and avoiding general and plural terms and multiple concepts (avoid, for example, 'and', 'of'). Be sparing with abbreviations: only abbreviations firmly established in the field may be eligible. These keywords will be used for indexing purposes.

Abbreviations

Define abbreviations that are not standard in this field in a footnote to be placed on the first page of the article. Such abbreviations that are unavoidable in the abstract must be defined at their first mention there, as well as in the footnote. Ensure consistency of abbreviations throughout the article.

AUTHOR INFORMATION PACK 6 Sep 2019 www.elsevier.com/locate/jsames 9

Acknowledgements

Collate acknowledgements in a separate section at the end of the article before the references and do not, therefore, include them on the title page, as a footnote to the title or

otherwise. List here those individuals who provided help during the research (e.g., providing language help, writing assistance or proof reading the article, etc.).

Formatting of funding sources

List funding sources in this standard way to facilitate compliance to funder's requirements:

Funding: This work was supported by the National Institutes of Health [grant numbers xxxx, yyyy];
the Bill & Melinda Gates Foundation, Seattle, WA [grant number zzzz]; and the United States Institutes of Peace [grant number aaaa].

It is not necessary to include detailed descriptions on the program or type of grants and awards. When funding is from a block grant or other resources available to a university, college, or other research institution, submit the name of the institute or organization that provided the funding. If no funding has been provided for the research, please include the following sentence: This research did not receive any specific grant from funding agencies in the public, commercial, or not-for-profit sectors.

Units

Follow internationally accepted rules and conventions: use the international system of units (SI). If other units are mentioned, please give their equivalent in SI.

Math formulae

Please submit math equations as editable text and not as images. Present simple formulae in line with normal text where possible and use the solidus (/) instead of a horizontal line for small fractional terms, e.g., X/Y. In principle, variables are to be presented in italics. Powers of e are often more conveniently denoted by exp. Number consecutively any equations that have to be displayed separately from the text (if referred to explicitly in the text).

Footnotes

Footnotes should be used sparingly. Number them consecutively throughout the article. Many word processors build footnotes into the text, and this feature may be used. Should this not be the case, indicate the position of footnotes in the text and present the footnotes themselves separately at the end of the article.

Electronic artwork

General points

• Make sure you use uniform lettering and sizing of your original artwork.
• Preferred fonts: Arial (or Helvetica), Times New Roman (or Times), Symbol, Courier.
• Number the illustrations according to their sequence in the text.
• Use a logical naming convention for your artwork files.
• Indicate per figure if it is a single, 1.5 or 2-column fitting image.
• For Word submissions only, you may still provide figures and their captions, and tables within a single file at the revision stage.
• Please note that individual figure files larger than 10 MB must be provided in separate source files.

A detailed guide on electronic artwork is available.

You are urged to visit this site; some excerpts from the detailed information are given here.

Formats

Regardless of the application used, when your electronic artwork is finalized, please 'save as' or convert the images to one of the following formats (note the resolution requirements for line drawings, halftones, and line/halftone combinations given below):

EPS (or PDF): Vector drawings. Embed the font or save the text as 'graphics'.
TIFF (or JPG): Color or grayscale photographs (halftones): always use a minimum of 300 dpi.
TIFF (or JPG): Bitmapped line drawings: use a minimum of 1000 dpi.
TIFF (or JPG): Combinations bitmapped line/half-tone (color or grayscale): a minimum of 500 dpi is required.

Please do not:

• Supply files that are optimized for screen use (e.g., GIF, BMP, PICT, WPG); the resolution is too low.

• Supply files that are too low in resolution.
AUTHOR INFORMATION PACK 6 Sep 2019 www.elsevier.com/locate/jsames 10
• Submit graphics that are disproportionately large for the content.
Color artwork
Please make sure that artwork files are in an acceptable format (TIFF (or JPEG), EPS (or PDF), or
MS Office files) and with the correct resolution. If, together with your accepted article, you submit usable color figures then Elsevier will ensure, at no additional charge, that these figures will appear in color online (e.g., ScienceDirect and other sites) regardless of whether or not these illustrations are reproduced in color in the printed version. **For color reproduction in print, you will receive information regarding the costs from Elsevier after receipt of your accepted article**. Please indicate your preference for color: in print or online only. Further information on the preparation of electronic artwork.
Figure captions
Ensure that each illustration has a caption. A caption should comprise a brief title (**not** on the figure itself) and a description of the illustration. Keep text in the illustrations themselves to a minimum but explain all symbols and abbreviations used.

Tables

Please submit tables as editable text and not as images. Tables can be placed either next to the relevant text in the article, or on separate page(s) at the end. Number tables consecutively in accordance with their appearance in the text and place any table notes below the table body. Be sparing in the use of tables and ensure that the data presented in them do not duplicate results described elsewhere in the article. Please avoid using vertical rules and shading in table cells.

ANEXO B – COMPROVANTE DE SUBMISSÃO DO ARTIGO

Zimbra **daniel.miranda@cprm.gov.br**

Confirming submission to Journal of South American Earth Sciences

De : Journal of South American Earth Sciences <em@editorialmanager.com> sex, 08 de mai de 2020 14:17
Remetente : em sames 0 6b2463 44b1d24a <em.sames.0.6b2463.44b1d24a@editorialmanager.com>
Assunto : Confirming submission to Journal of South American Earth Sciences
Para : Daniel Augusto de Miranda <daniel.miranda@cprm.gov.br>
Responder para : Journal of South American Earth Sciences <sames@elsevier.com>

This is an automated message.

A mineral system approach on the Paleoproterozoic Au-bearing quartz veins of the Serra de Jacobina, Northeastern of the São Francisco Craton, Brazil

Dear Mr. Miranda,

We have received the above referenced manuscript you submitted to Journal of South American Earth Sciences.

To track the status of your manuscript, please log in as an author at https://www.editorialmanager.com/sames/, and navigate to the "Submissions Being Processed" folder.

Thank you for submitting your work to this journal.

Kind regards,
Journal of South American Earth Sciences

More information and support

You will find information relevant for you as an author on Elsevier's Author Hub: https://www.elsevier.com/authors.

FAQ: How can I reset a forgotten password?
https://service.elsevier.com/app/answers/detail/a_id/28452/supporthub/publishing/kw/editorial+manager/

For further assistance, please visit our customer service site: https://service.elsevier.com/app/home/supporthub/publishing/. Here you can search for solutions on a range of topics, find answers to frequently asked questions, and learn more about Editorial Manager via interactive tutorials. You can also talk 24/7 to our customer support team by phone and 24/7 by live chat and email.